UNIVERSITY OF CALGARY

The Reflection of Topography in the Plant Tolerance Curve

by

Marianne Nicole Chase

A THESIS

SUBMITTED TO THE FACULTY OF GRADUATE STUDIES

IN PARTIAL FULFILMENT OF THE REQUIREMENTS FOR THE

DEGREE OF MASTER OF SCIENCE

DEPARTMENT OF BIOLOGICAL SCIENCES

CALGARY, ALBERTA

DECEMBER, 2010

UNIVERSITY OF
CALGARY

Abstract

Plant distribution is known to be controlled by moisture at the watershed scale. Moisture is determined by the complex flow of the precipitation input by the hydrology and geomorphology of the landscape. In this paper I use a landscape evolution model, CHILD, to create landscapes dominated by: creep, overland flow, and landsliding processes, and a topographic index to approximate soil moisture to show that: 1) different geomorphic processes create different patterns of soil moisture which influence the distribution of plants and 2) transects on a landscape using slope position alone do not adequately define the soil moisture gradient.

Acknowledgements

Table of Contents

List of Tables

List of Figures and Illustrations

List of Symbols, Abbreviations and Nomenclature

Symbol	Definition
D_d	Drainage density (m^{-1})
L	Channel length (m)
A	Basin (Contributing) area (m^2)
l_o	Hillslope length (m)
α	Contributing area (m^2)
$\tan \beta$	Tangent slope, dimensionless
z	Elevation (m)
t	Time (yr)
U	Rate of tectonic uplift (m yr^{-1})
z_i	Elevation of cell i (m)
Λ_i	Surface area of cell i (m^2)
Q_{si}	Rate of sediment exiting cell i (m^3 yr^{-1})
Q_{sj}	Rate of sediment entering cell i from cell j (m^3 yr^{-1})
N_i	All neighbouring cells that drain into cell i
D_{ci}	Potential erosion (detachment) rate for cell i (m yr^{-1})
ϕ_i	Erosion/ deposition rate for cell i if the material was loose sediment (m yr^{-1})
D_c	Detachment capacity (m yr^{-1})
Q_{ci}	Potential transport rate for cell i (m^3 yr^{-1})
KB	Bedrock erodibility (m yr^{-1} (Pa)$^{-P}$)
τ	Shear stress (Pa)
τ_c	Critical shear stress to be overcome for erosion to occur (Pa)
P_b	Shear stress exponent, dimensionless
K_t	Coefficient for shear stress (Pa per (m^2 s^{-1})$^{Mb \text{ or } Mf}$)
Q	Discharge (m^3 yr^{-1})
W	Channel (or rill) width (m)
M_b	Detachment discharge exponent, dimensionless
S	Slope, dimensionless
N_b	Detachment slope exponent, dimensionless
Q_c	Sediment transport capacity (m^3 yr^{-1})
K_f	Sediment transport efficiency factor (m^3 yr^{-1} Pa^{-1})
P_f	Shear stress exponent, dimensionless
M_f	Transport discharge exponent, dimensionless
N_f	Transport slope exponent, dimensionless

R	Runoff rate (m yr^{-1})
P	Rainfall intensity (m yr^{-1})
I	Soil infiltration rate (m yr^{-1})
Q_{total}	Total discharge (m^3 yr^{-1})
$Q_{subsurface}$	Subsurface discharge (m^3 yr^{-1})
b	Contour width (m)
T	Transmissivity (m^2 yr^{-1})
W_b	Bank-full width (m)
K_w	Bank-full width coefficient
Q_b	Bank-full discharge (m^3 yr^{-1})
w_b	Downstream width exponent, dimensionless
w_s	At-a-station width exponent, dimensionless
$\tau_{c,s}$	Resistance of soil (Pa)
V	Vegetation density, proportion
$\tau_{c,v}$	Shear stress imparted by vegetation (Pa)
T_v	Time required for vegetation to become a resistive force to erosion (yr)
K_v	Erodibility of vegetation (Pa^{-1} yr^{-1})
$\overline{q_s}$	Sediment flux (m^3 yr^{-1})
K_D	Diffusion coefficient (m^2 yr^{-1})
∇z	Hillslope gradient, dimensionless
S_c	Critical slope gradient, dimensionless
S_{ij}	Slope gradient between cell i and j of the CHILD network, dimensionless
w_{ij}	Width of the Voronoi face cells i and j in the CHILD triangular irregular network share (m)
z_j	Elevation of cell j (m)
λ_{ij}	Length of the Voronoi edge cells i and j in the CHILD triangular irregular network share (m)
S_t	Threshold slope for failure by pore-pressure landsliding, dimensionless
$C_r^{'}$	Normalized cohesive resistance of roots
ϑ	Slope, dimensionless
ϕ	Friction angle of soil particle (deg)
p_w	Water density (kg m^{-3})
p_s	Bulk density of soil (kg m^{-3})
Γ	Inverse saturation threshold (m^{-1})
C_r	Cohesive resistance of roots (Pa)
h_s	Soil depth (m)
g	Gravity (m s^{-2})

Introduction

One of the basic goals of plant ecology is to describe and understand the distribution of plants on the landscape. Tolerance curves are one tool used to describe the local distribution of plants, and are a core concept in Ecology (e.g., Smith and Smith 2001). Tolerance curves are one or more dimensional curve(s) that describe the abundance of a species along one or more environmental gradient(s). Local here will mean the scale of hillslopes and low order watersheds (this will be defined more carefully shortly). Tolerance curves are generally symmetrical and unimodal; however, several studies have also found skewed and bimodal distributions and the shape of these curves have been a subject of some debate (e.g., Austin et al. 1984, Austin 1987, Minchin 1989, Oksanen and Minchin 2002). Regardless of the discrepancy in the shape of the curve from one study to the next, gradient methods used to derive the curves often come to similar conclusions: soil moisture is the principal axis of changes in abundance in tolerance curves (e.g., Curtis and McIntosh 1951, Whittaker 1956, Waring and Major 1964, Bridge and Johnson 2000, Zinko et al. 2005 and many others).

However, the reason the landscape organization results in moisture being so important is rarely explored in any detail in ecology (for an exception see Hack and Goodlett 1960). Over the last several decades geomorphologists have gained a better understanding of the processes of uplift and erosion that act upon landscapes to give them their characteristic forms (e.g., Dietrich and Montgomery 1998) and hydrologists have shown the connections between topography and soil moisture (e.g., Beven and Freer 2001). An understanding of earth surface processes can help explain what makes moisture (and nutrient) gradients so universally important in determining local plant

distribution and why an understanding of these processes which shape landscapes are necessary to understand both plant distribution on the landscape and the determination of their tolerance curves.

The *purpose* of this paper is to show how a process-based geomorphic understanding of landforms can be used to understand how soil moisture is distributed differently on landscapes with different uplift and erosion processes. This in turn can then show how distribution and abundance (tolerance curves) of different plants would be placed on landscapes. Models of uplift and erosion processes have been used to explore the development of landscapes (Harmon and Doe 2001, Pelletier 2008) in geomorphology because of the complexity of landscapes and the interaction of the processes that shape them. I use a landscape evolution model to create three landscapes in which the geomorphic processes acting upon each landscape are known and the relative strengths of these processes can be controlled.

The first is a landscape in which the dominant process is soil creep, the second is dominated by water overland flow, and the dominant process of the third is pore pressure landsliding. A topographic index is used as an approximation of soil moisture. The index incorporates how water moves over hillslopes to contribute to the soil moisture at a particular location (Kirkby 1975, Grayson et al. 1997). Because of the way the index is constructed, locations with similar indexes will have similar moisture (Beven 2001). This allows comparison of similar xeric, mesic, and wet locations on landscapes produced by different processes. The gradient of the topographic index can then be related to species abundance i.e. tolerance curves. There are two specific *objectives*: 1. To determine the effectiveness of three different transect methods (channel to ridgeline, path of steepest

ascent from channel to ridgeline, and path of steepest descent from ridgeline to channel) in describing moisture gradients and tolerance curves. 2. To determine whether the present idea of tolerance, particularly the 1-dimensional assumption for moisture, reflects appropriately our understanding of landscape process and organization.

Tolerance Curves

Generally two approaches are used to construct plant tolerance curves. The first determines gradients of soil moisture indirectly by using the similarity in stand plot composition and abundance. This approach uses multivariate statistical techniques which define the axis of principal variation (Gauch 1982). This approach has always had several technical problems, mainly due to the fact that there is no good underlying statistical model that is widely accepted. Because the gradients, and thus the tolerance curves, are constructed by putting stands/plots with similar species composition close together on the axes, there is not necessarily any *relationship of these gradients to specific landscape positions*. The second approach uses transects or categories to define the moisture gradients directly. The moisture transects are based on the assumption that a 1-dimensional transect up a hill will approximate a gradient of decreasing moisture (e.g., Whittaker 1956, 1967, Racine 1971, Smithson et al. 2002). Likewise, the categorical approach attempts to organize the landscape into regions of high and low soil moisture using topographic features such as valley bottoms and crests of ridges (e.g., Whittaker 1956). However, often the hillslopes used, the arrangement of transects, and the position of transects or categories in the landscape are not well specified with respect to the landscape's geomorphology and hydrology. This, as I will show later, is often at variance with the way water moves on hillslopes.

Landscape Organization

Landscapes have characteristics that are shared; all watersheds consist of peaks (local elevation maxima), saddles (two peaks with a minimum along a ridgeline), and streams (local minima) (Warntz 1975, Werner 1988, 1991, Dawes and Short 1994). Besides these, there are contour lines (delineating areas of equal elevation) and flow lines (lines orthogonal to contours). Flow lines indicate the direction of steepest descent. They usually connect ridgelines and stream courses.

While the basic elements of a landscape are similar for all landscapes, the degree of dissection or drainage density will vary. A highly dissected landscape will have more channelization per unit area than a less dissected landscape. This can be represented by drainage density, D_d (Horton 1945):

$$D_d = \frac{\sum L}{A} \tag{1}$$

where L is channel length and A is the total area of the basin. The average length of a hillslope (or length of overland flow), l_o (Horton 1945), is:

$$l_o = \frac{1}{2D_d} \tag{2}$$

Thus, a landscape that is more dissected will have shorter hillslopes on average than one that is less dissected.

Landscapes evolve according to the strength and type of tectonics that uplift masses and the erosive processes that lower them. When the erosive forces overcome the resistive forces imparted by soil and vegetation (e.g., Istanbulluoglu and Bras 2005), material is transported downslope. Hillslopes deliver sediment by a number of processes

to channels that then transport the sediment through the channel. Hillslope processes delivering sediment include soil creep, overland flow, and landsliding.

Soil creep is the gradual downhill movement of soil due to gravity (Culling 1963), aided by events such as freeze-thaw (Davison 1889) and wetting and drying cycles (Fleming and Johnson 1975), bioturbation (Black and Montgomery 1991, Roering et al. 2002, Yoo et al. 2005), and rain splash (Moeyersons 1975). Vegetation, however, may act as a form of resistance to many erosive processes as roots help anchor soil in place and hinder the movement of soil (e.g., Thornes 1990). Soil creep may be considered a linear process, increasing as slope increases for low to moderate slopes (Gilbert 1909, Culling 1960, McKean et al. 1993, Small et al. 1999); however, in regions characterized by steep slopes, soil creep becomes an increasingly nonlinear process as slope increases (Howard 1994, Roering et al. 1999, Martin 2000). Regions in which soil creep is a dominant process tend to have hillslopes that are very rounded (Davis 1892, Gilbert 1909, Anderson 1994).

Two forms of overland flow that contribute to erosion are infiltration excess overland flow (Hortonian overland flow) (Horton 1933) and saturation excess overland flow (Kirkby and Chorley 1967). Under conditions of poor infiltration, infiltration excess overland flow may occur uniformly over the hillslope (Horton 1933). Saturation excess overland flow is the more common form of overland flow in humid to temperate watersheds (Kirkby and Chorley 1967). In these watersheds, water moves primarily as shallow subsurface flow, travelling through the porous spaces in soil and rock along paths of steepest descent that are orthogonal to the contour lines. The flow of water downslope causes the water table to rise. If the rise of the water table is great enough, it may result in

groundwater seeping to the surface. Any subsequent precipitation is unable to infiltrate

the soil and further contributes to saturation overland flow. Since the water table is

closest to the surface at the bases of hillslopes and water moves downhill, saturation

overland flow will first occur at the bases of slopes and then spread uphill with increased

precipitation. The volume of water flowing over a location, the water discharge, may be

approximated by multiplying runoff and the contributing area (Tucker and Bras 1998). If

the water discharge is great enough, it may become an erosive force by overcoming the

shear stress necessary to move soil particles and result in the formation of small channels,

or rills.

Soil moisture depends on a number of factors including precipitation, slope

gradient, topographic convergence and divergence, porosity of substrate, depth of soil,

and evapotranspiration (Beven 2001). Note that in geomorphology the term gradient

specifically refers to the change in elevation with distance whereas in ecology gradient

may be used to indicate the change in any environmental variable that affects plant

distribution. In humid to temperate watersheds where water moves primarily as

subsurface flow and precipitation is greater than evapotranspiration, soil moisture can be

reasonably estimated using a topographic index that considers certain assumptions about

the topography that determine soil moisture (Kirkby 1975, Grayson et al. 1997). If the

subsurface flow and precipitation travel uniformly throughout the watershed such that it

is in a steady state and the surface slope approximates the slope of the water table, then

the likelihood of saturation at any given locale depends upon the soil transmissivity, the

flow path to that location, and the local slope which indicates the ability of the soil to

retain water. Flow paths cannot cross, but can coalesce into one path. Thus, if a collection

of adjacent flow paths are combined, they give the water contributed to the specified contour width. If soil transmissivity is homogeneous and decreases exponentially with depth throughout the watershed, a reasonable approximation of saturated soil moisture at a particular location is the topographic index, $\ln\left(\frac{\alpha}{\tan\beta}\right)$, where α is the contributing area at a given contour width and $\tan\beta$ is the local slope (Kirkby 1975). The advantage of the topographic index is that, as a similarity index, it allows for direct comparison of sites with the same index while considering the role of the 3-dimensional structure of the landscape in determining water flow. Other similarity indices approximating saturated soil moisture have also been developed (O'Loughlin 1981, 1986, Hjerdt et al. 2004). However, the topographic index is widely used and has often been expanded upon (Beven 2001).
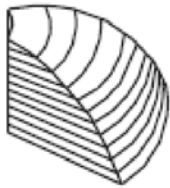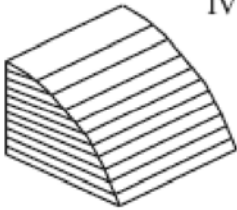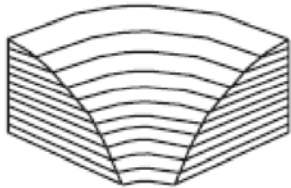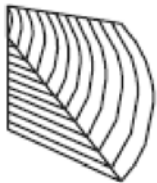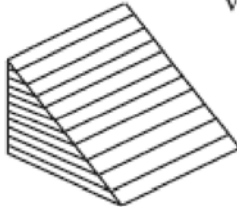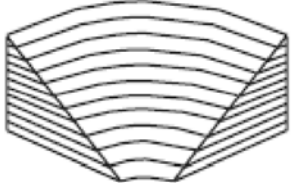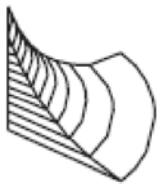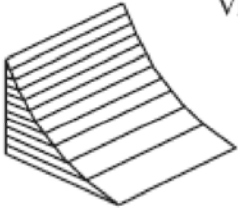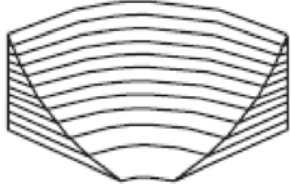
Saturated conditions contribute to pore-pressure landsliding. The likelihood of pore-pressure landsliding increases as the friction angle of soil, local slope, and vegetative cover decrease, and as precipitation and contributing area increase (Wu and Sidle 1995, Benda and Dunne 1997, Lancaster et al. 2003, Istanbulluoglu and Bras 2005). Pore-pressure landsliding tends to occur more often at headslopes than sideslopes because flow is always convergent at headslopes and therefore saturated conditions are common (Tucker and Bras 1998). Threshold landsliding may also occur in landscapes when the slope of a site becomes too steep (Howard 1994).

Due to a larger area of the landscape being comprised of hillslopes than channels, the topographic index *distributions* for watersheds are generally all right skewed (Beven 2001). Within a watershed, points on or near ridgelines have little or no contributing area

above them and thus have low topographic index values. As one moves down slope, the topographic index tends to increase as the contributing area increases. Also, different hillslopes will have different contributing areas, depending on their convergence/divergence, length of the hillslope, and the differing abilities to retain water according to the slope. Each landscape should have its own specific set of hillslope forms according to the processes at work that dictate lengths, contributing areas, and slope gradients.

Landscapes can be further divided into somewhat larger units that are hydrologically similar by separating hillslopes into headslopes and sideslopes (Bogaart and Troch 2006). Headslopes are those hillslopes for which subsurface flow drains towards the beginning of a headwater, or first order channel. Sideslopes are those slopes for which subsurface flow drains into one side of a channel link (the channel sections between stream junctions). As one would expect curvature distributions of head vs. sideslopes show that headslopes tend to be more convergent than sideslopes (Bogaart and Troch 2006). Furthermore, the frequency distribution of distance to the channel for cells on a digital elevation model (DEM) differs between headslopes and sideslopes. Distances to the channel for headslope cells have a slightly right skewed distribution with a high degree of variance about a mean of intermediate distance, while distances to the channel for sideslope cells have longer right skewed tails with a lower range of variation about a mean of low distance (Bogaart and Troch 2006).

Hillslopes can be further subdivided so as to create nine categories of hillslopes (Fig. 1) that should each show hydrological similarity by considering two measures of curvature (Suzuki 1977 presented in Tsukamoto and Ohta 1988, Aryal et al. 2002). The

Figure 1. Nine different hillslope types that may be identified based on planform and profile curvature (from R. Suzuki, as presented in Tsukamoto and Ohta 1988 and Aryal et al. 2002). Reprinted from Tsukamoto and Ohta 1988 with permission from Elsevier. Aryal et al. 2002 reproduced/modified by permission of American Geophysical Union.

first, planform curvature, is determined by the convergence ratio, which is the ratio of length of the ridgeline to the length of outlet for a hillslope (according to the definition by Suzuki 1977 presented in Tsukamoto and Ohta 1988, Aryal et al. 2002). Headslopes should have large convergence ratios because the ridgeline of the hillslope is much larger than the headwater channel towards which the subsurface flow paths of the hillslope drain. Sideslopes can be separated into parallel hillslopes and divergent hillslopes. Parallel hillslopes have convergence ratios that are close to one because the top of the hillslope and the base of the hillslope have nearly equal lengths and flow paths are parallel. Divergent hillslopes have a ratio that is less than one because flow paths are divergent and water drains from a smaller area at the ridgeline to a larger area at the channel link. The second measure of curvature is profile curvature which is the change in slope along a profile. Profile curvature separates hillslopes into concave, planar, or convex types; combined with the three planform types, it allows for a total of nine hillslope types to be identified (Fig. 1).

This study will link landscape formation to patterns of soil moisture and show that traditional methods used to derive tolerance curves are not adequate because they do not properly consider the controls on soil moisture. A landscape evolution model will be used to simulate three landscapes differing in dominant geomorphic process.

The Landscape Evolution Model

There are several landscape evolution models (e.g., Willgoose et al. 1991b, Tucker and Slingerland 1994, Braun and Sambridge 1997, Martin 2000). Here Iwill use the Channel Hillslope Integrated Landscape Development model (CHILD) (Tucker et al.

2001). This model incorporates known processes for non-glaciated landscapes. CHILD simulates uplift and erosion according to the general equation:

$$\frac{\partial z}{\partial t} = U + \left.\frac{\partial z}{\partial t}\right|_{fluvial} + \left.\frac{\partial z}{\partial t}\right|_{creep} + \left.\frac{\partial z}{\partial t}\right|_{landsliding} \tag{3}$$

where z is elevation, t is time, and U is uplift rate.

The model considers every cell to behave like a channel cell. The change in elevation of each cell, z_i, with time due to fluvial erosion is:

$$\left.\frac{\partial z_i}{\partial t}\right|_{fluvial} = \frac{1}{\Lambda_i}\left(-Q_{Si} + \sum_{j=1}^{N_i} Q_{Sj}\right) \tag{4}$$

where Λ_i is the surface area of the cell, Q_{Si} is the rate of sediment exiting the cell by fluvial transport, N_i is the number of neighbouring cells that drain into the cell, and Q_{Sj} is the rate of sediment entering the cell by fluvial transport from neighbour j. The rate of sediment exiting the cell, Q_{si} is:

$$Q_{si} = \begin{cases} \Lambda_i D_{ci} : \phi_i > D_c \\ Q_{ci} : \phi_i \leq D_c \end{cases} \tag{5}$$

where ϕ_i, the erosion/deposition of loose material is:

$$\phi_i = \frac{1}{\Lambda_i}\left(Q_{ci} - \sum_{j=1}^{N_i} Q_{Sj}\right) \tag{6}$$

Thus, in the case of resistant bedrock material (low detachment capacity, D_c), the sediment flux will be given by the potential detachment capacity, D_{ci}, i.e. a detachment limited state. Otherwise, in the case of easily detachable bedrock (high D_c), sediment

flux is given by the potential transport capacity of the stream, Q_{ci}, i.e. a transport limited state.

For this study the detachment of material will be modelled using the following power law equation:

$$D_c = KB(\tau - \tau_c)^{P_b} \qquad (7)$$

where KB is bedrock erodibility, τ is shear stress, τ_c is the critical shear stress to be overcome for erosion to occur, and P_b is a parameter. Shear stress, τ, is calculated as:

$$\tau = K_t\left(\frac{Q}{W}\right)^{M_b} S^{N_b} \qquad (8)$$

where K_t, M_b and N_b are parameters, Q is surface discharge, W is channel or rill width, and S is local slope.

There are several sediment transport laws that have been incorporated into CHILD. The transport law chosen for this study is based upon the Meyer-Peter Müller formula where sediment transport capacity, Q_c, is:

$$Q_c = K_f W(\tau - \tau_c)^{P_f} \qquad (9)$$

where K_f is a sediment transport efficiency parameter, P_f is a parameter and τ is instead:

$$\tau = K_t\left(\frac{Q}{W}\right)^{M_f} S^{N_f} \qquad (10)$$

where M_f and N_f are parameters.

Fluvial erosion occurs during storms and storm intensity, duration, and time between storms may be either modeled as constant values or as exponential distributions

centred around a mean (Eagleson 1978, Tucker and Bras 2000). This study will use

constant values.

Overland flow may be modeled as infiltration excess overland flow (Hortonian)

or as saturation excess flow. In the case of infiltration excess overland flow, surface

discharge, Q, is:

$$Q = R \times A \qquad (11)$$

where A is contributing area and runoff, R, is:

$$R = P - I \qquad (12)$$

where P is rainfall intensity and I is the infiltration capacity of the soil.

In saturation overland flow, surface discharge is calculated using equations based

upon O'Loughlin's (1986) topographic index:

$$Q = Q_{total} - Q_{subsurface} \qquad (13)$$

where total discharge, Q_{total}, is:

$$Q_{total} = A \times P \qquad (14)$$

and subsurface flow, $Q_{subsurface}$, is:

$$Q_{subsurface} = S \times b \times T \qquad (15)$$

where S is the local slope, b is contour width (or distance between nodes of the triangular

irregular network system in CHILD), and T is soil transmissivity.

The channel geometry used in the model runs has been modeled after Leopold

and Maddock's (1953) empirical relationships, and bank-full width, W_b, is:

$$W_b = K_w Q_b^{w_b} \qquad (16)$$

where Q_b is bank-full discharge, K_w is a coefficient, and w_b is the downstream (channel length) hydraulic geometry exponent, and:

$$\frac{W}{W_b} = \left(\frac{Q}{Q_b}\right)^{w_s} \tag{17}$$

where w_s is the at-a-station (channel cross section) hydraulic geometry exponent.

Vegetation is included in the model as a form of resistance to erosion and thus increases critical shear stress (Collins et al. 2004):

$$\tau_c = \tau_{c,s} + V\tau_{c,v} \tag{18}$$

where $\tau_{c,s}$ is the resistive force of the soil, V is the proportionate density of vegetation, and $\tau_{c,v}$ is the resistive force of the vegetation. The density of vegetation is determined both by the rate at which plants colonize the substrate and the rate at which they are removed from it. Plant colonization of the substrate over time is given by:

$$\frac{\partial V}{\partial t} = \frac{1}{T_v}(1-V) \tag{19}$$

where T_v is the time required for the plant community to reach a point at which it serves as a resistance to erosion. Removal of vegetation over time is:

$$\frac{\partial V}{\partial t} = \begin{cases} -K_v V (\tau - \tau_c) : \tau > \tau_c, \\ 0 : \tau \le \tau_c \end{cases} \tag{20}$$

where K_v is the erodibility of the plant community or population and τ is the shear stress of the erosive force.

Soil creep has been modeled using the Roering et al. (1999) adaptation of the (Howard 1994) equation that models creep as a nonlinear process:

$$\overline{q}_s = \frac{K_D \nabla z}{1 - (|\nabla z|/S_c)^2} \qquad (21)$$

where $\overline{q}_s$ represents the diffusive sediment flux, K_D is a diffusion coefficient, ∇z represents the hillslope gradient that is equal to the tangent of the slope angle, and S_c is a critical hillslope gradient. In the model, the change in elevation of each cell over time due to nonlinear soil creep is:

$$\left.\frac{\partial z_i}{\partial t}\right|_{creep} = \frac{-K_D}{\Lambda_i} \sum_{j=1}^{M_i} \frac{S_{ij}}{1 - \left(S_{ij}/S_c\right)^2} w_{ij} \qquad (22)$$

where S_{ij}, the slope between cells i and j of the triangular irregular network in CHILD is:

$$S_{ij} = \frac{(z_i - z_j)}{\lambda_{ij}} \qquad (23)$$

where λ_{ij} is the length of the Voronoi edge between cell i and cell j, and w_{ij} is the width of the Voronoi face the two cells share.

Ihave extended the program code to incorporate pore pressure landsliding. This modified version of the program has not been benchmarked. Pore pressure landsliding occurs when the local slope exceeds a threshold slope, S_t (Wu and Sidle 1995, Benda and Dunne 1997, Lancaster et al. 2003, Istanbulluoglu and Bras 2005):

$$S_t = \frac{C_r' V}{\cos \vartheta} + \tan \phi \left(1 - p_w / p_s \min\left(\Gamma \frac{A}{S}, 1\right)\right) \qquad (24)$$

where ϑ is the slope, ϕ is the friction angle of the soil particle, p_w is water density, p_s is the bulk density of soil, and C_r' is:

$$C'_r = \frac{C_r}{h_s p_s g} \tag{25}$$

and Γ, the inverse saturation threshold, is:

$$\Gamma = \frac{P}{T} \tag{26}$$

C_r is the cohesive resistance of roots, h_s is soil depth, and g is gravity. If the local slope exceeds the threshold slope, 0.5m of sediment is removed and assumed to exit the watershed. Therefore, the change in elevation with time due to landsliding is:

$$\left.\frac{\partial z_i}{\partial t}\right|_{landsliding} = \begin{cases} -0.5m : S > S_t \\ 0m : S \leq S_t \end{cases} \tag{27}$$

Methods

    Three different landscapes were created using the landscape evolution model. A topographic index approximating soil moisture was distributed on each landscape, and its distribution related to the geomorphology of each landscape. Each landscape was then divided into hillslopes and three different transects were taken on each hillslope; channel to ridgeline, steepest ascent, and steepest descent. The ability of each transect type to construct moisture gradients was assessed. A mesic plant was then placed on each landscape, and its distribution related to the geomorphology of the landscapes through the moisture index. Finally, the ability of the three transect types to generate plant tolerance curves were assessed.

    The Channel Hillslope Landscape Development model (CHILD) version RI8.12 (Tucker et al. 2001) was used to generate three Digital Elevation Models (DEM's) of landscapes three kilometers by two kilometers with elevation contours of 15 meters. This

scale was chosen to represent a small watershed. All three landscapes had a single outlet

point through which all water that carried sediment exited.

Table 1 provides the parameters used in each of the landscapes. The landscapes

were not designed to represent any specific real world landscapes. Parameter values were

chosen on the basis that they created landforms characteristic of different geomorphic

processes (e.g., Tucker and Bras 1998). Landscape DEM's and slope-area plots generated

for each landscape reflect the dominant processes that shaped the landscape (see results

for explanation and e.g., Willgoose et al. 1991a, Montgomery and Foufoula-Georgiou

1993, Tucker and Bras 1998).

After the DEM's were created they were converted from triangular networks into raster

grids, and TARDEM (Tarboton 1989, Tarboton 1997) was used to fill pits. Slope

gradients were calculated, as were flow directions out of each cell using the D8 and Dinf

grid cell methods (Tarboton 1989, Tarboton 1997). The dinf flow directions were

subsequently used in TARDEM to determine contributing areas for each grid cell of the

DEM and the contributing area derived using this method was used in the calculation of

the topographic index because, unlike the D8 method, dinf allows for divergence of flow

paths (O'Callaghan and Mark 1984, Costa-Cabral and Burges 1994). The D8 flow

directions were used to define channels and divide the landscapes into hillslopes using

the hsB toolkit (Troch et al. 2003, Bogaart and Guardiola 2007).

Each basin was divided into hillslopes using the hsB toolkit (Troch et al. 2003,

Bogaart and Guardiola 2007). In order to define hillslopes, the channels were first

defined by arbitrarily setting a critical contributing area of 50,000 m^2, above which

conditions were considered saturated. Next the hsB toolkit divided the channels into

Table 1. Parameter values used in the landscape evolution model simulations to generate the three landscapes. Values for the overland flow-dominated and landslide-dominated landscapes are the same as for the creep-dominated landscape unless otherwise indicated.

Parameter	Value
Landscape 1: Creep-Dominated	
Spacing between nodes	15 m
Uplift rate, U	0.00003 m yr^{-1}
Diffusion coefficient, K_D	0.005 m^2 yr^{-1}
Bedrock erodibility, KB	0.000003 m yr^{-1} (Pa)$^{-p}$
Transmissivity, T	6209 m^2 yr^{-1}
Critical shear stress of soil, $\tau_{c,s}$	5 Pa
Shear stress imparted by vegetation, $\tau_{c,v}$	80 Pa
Erodibility of vegetation, K_v	1 Pa^{-1} yr^{-1}
Time for vegetation to grow to point where limits erosion, T_v	5 y
Storm intensity	5.22 m yr^{-1}
Storm duration	0.885 yr
Between storm duration	29.5 yr
Soil internal friction angle, ϕ	30 deg
Bulk density of soil, p_s	1500 kg m^{-3}
Cohesive resistance of roots, C_r	200 Pa
Landscape 2: Overland Flow Dominated	
Uplift rate, U	0.00007 m yr^{-1}
Bedrock erodibility, KB	0.000004 m yr^{-1} (Pa)$^{-p}$
Infiltration rate, I	1.74 m yr^{-1}
Shear stress imparted by vegetation, $\tau_{c,v}$	40 Pa
Cohesive resistance of roots, C_r	100 Pa
Landscape 3: Landslide-Dominated	
Uplift rate, U	0.007 m yr^{-1}
Bedrock erodibility, KB	0.000004 m yr^{-1} (Pa)$^{-p}$
Transmissivity, T	22314 m^2 yr^{-1}
Storm intensity	12.77 m yr^{-1}
Storm duration	0.989 yr
Between storm duration	7.89 yr
Soil internal friction angle, ϕ	32.5 deg
Bulk density of soil, p_s	1720 kg m^{-3}

links. A hillslope was represented by all cells that either drain into one side of a channel link (sideslopes) or all cells that drain into the first cell (channel head) of the first order channel (headslopes). The base of a hillslope was then defined as the hillslope cells that drain immediately into a channel cell (the channel outlet). The top of a hillslope was defined by the ridgeline, the topmost cells that drain into that particular side of the channel link or the channel head.

Soil moisture was then approximated for all cells on each landscape using the Kirkby (1975) topographic index.

A mesic Gaussian plant tolerance curve "species" was created (Fig. 2) with abundance at different topographic indices. This plant may represent any species with a mesic distribution. The plant was designed with a broad range along the topographic index so that it was present on all three landscapes, and sampled by each transect. The relationship between species abundance and topographic index was then used to map abundance on the synthetic landscapes using the topographic index for each location.

The assumption was made that distance from the channel to the ridgeline indicated a gradient of decreased topographic index (i.e. moisture) and the abundance of each species as a function of *distance* along the transect would yield a "tolerance curve". Transects were then taken on each landscape within each of the nine hillslope categories using three different methods. In the first method transects were laid from the centre of the base of the hillslope to the centre of the ridgeline for each hillslope. The second transect method followed a path of steepest *ascent* starting at the middle of the base of each hillslope. The third method was to follow a path of steepest *descent* from the middle of the ridgeline of each hillslope. Transects were sampled for contributing area, slope,
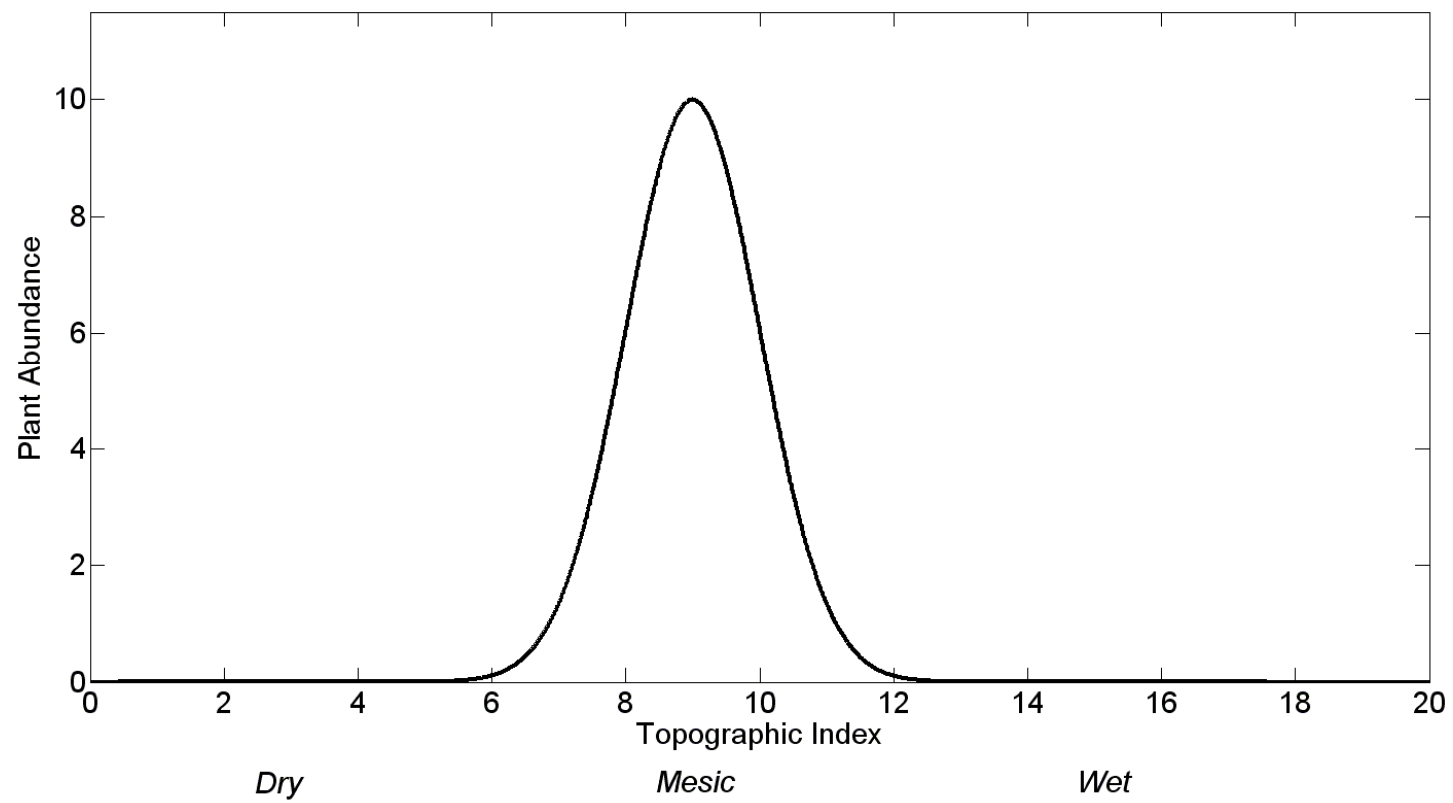
Figure 2. The plant species created where abundance is a function of the topographic index.

topographic index, and the abundance of the plant every 25 m for the channel to ridgeline

method, or every cell for the ascent and descent transects.

Results

Landscapes

All landscapes have a common structure of ridges and channels with hillslopes in

between; however, different geomorphic processes of uplift and erosion leave distinct

signatures on the landforms that determine the distribution of soil moisture and thus

plants with different tolerance distributions.

<u>Creep-Dominated</u>

The DEM of the creep-dominated landscape (Fig. 3a) has the characteristic

rounded hilltops. The slope-area plot (Fig. 3b) has a strong initial increase in slope with

contributing area (region I of Fig. 3b) which indicates slope convexity and dominance of

soil creep (Willgoose et al. 1991a, Tucker and Bras 1998). Following this, there is a

decrease in slope with increasing contributing area (region II, Fig. 3b) that indicates pore-

pressure landsliding occurred on slopes that may not have been completely saturated but

were steep enough to fail. This is followed by a levelling out of slope with increasing

contributing area (region III, Fig. 3b), which indicates a threshold for landsliding where

the combined slope and contributing area were great enough that fully saturated

landsliding occurred (Montgomery and Dietrich 1988, Montgomery and Dietrich 1989,

Montgomery and Dietrich 1992, 1994, Tucker and Bras 1998). These pore-pressure

landslides are not readily apparent on the DEM (Fig. 3a), likely because many of the

older gullies created were filled by creep over time. A final decrease in slope with

contributing area (region IV, Fig. 3b) indicates fluvial processes, including overland flow
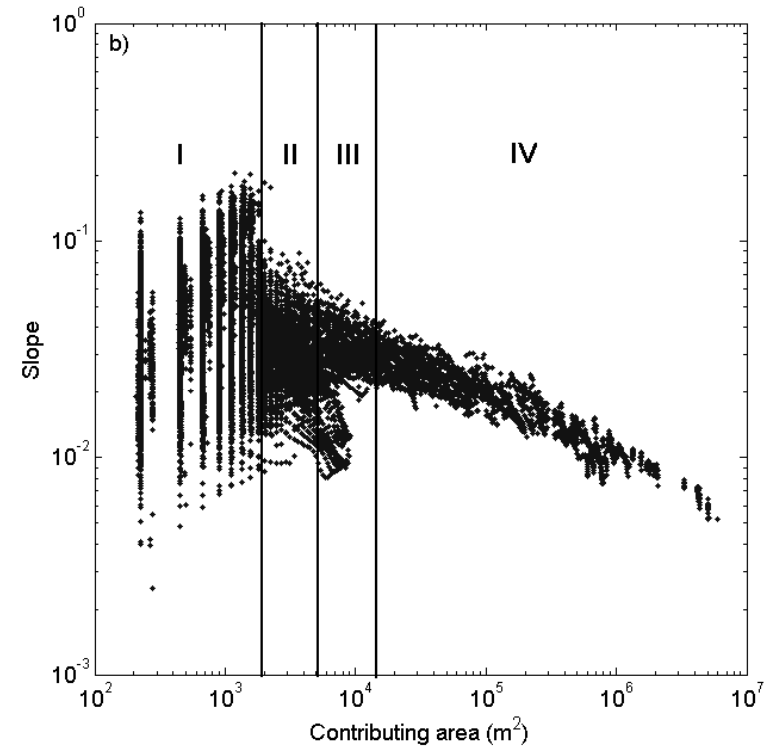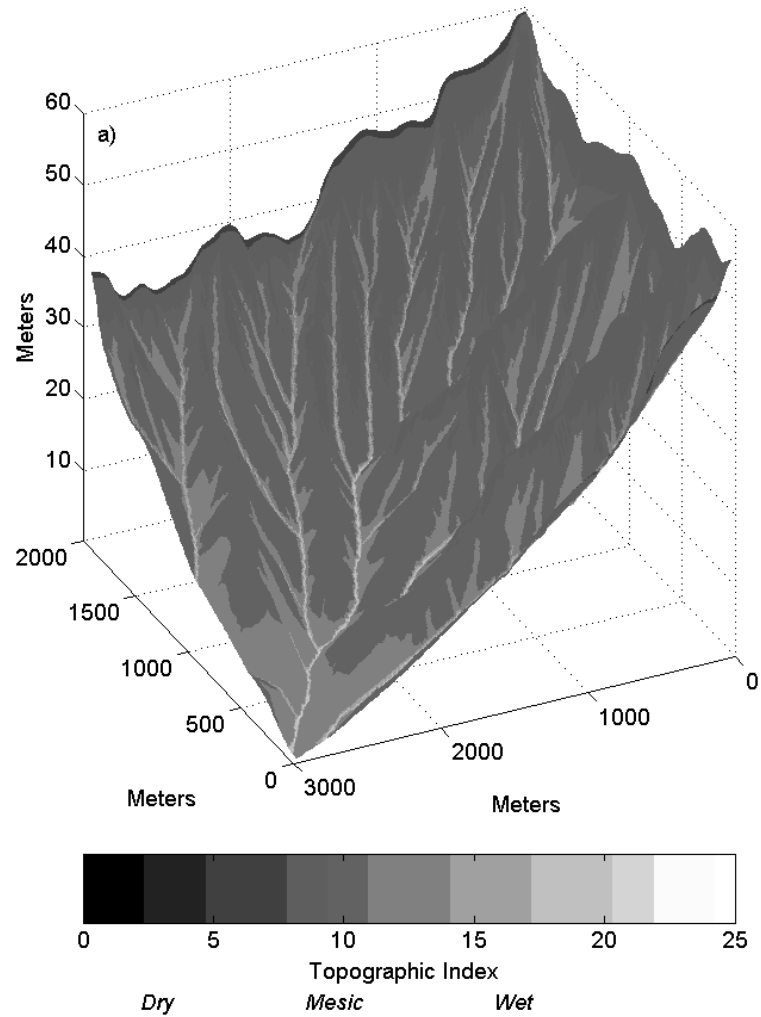
Figure 3. Creep-dominated landscape a) digital elevation model colored by topographic index and b) slope-area plot. Refer to text for interpretation of the regions of the slope-area plot.

(Montgomery and Dietrich 1988, 1989, Willgoose et al. 1991a, Montgomery and Dietrich 1992, 1994, Tucker and Bras 1998). This landscape is similar to one that experiences a low rate of tectonic uplift, moderate rainfall and has shrub-like vegetation, like some regions of Marin County, California.

Of the three landscapes, the creep-dominated landscape had the lowest maximum relief (60 m) (where relief is the difference in elevation between the highest and lowest points of a landscape) as well as the lowest mean slope. The average hillslope length calculated using equation 2 was 162.2 m.

Overland flow-Dominated

The DEM of the overland flow-dominated landscape (Fig. 4a) has sharper peaks than the creep-dominated landscape. An initial increase in slope with area in the slope area plot (region I, Fig. 4b) indicates soil creep did occur on hilltops; however, this is less pronounced than in the creep-dominated landscape. Rather, overland flow erosion was the dominant process as indicated by a strong fluvial trend in the slope-area plot (region IV, Fig. 4b). Unlike the other two landscapes, this landscape experienced infiltration excess overland flow rather than saturation excess overland flow. A similar natural landscape would be one that has moderate rainfall, scattered vegetation, and experiences uniform overland flow. The landscape was evolved with higher tectonic uplift and bedrock erodibility than the creep-dominated landscape and this contributed to a greater maximum relief (84 m) and slightly higher mean slope. The average hillslope length was 166.5 m.

23

Figure 4. Overland flow-dominated landscape a) digital elevation model colored by topographic index and b) slope-area plot. Refer to text for interpretation of the regions of the slope-area plot.

<u>Landslide-Dominated</u>

The pore-pressure landsliding-dominated landscape (Fig. 5a), like the overland flow-dominated landscape, has hillslopes that appear planar in comparison to the creep-dominated landscape. The initial increase of slope with area in the slope-area plot (region I, Fig. 5b) does indicate that creep occurred, but, like the overland flow-dominated landscape, this region is much less pronounced than in the creep-dominated landscape (Fig. 3b). The decrease of slope with area that followed (region II, Fig. 5b) and then levelling off of slope with area (region III, Fig. 5b) is pronounced and indicates that pore-pressure landsliding was the dominant process in this landscape's evolution. As with the other two landscapes, the final decrease in slope with area (region IV, Fig. 5b) is indicative of fluvial processes. Natural landscapes similar to this one are regions that are humid with high tectonic uplift and abundant vegetation, such as Taiwan. This landscape was developed with notably higher tectonic uplift than the other two landscapes, resulting in much higher maximum relief (882 m), and steeper slopes. The average hillslope length was 154.5 m.

Each of the three landscapes was dominated by a different geomorphic process as indicated in the distinctive signatures of their slope-area plots and the shapes of their DEMs. Next, it was determined whether these differences in geomorphology were reflected by differences in soil moisture using the topographic index.

Soil moisture

The frequency of the topographic index (Fig. 6) for all pixels on each landscape had a right skewed distribution with different means and ranges. As previously
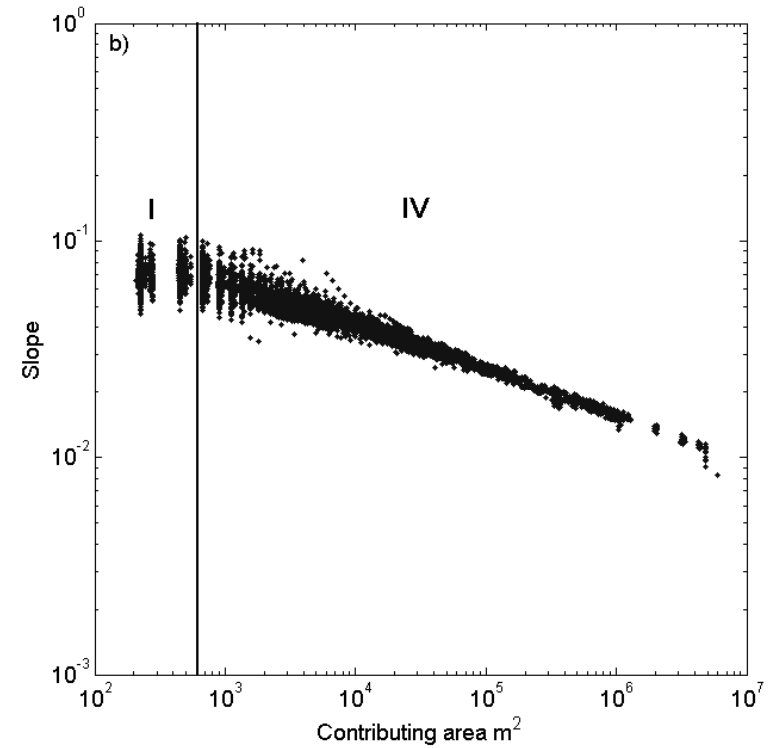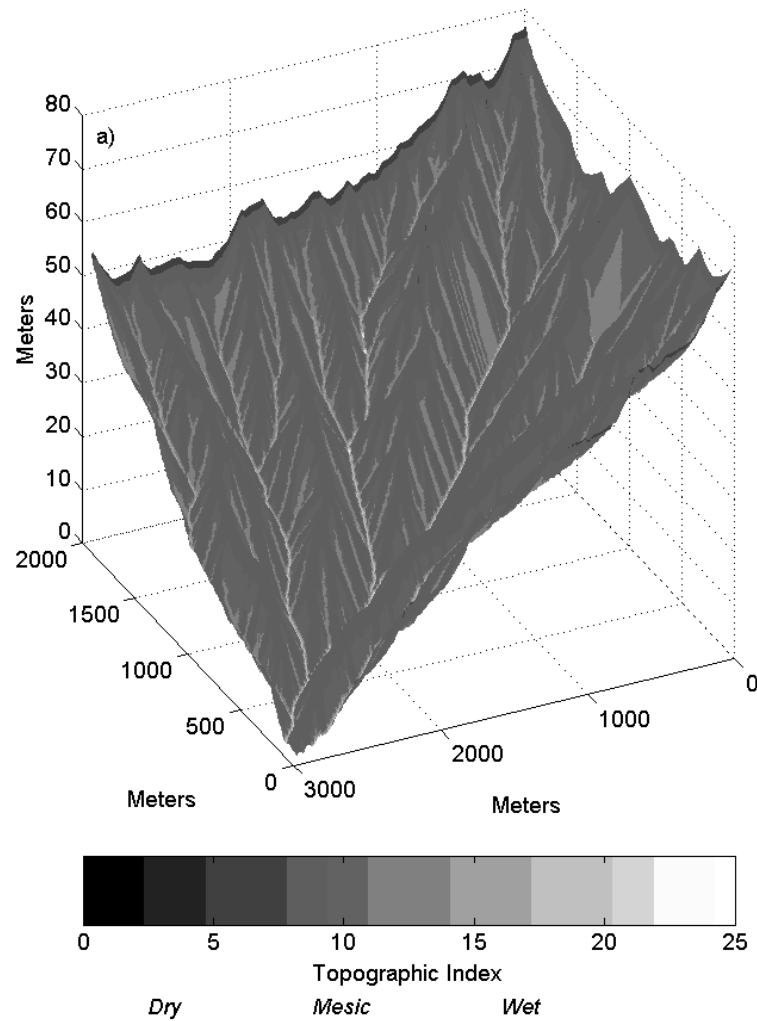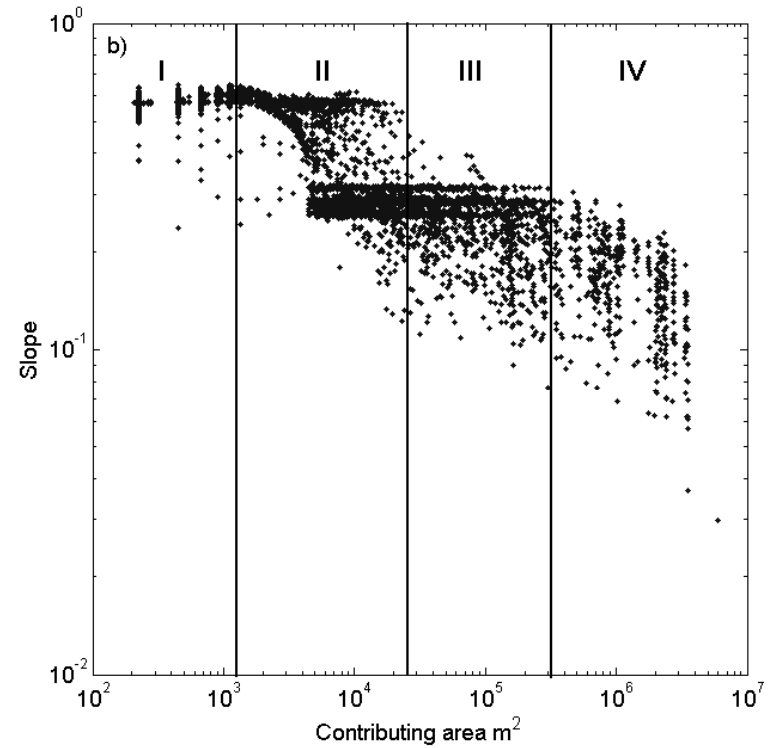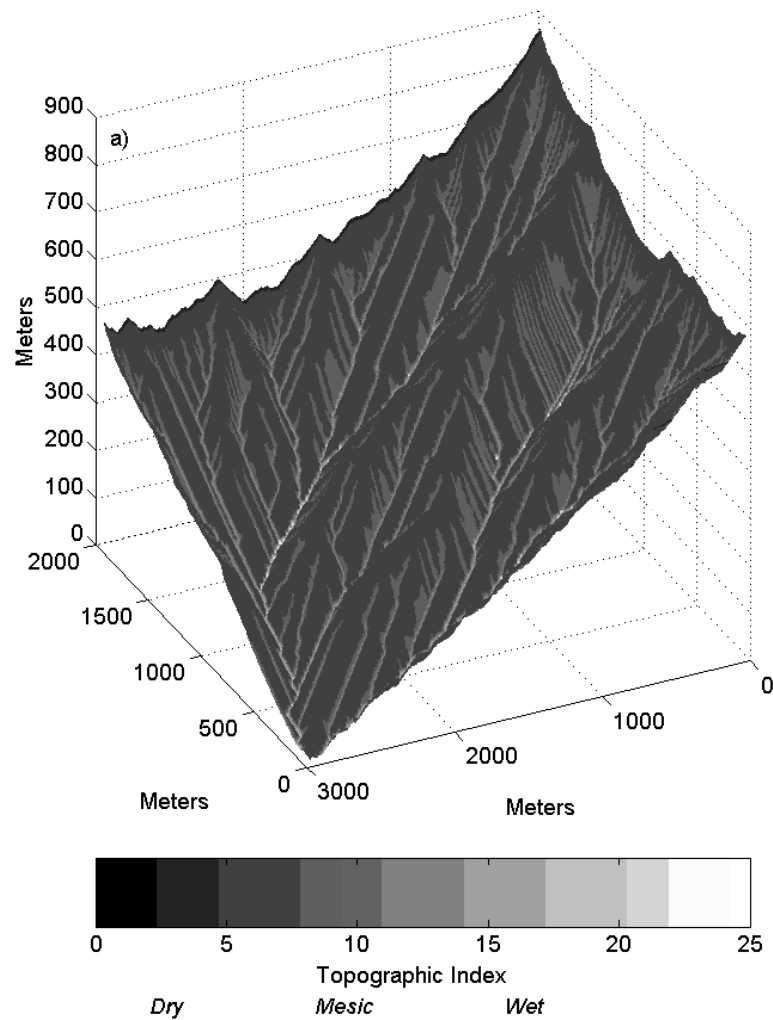
Figure 5. Landslide-dominated landscape a) digital elevation model colored by topographic index and b) slope-area plot. Refer to text for interpretation of the regions of the slope-area plot.
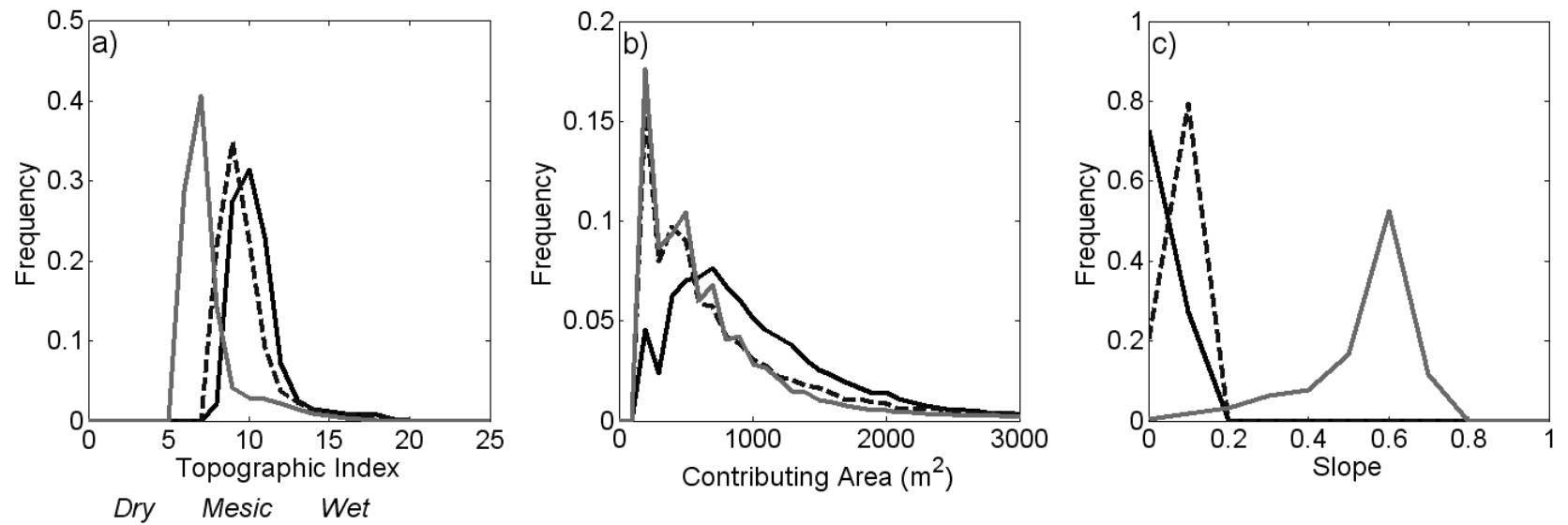
Figure 6. Probability density function of the a) topographic index, b) contributing areas, and c) slopes for the three landscapes. The solid black line represents the creep-dominated landscape, the dashed line represents the overland flow-dominated landscape, and the solid grey line represents the landslide-dominated landscape. Note: the contributing area plot has been cut-ff at 3,000 m2 because all distributions are very right-skewed.

mentioned the topographic index is a surrogate for soil moisture (Kirkby 1975, Grayson et al. 1997). The three landscapes have similarly shaped frequency distributions because they are all constructed of a ridgeline, hillslope, and streamcourse pattern. However, the different means and ranges reflect the different processes that shaped this basic plan.

The mean and median topographic index values of the landslide-dominated landscape are lower, i.e. a more xeric landscape than the other two landscapes, and the minimum and maximum topographic index values are also lower than the other two landscapes, spanning values from 5.8 to 19.9 (Fig. 6). The median contributing areas of the landslide-dominated and overland flow-dominated landscapes are comparable and lower than those of the creep-dominated landscape (Fig. 6b). However, the mean and median slopes of the landslide-dominated landscape are much higher than those of the other two landscapes, and this results in generally lower topographic index values (Fig. 6c).

The overland flow-dominated landscape has topographic index values that span from 7.7 to 22.6 (Fig. 6a). While median contributing areas of the overland flow-dominated landscape are comparable to those of the landslide-dominated landscape (Fig. 6b), mean and median slopes are much lower, yet slightly higher than the creep-dominated landscape (Fig. 6c). Thus, topographic index values tend to be greater than the landslide-dominated landscape and lower than the creep-dominated landscape.

The creep-dominated landscape is the wettest of the three and the topographic index ranges from 7.0 to 22.0 with mean and median topographic index values greater for this landscape than the other two (Fig. 6a). This is a result of greater median contributing areas and lower mean and median slopes than the other two landscapes (Fig. 6b, c).

The differences in topographic index values are also apparent on the landscape DEMs and can be thought of as how xeric, mesic, and wet tolerance curve species would be distributed on the landscape. On the creep-dominated landscape (Fig. 3a), wet areas radiate outwards from headwaters or concave valleys, where contributing areas are large, and the driest areas are restricted to ridgelines. The overland flow-dominated landscape (Fig. 4a) is drier than the creep-dominated landscape, and wet regions tend to occur lower on the hillslopes. On the landslide-dominated landscape (Fig. 5a), wet areas are restricted to the channels, and the ridgelines are much drier than those of the other two landscapes.

Curvature influences the topographic index because it dictates whether flow paths of water movement converge, diverge, or run parallel (e.g., Warntz 1975) and thus, along with slope length, determines contributing areas. As described previously, hillslopes can be separated into nine categories (Fig. 1) that consider planform and profile curvature and are hydrologically similar (Suzuki 1977 presented in Tsukamoto and Ohta 1988, Aryal et al. 2002). The planform shape of these nine types indicates whether flow paths should converge, diverge, or run parallel to one another. The profile shape indicates how rapidly the rate of change in topographic index of each of these categories should occur.

The frequency distribution of hillslopes in the nine groups (Fig. 7) is similar for each of the three landscapes. Convergent-concave and divergent-concave hillslope types are the most common hillslope types in all three landscapes. Convergent-concave hillslopes are the dominant hillslope type at first-order channels, the most common channel order. Divergent-concave hillslopes are the second most common hillslope type found alongside first-order channels in the overland flow- and landslide-dominated

29
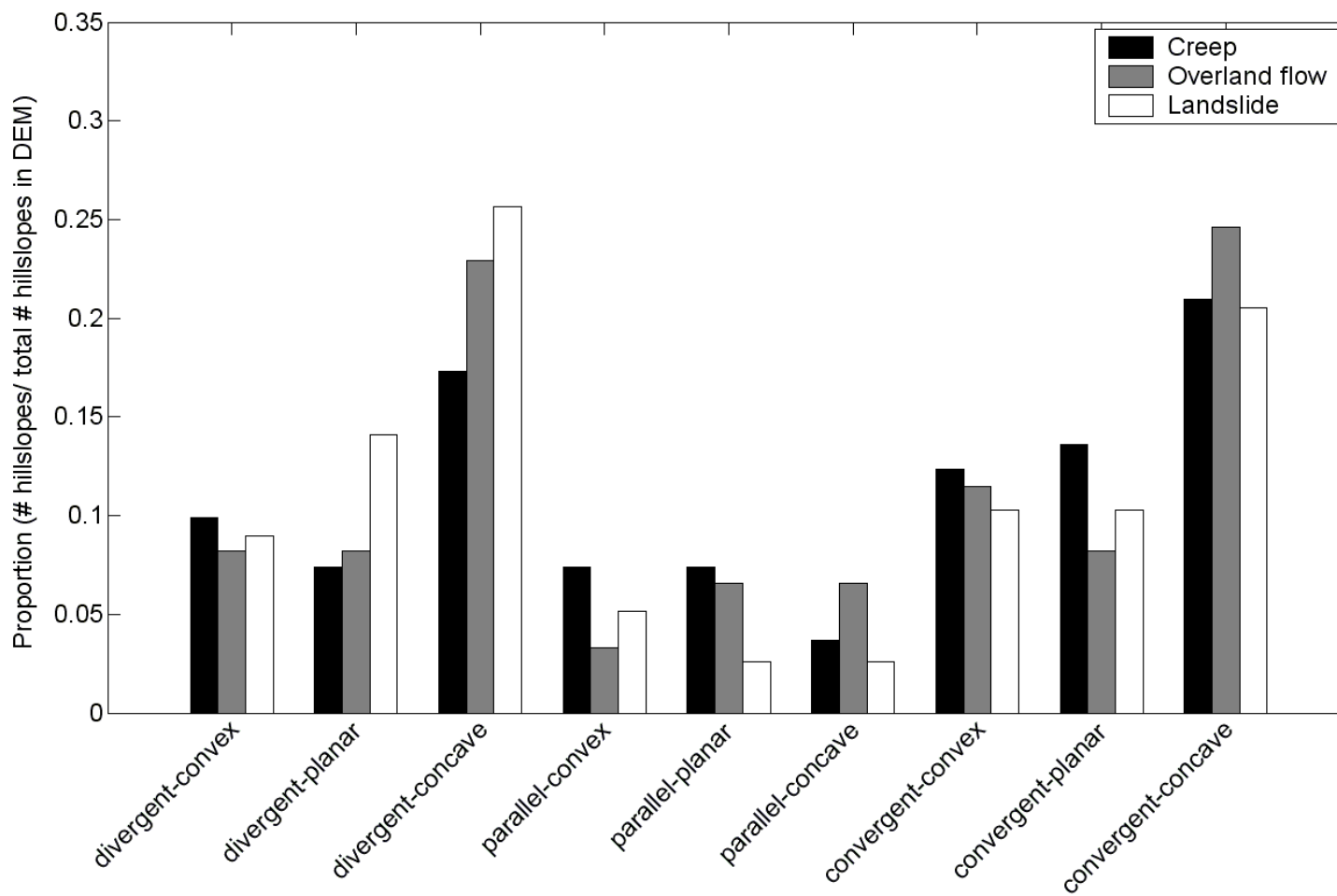
Figure 7. Proportion of each hillslope type in each of the three landscapes.

landscapes. Divergent-concave hillslopes are the dominant hillslope type at second-order channels for all three landscapes.

Up to this point it has been shown that all landscapes share the same basic structure but have unique signatures due to different geomorphic processes of uplift and erosion. In the last section nine hillslope types were introduced that show how the flow of water should move.

Transects

Since plant abundance is determined by soil moisture, in this section traditional approaches to determining moisture gradients and species tolerances curves using 1-dimensional transects will be taken in each of the nine hillslope categories along with the topographic indexes along the transects as the moisture gradient. It is expected that the topographic index will decrease from the channel towards the ridgeline.

The channel to ridgeline transects (Fig. 8) gave topographic index values that were variable, but tended to decrease as distance from the channel increased for all three landscapes. However on several transects the topographic index values increased and decreased repeatedly along the length of the transect (i.e. did not consistently decrease). The nine hillslope categories did not yield any patterns in the topographic index for any of the three landscapes (Appendix A). The mean length of the transects for the creep-dominated landscapes was 162.8 m (+/- 11.2 m), for the overland flow-dominated landscape was 160.2 m (+/- 10.8 m), and for the landslide-dominated landscape was 170.5 m (+/- 11.4 m).

One reason the channel to ridgeline transects had variable topographic index values with distance from the channel is because they do not always follow the flow

31
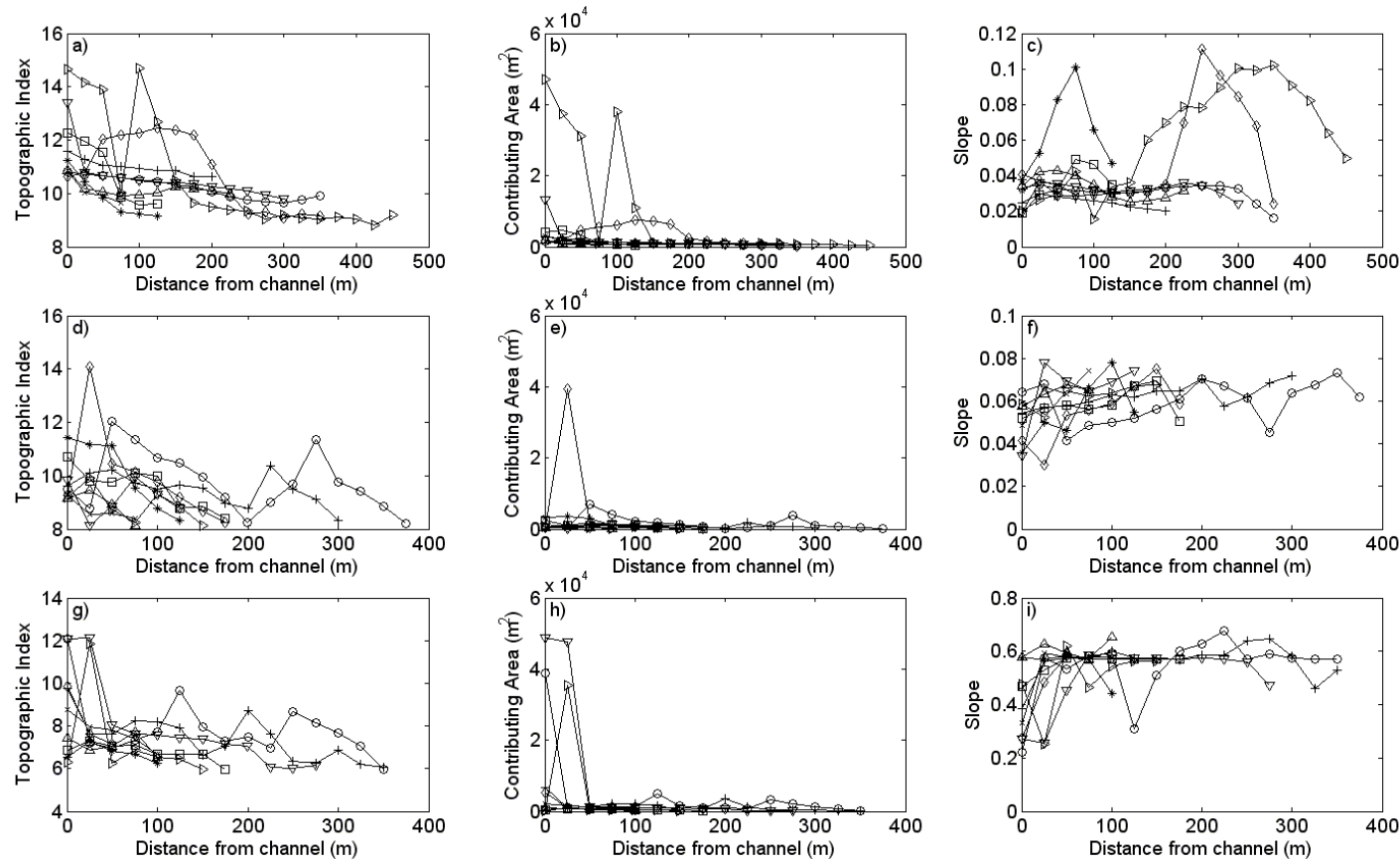
Figure 8. Channel to ridgeline transects topographic index, contributing area, and slope as a function of distance from the channel for nine hillslopes (one of each hillslope type) for the a) - c) creep-dominated landscape, d) - f) overland flow-dominated landscape, and g) – i) landslide-dominated landscape. Plus signs represent divergent-convex hillslope transects, circles represent divergent-planar, an asterisk represents divergent-concave, x's represent parallel-convex, squares represent parallel-planar, diamonds represent parallel-concave, upward triangles represent convergent-convex, downward triangles represent convergent-planar, and right pointing triangles represent convergent-concave hillslope transect

32

paths of water down slopes (Fig. 9). For example, a transect may have intercepted a region where the flow of water is largely parallel or divergent, resulting in a low contributing area, and then further upslope intercepted a region where several flow paths converged, resulting in a high contributing area (Fig. 8). This may have resulted in a lower topographic index closer to the channel than at a point closer to the ridgeline. Variable slope gradients (Fig. 8) also contributed to fluctuations in the index by a similar argument.

The steepest ascent transects gave topographic index values (Fig. 10) which were mid to low values for the first couple hundred meters from the channel, and lower values after that point. While it is difficult to identify individual transects within these plots, it is apparent that the variability in topographic index value along transects is diminished in comparison to that apparent in the channel to ridgeline transects. Similar to the channel to ridgeline method, the topographic index of most of the transects increased and decreased over the first couple hundred meters, but then tended to level out around low index values. Separating transects into the nine hillslope categories did not yield any patterns among hillslope types. The mean length of transects for the creep-dominated landscape was 921.0 m (+/- 55.6 m), for the overland flow- dominated landscape was 518.3 m (+/- 29.9 m), and for the landslide-dominated landscape was 466.6 m (+/- 25.4 m).

The steepest ascent transects (Fig. 10) tended to have low topographic index values along most of their distance because the path of steepest ascent was not likely to be the same as the path of steepest descent that water tends to follow (see flow lines in Fig. 9). Flow paths tend to follow directions of steepest descent and, in areas of

Figure 9. The three different types of transects on a hillslope of the creep-dominated landscape. The different shaded regions indicate different hillslopes. The white grid cells represent the channel network. Although the topographic index was calculated using contributing areas based on a dinf flow routing scheme, the d8 (path of steepest descent, and direction most of the flow will follow) flow lines are depicted as thin grey lines instead for the sake of simplicity.
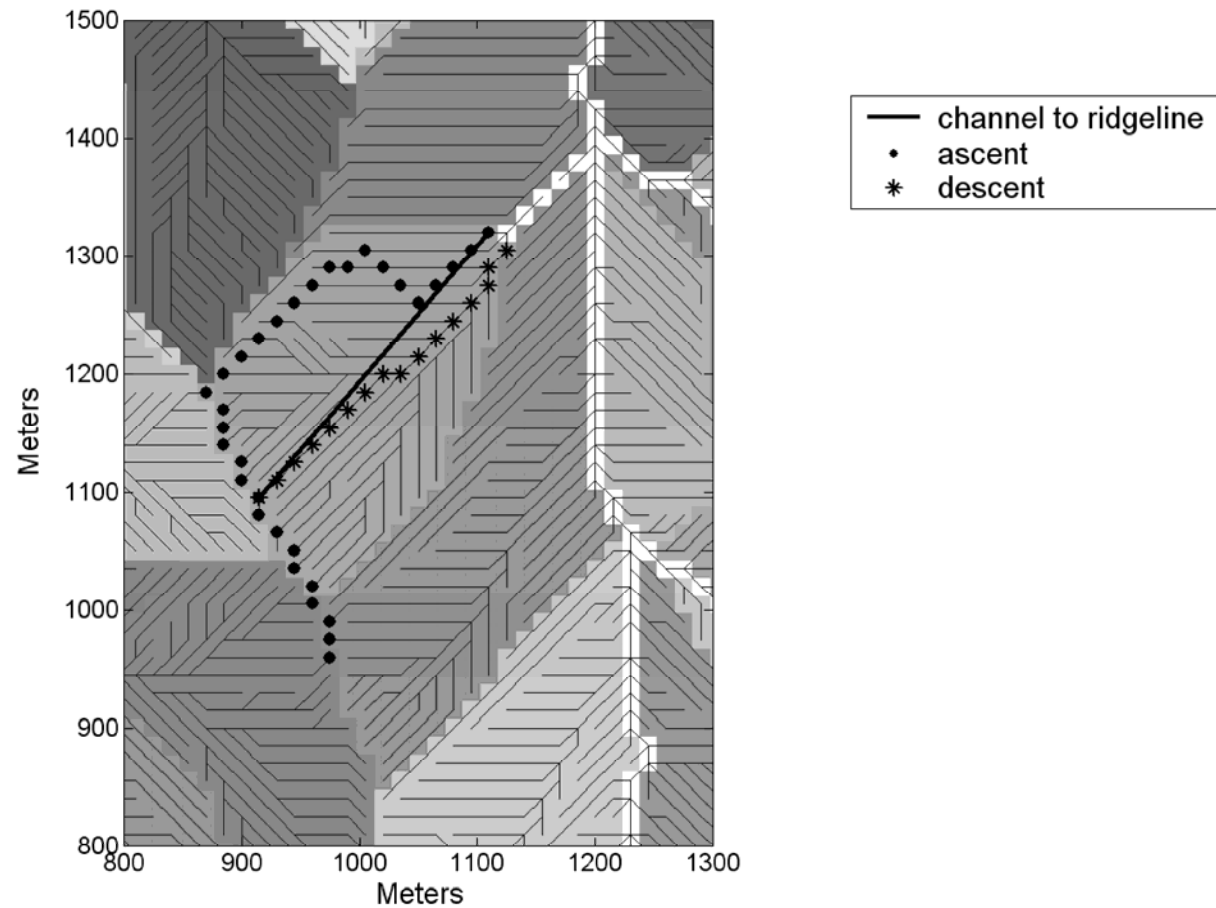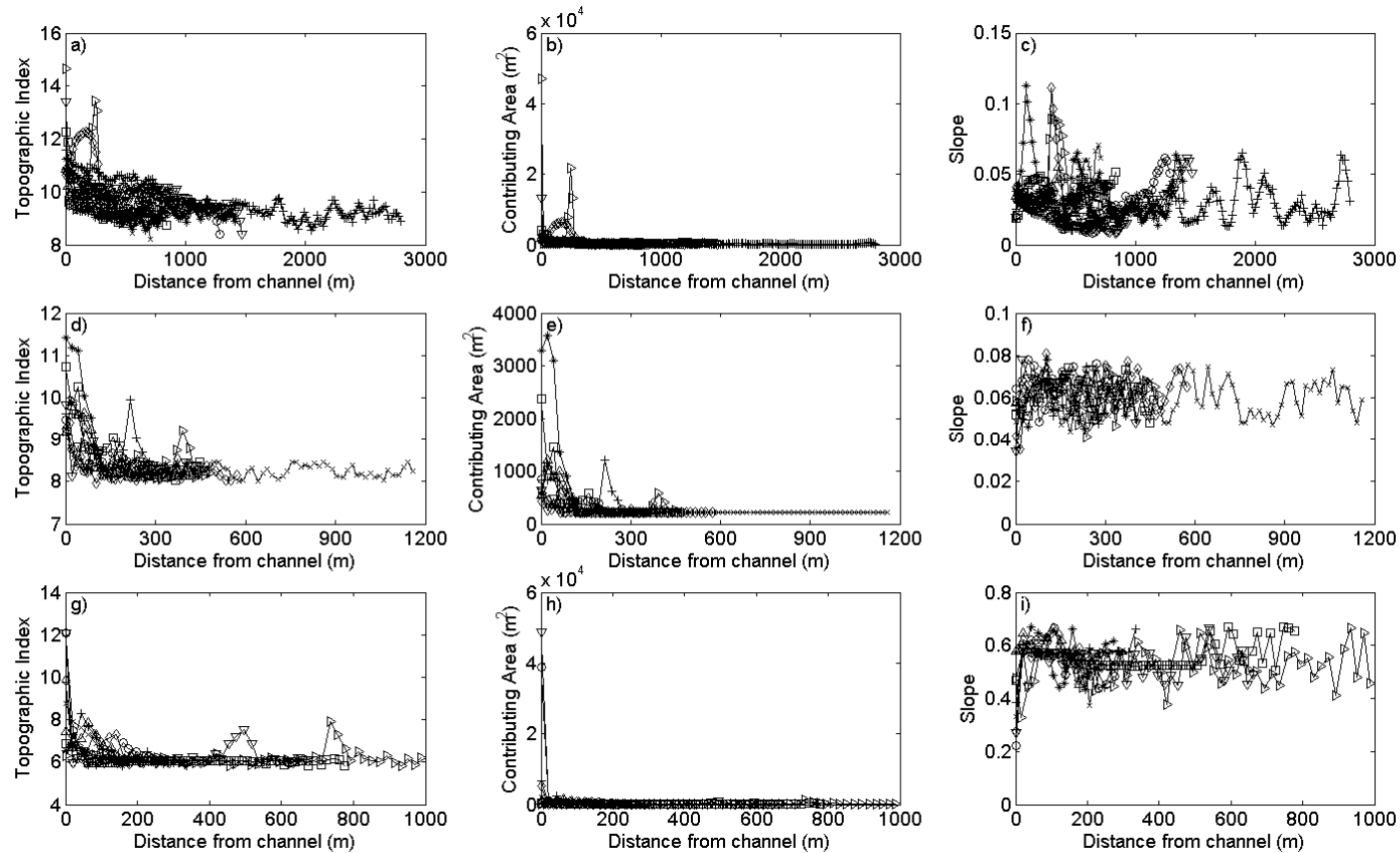
Figure 10. Ascent transects topographic index, contributing area, and slope as a function of distance from the channel for nine hillslopes (one of each hillslope type) for the a) - c) creep-dominated landscape, d) - f) overland flow-dominated landscape, and g) - i) landslide-dominated landscape. Plus signs represent divergent-convex hillslope transects, circles represent divergent-planar, an asterisk represents divergent-concave, x's represent parallel-convex, squares represent parallel-planar, diamonds represent parallel-concave, upward triangles represent convergent-convex, downward triangles represent convergent-planar, and right pointing triangles represent convergent-concave hillslope transects.

convergence, will accumulate in regions of low elevation. Taking a path of steepest ascent tends to avoid these regions because, while descent seeks out low elevation values, ascent seeks out high elevations. Therefore the contributing areas at points along a path of steepest ascent tend to be low. Slope gradients were also variable (Fig. 10) and contributed to fluctuations in the index.

The steepest descent transects (Fig. 11) tended to show an increase in the topographic index in a concave upward pattern as the distance to the channel decreased along transects on all three landscapes. Some of the transects did have increases and decreases in the topographic index, but these oscillations were not as pronounced as in the other two transect methods. The mean length of transects for the creep-dominated landscape were 188.8 m (+/- 11.9 m), for the overland flow dominated landscape was 175.5 m (+/- 12.4 m), and for the landslide-dominated landscape was 181.8 m (+/- 13 m).

The steepest descent transects tended to increase in a convex form from the ridgeline to the channel because these transects considered the flow paths of water (Fig. 9). However, these transects also had some increases and decreases in the topographic index. This was due in part to variable slope gradients , and also to divergent flow (Fig. 11).

It has been shown that the different structures of landscapes resulted in different patterns of the topographic index and values and rates of change of the index along transects. The transect method of steepest descent tended to have the least amount of increases and decreases in the topographic index because the method tended to follow flow lines.
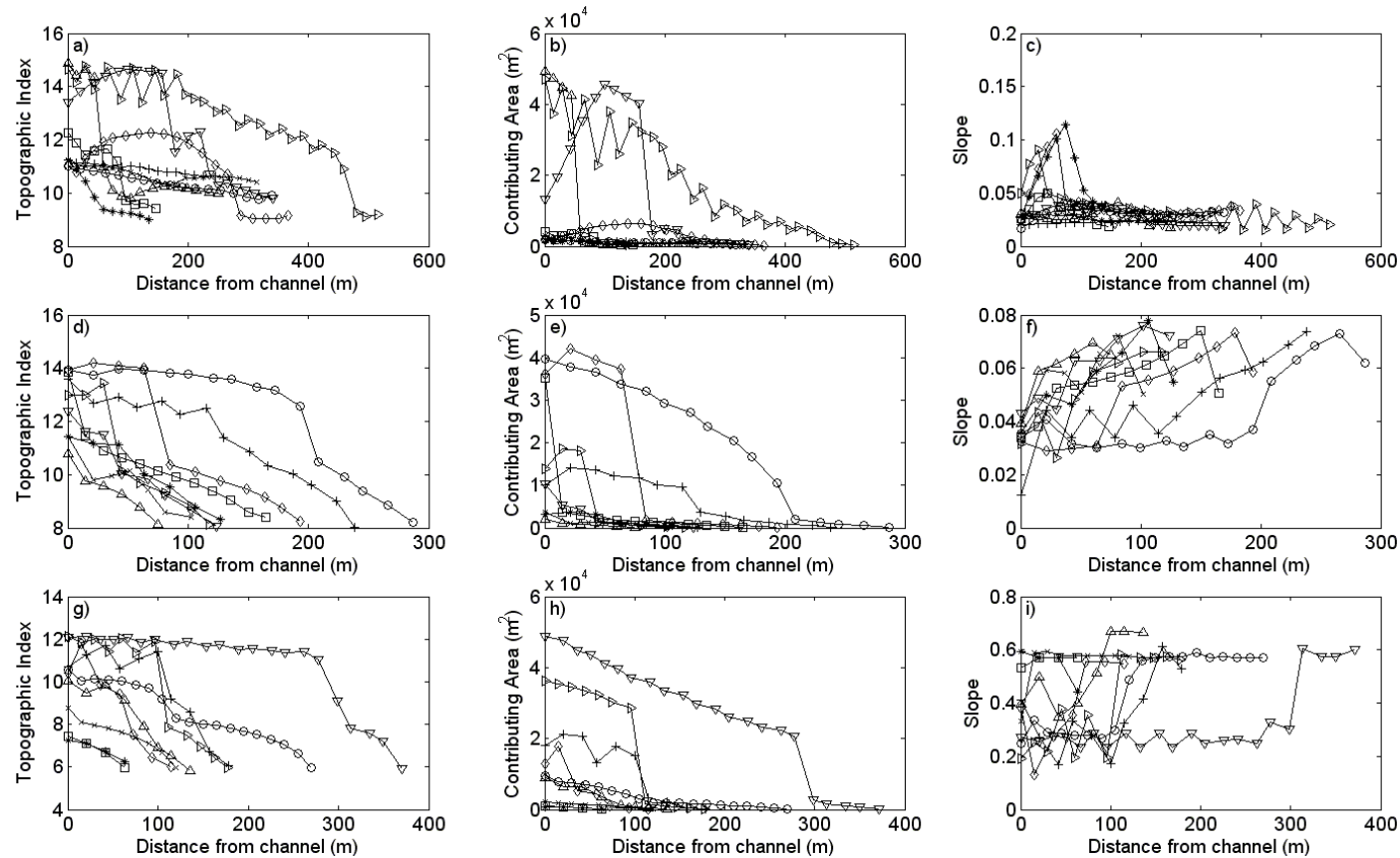
Figure 11. Descent transects topographic index, contributing area, and slope as a function of distance from the channel for nine hillslopes (one of each hillslope type) for the a) - c) creep-dominated landscape, d) - f) overland flow-dominated landscape, and g) - i) landslide-dominated landscape. Plus signs represent divergent-convex hillslope transects, circles represent divergent-planar, an asterisk represents divergent-concave, x's represent parallel-convex, squares represent parallel-planar, diamonds represent parallel-concave, upward triangles represent convergent-convex, downward triangles represent convergent-planar, and right pointing triangles represent convergent-concave hillslope transects.

37

I will next show a) how the shapes of the different landscapes influence plant distribution by placing the designed plant on the landscapes according to the topographic index, and b) how the different transect methods affect the shape of the resulting plant tolerance curves.

Plant Distribution

A designed plant with a mesic distribution of tolerance (Fig. 2) is abundant on and near ridges of the creep-dominated landscape (Fig. 12); however, its numbers rapidly decline downslope towards the channels. On the overland flow-dominated landscape the mesic tolerant plant is widely distributed with intermediate abundance on the ridges, high abundance below the ridges, and intermediate to low abundance further downslope. On the landslide-dominated landscape the plant is least common and is absent from ridges, usually appearing in a narrow band part way down the hillslopes.

The accuracy of the three transect methods should be reflected in how well they can reproduce the tolerance curve of Fig. 2. The channel to ridgeline transect method resulted in plant tolerance curves that were variable for each transect (Fig. 13). Ranges, maximum abundance, modes, and degree of modality all varied between transects. Normalizing transect distances by total transect distance did little to resolve the variation. For the nine hillslope types and the three landscapes when transects were combined and abundances binned by distance, defining bin width by the square root of sample size, modes, and degree of modality of the average tolerance curve also varied. Curves remained at mid to high values for the convergent-convex and convergent-planar slopes of the creep-dominated and several of the overland flow dominated hillslope categories (see also Appendix B). Several of the creep-dominated and overland flow-dominated

38
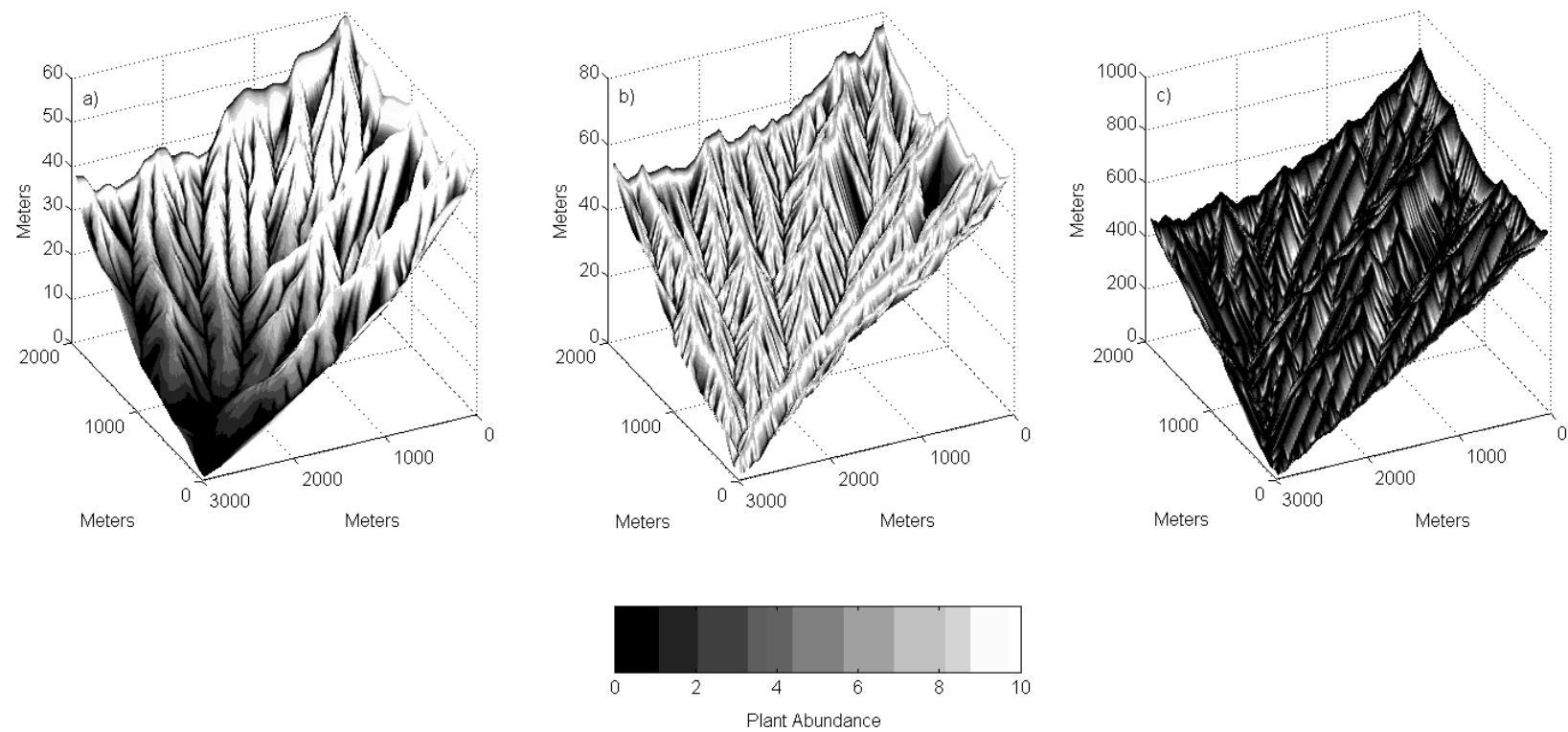
Figure 12. Distributions of a mesic tolerant plant (Fig. 2) on each of the three landscapes; a) creep-dominated, b) overland flow-dominated, and c) the landslide-dominated landscape.
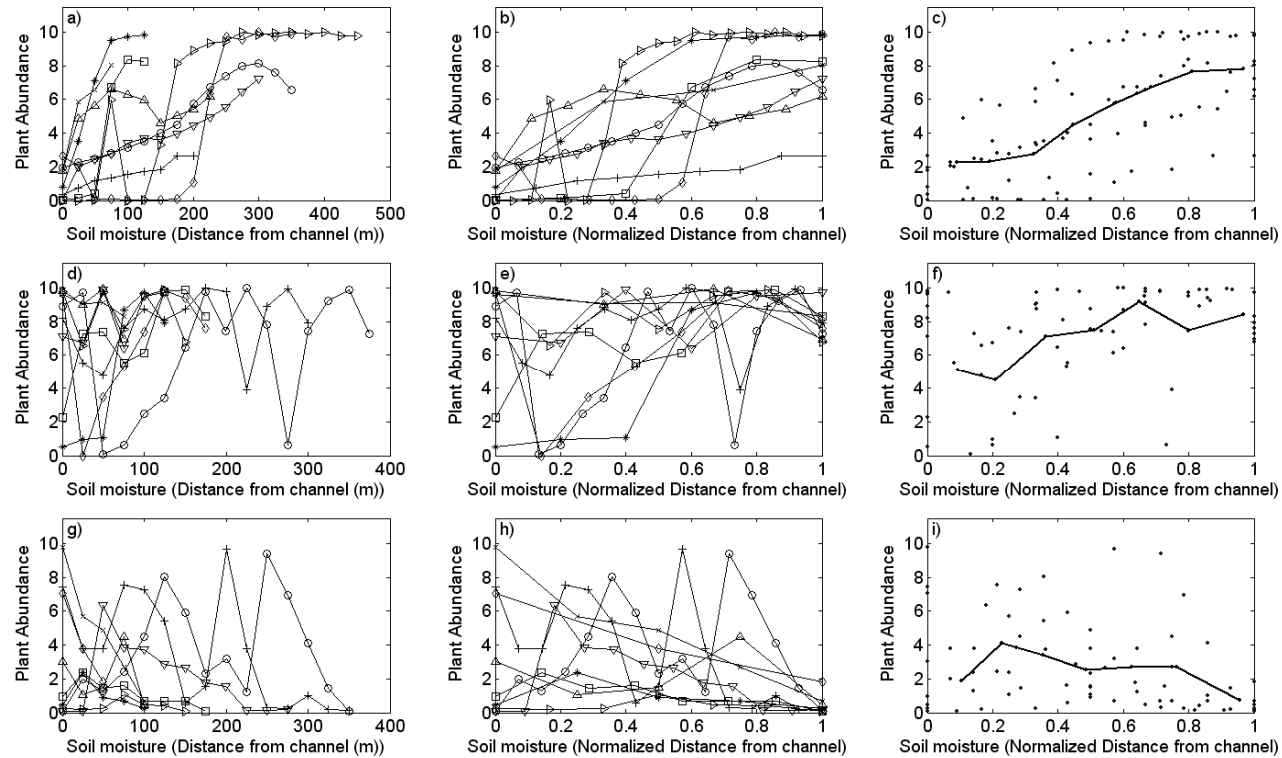
Figure 13. Channel to ridgeline transects mesic plant tolerance curves (Fig. 2) for one of each of the nine hillslope types where soil moisture is approximated by distance from the channel (wet) to the ridgeline (dry), normalized distance, and by binning by distance for the a) - c) creep-dominated landscape, d) - f) overland flow-dominated landscape, and g) - i) landslide-dominated landscape. Plus signs represent divergent-convex hillslope transects, circles represent divergent-planar, an asterisk represents divergent-concave, x's represent parallel-convex, squares represent parallel-planar, diamonds represent parallel-concave, upward triangles represent convergent-convex, downward triangles represent convergent-planar, and right pointing triangles represent convergent-concave hillslope transects. The solid line in c), f), and i) indicates the mean obtained from binning using all data points (shown as dots) for the nine transects.

40

curves suggest only part of the species range was sampled. The peak abundances of the

plant on the landslide-dominated landscape tended to be lower than those of the other two

landscapes.

Tolerance curves obtained from the steepest ascent transects (Fig. 14a, d, g)

tended to have values that oscillated around mid to high abundance for the mesic plant

species over several hundred meters for the overland flow- and creep-dominated

landscapes. The tolerance curves of the landslide-dominated landscape did not oscillate

around mid to high abundances. Instead, tolerance curves indicated unimodal to

multimodal distributions with variable ranges and skews and the plant was absent or had

abundance near zero from many of the points sampled. Normalization of distance (Fig.

14b, e, h) failed to resolve much of the variation in the curves for the three landscapes.

Tolerance curves obtained by binning distance values for each of the nine hillslope types

tended to indicate unimodal curves for the creep-dominated landscape (Fig. 14c). The

curves of the overland flow-dominated landscape remained at mid to high values across

the entire gradient (Fig. 14f). The landslide-dominated landscape tended to have

consistently low values of plant abundance along the gradient (Fig. 14i) (see also

Appendix B).

The tolerance curves obtained using the path of steepest descent method (Fig. 15)

suggested that only half the range was sampled on transects from each of the nine

hillslope types for both the landscape dominated by creep (Fig. 15a) and the one

dominated by overland flow (Fig. 15d). Ranges varied from transect to transect, as did

the position of the mode, which was located near the ridge (dry end of the gradient) for

all tolerance curves (Fig. 15a, d, g). The peak abundance for each curve was
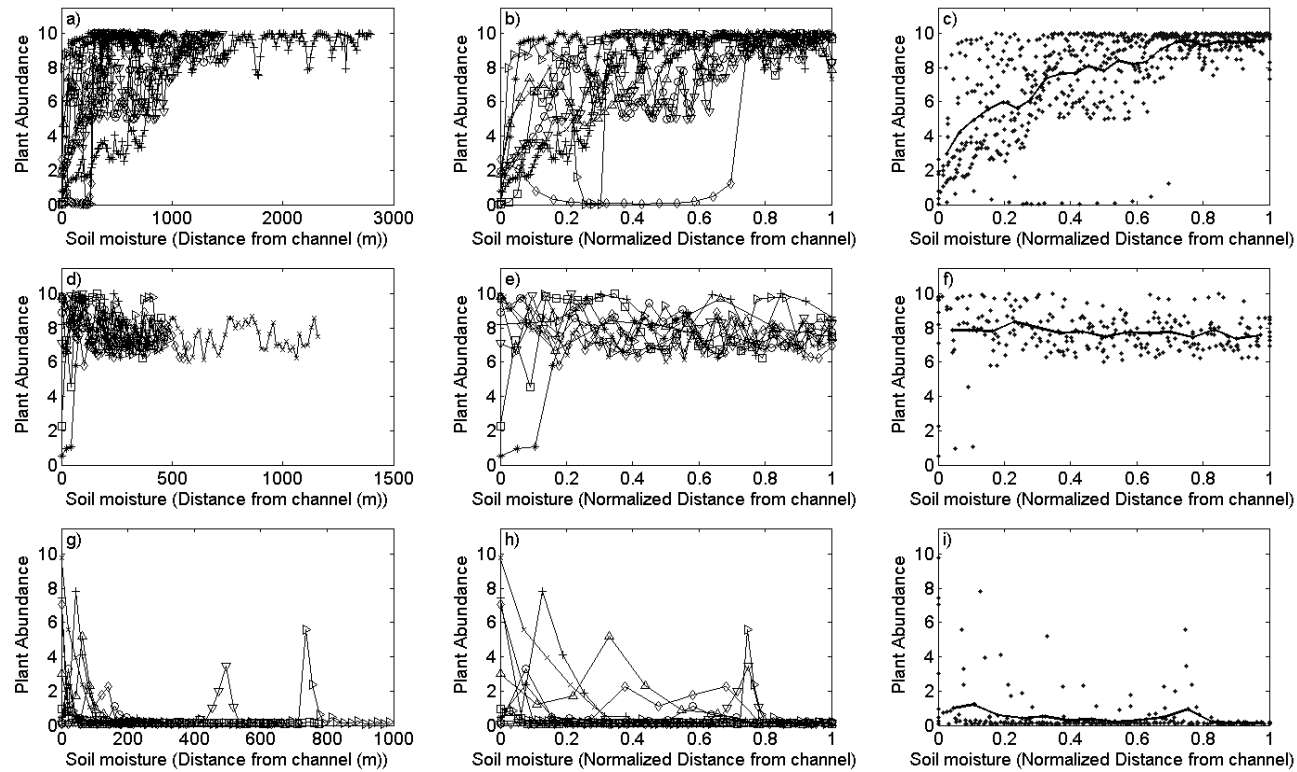
Figure 14. Ascent transects mesic plant tolerance curves (Fig. 2) for one of each of the nine hillslope types where soil moisture is approximated by distance from the channel (wet) to the ridgeline (dry), normalized distance, and by binning by distance for the a) - c) creep-dominated landscape, d) - f) overland flow-dominated landscape, and g) - i) landslide-dominated landscape. Plus signs represent divergent-convex hillslope transects, circles represent divergent-planar, an asterisk represents divergent-concave, x's represent parallel-convex, squares represent parallel-planar, diamonds represent parallel-concave, upward triangles represent convergent-convex, downward triangles represent convergent-planar, and right pointing triangles represent convergent-concave hillslope transects. The solid line in c), f), and i) indicates the mean obtained from binning using all data points (shown as dots) for the nine transects.
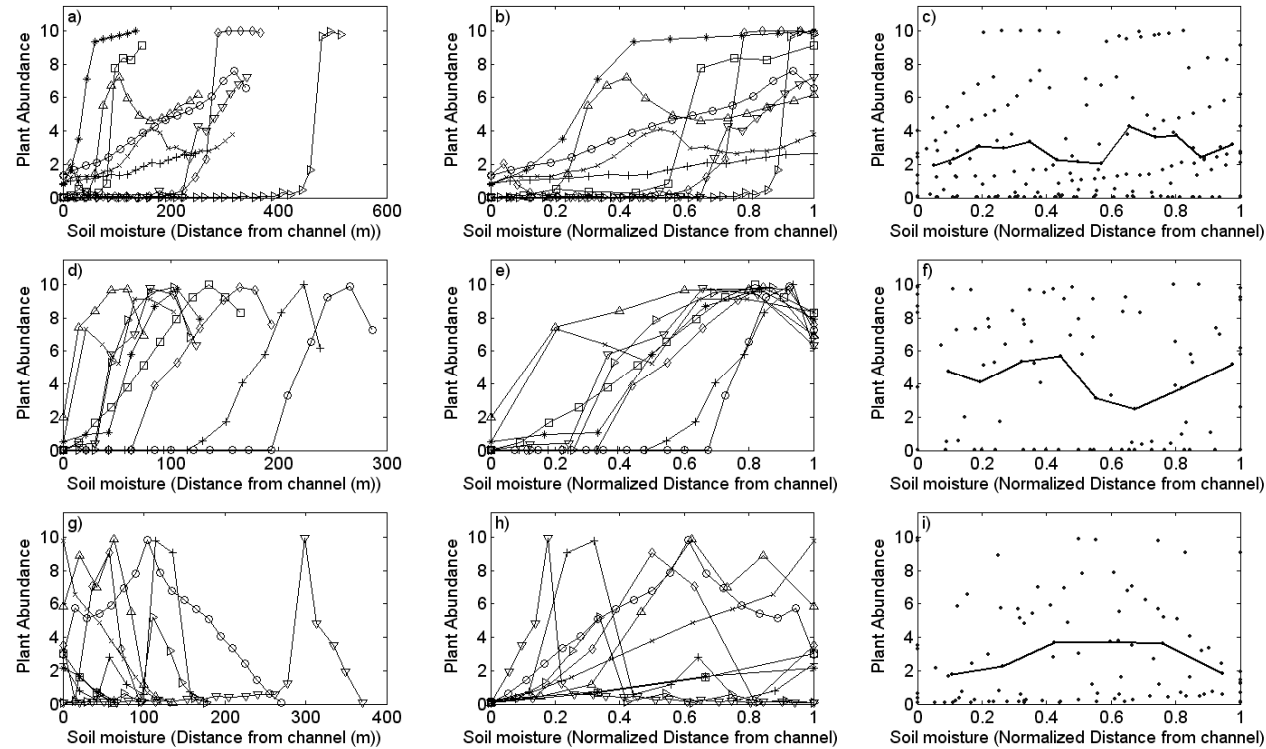
42

Figure 15. Descent transects mesic plant tolerance curves (Fig. 2) for one of each of the nine hillslope types where soil moisture is approximated by distance from the channel (wet) to the ridgeline (dry), normalized distance, and by binning by distance for the a) - c) creep-dominated landscape, d) - f) overland flow-dominated landscape, and g) - i) landslide-dominated landscape. Plus signs represent divergent-convex hillslope transects, circles represent divergent-planar, an asterisk represents divergent-concave, x's represent parallel-convex, squares represent parallel-planar, diamonds represent parallel-concave, upward triangles represent convergent-convex, downward triangles represent convergent-planar, and right pointing triangles represent convergent-concave hillslope transects. The solid line in c), f), and i) indicates the mean obtained from binning using all data points (shown as dots) for the nine transects.

approximately 10 individuals. Distance normalization did not resolve much of the variation in transects for the three landscapes (Fig. 15b, e, h). Binning resulted in variable modes, modality, and skew for all three landscapes with mid to low peak abundances (Fig. 15c, f, i) (see also Appendix B).

The tolerance curves obtained from the path of steepest descent on the landslide-dominated landscape were more variable than for the other two landscapes. Peak abundances reached approximately 10 on several transects, and the mode region tended to be closer to the ridgeline than the channel. However, several transects indicated the tolerance curves were multimodal, while other transects indicated unimodal tolerance curves. Some curves indicated minimal, if any, skew, while others indicated indicated right or left skews (Appendix B).

Lastly, plant abundance was plotted as a function of the topographic index rather than distance (Fig. 16). This gave symmetrical, unimodal, complete or partial curves, depending on the topographic index values found on each transect.

Discussion

The objectives of this study were to assess the ability of different transect methods to construct gradients for plant tolerance curves and the usefulness of plant tolerance curves to describe abundance and distribution of plants on a landscape. A landscape evolution model (CHILD) was used to simulate three landscapes that differed in dominant geomorphic process: 1) creep, 2) overland flow, and 3) pore-pressure landsliding. The geomorphic processes incorporated in landscape evolution models are well studied, and visual comparisons of DEM's and slope-area plots produced by simulated landscapes to actual landscapes indicate that these processes are appropriately represented in modelling
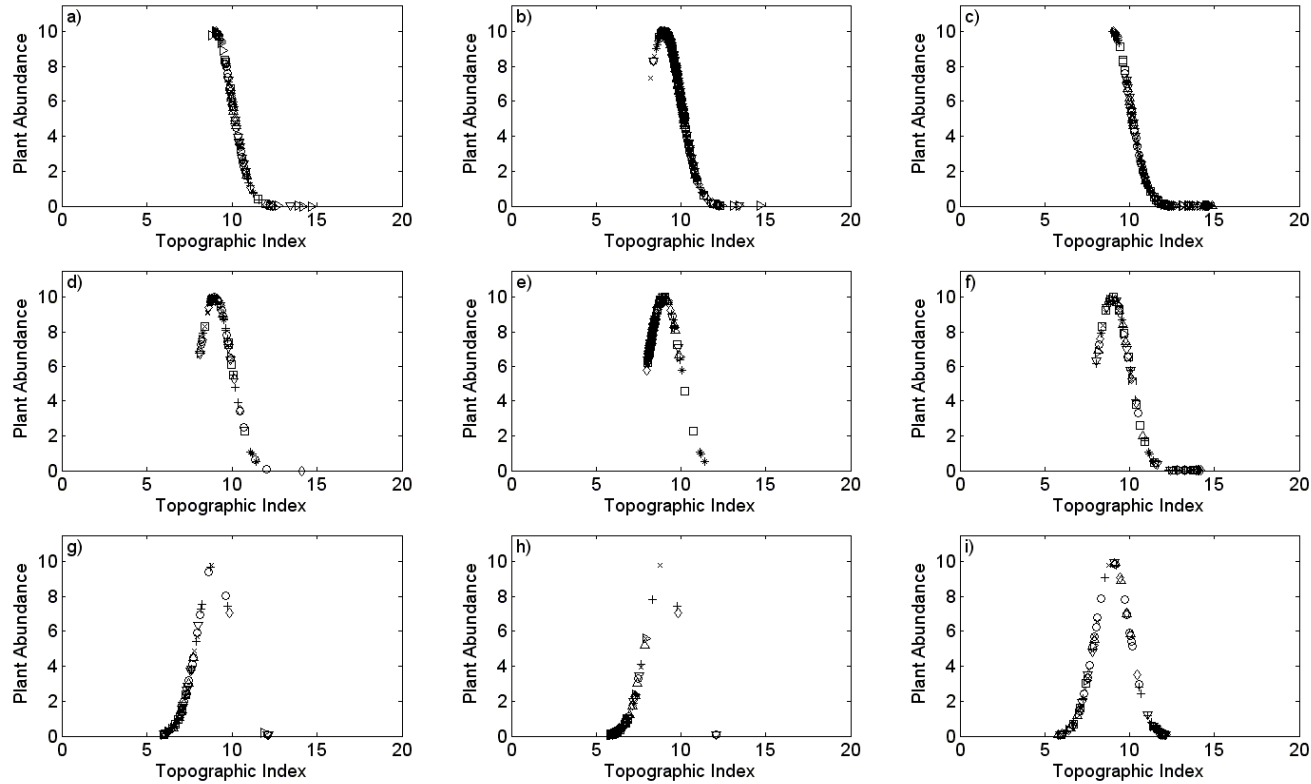
Figure 16. Mesic plant tolerance curves (Fig. 2) for one of each of the nine hillslope types when the topographic index is plotted against plant abundance for the channel to ridgeline (left), ascent (middle), and descent (right) methods for the a) - c) creep-dominated landscape, d) - f) overland flow-dominated landscape, and g) - i) landslide-dominated landscape. Plus signs represent divergent-convex hillslope transects, circles represent divergent-planar, an asterisk represents divergent-concave, x's represent parallel-convex, squares represent parallel-planar, diamonds represent parallel-concave, upward triangles represent convergent-convex, downward triangles represent convergent-planar, and right pointing triangles represent convergent-concave hillslope transects.

45

studies (e.g., Willgoose 1994, Tucker and Bras 1998). The advantage to the use of a landscape evolution model over an actual DEM was the ability to control parameters and relate known processes incorporated in the model to the shape of the resultant landscape as indicated in both the DEM and slope-area plots (Figs. 3, 4, and 5). The characteristic signatures of the different landscape processes that dominated each landscape were evident in the DEMs and slope-area plots. However, it is important to notice a marked characteristic in all slope-area curves, either in actual landscapes (Montgomery and Dietrich 1988, McNamara et al. 2006) or in simulated landscapes (Willgoose et al. 1991a, Tucker and Bras 1998, Fig. 3b, 4b, 5b): there is a large variation in slope at a particular watershed size. Thus, although the 2-dimensional plot of slope and area captures the principal processes occurring in the landscapes, more variables are needed to explain all the variation.

In order to deal with this more 3-dimensional importance in landscape moisture distribution, I have used a topographic index that defines hydrologically similar points (Kirkby 1975). It does this by making simple assumptions (see Landscape Organization) about water flow on hillslopes that allow the index to both take into account the 3-dimensional flow of water on the landscape and compare points with the same index on one landscape and between landscapes. This is particularly useful to ecologists because it indicates where plants will be found as their distribution and abundance pertains solely to soil moisture.

The 3-dimensional structures of landscapes influence the topographic index (and therefore soil moisture) through both contributing area and slope gradient. Landscapes have regions of convexity and flow path divergence and concavity and flow path

convergence, which along with hillslope length, determine contributing areas. Furthermore, curvature means that slope gradients are not constant. The advantage of the topographic index is that it accounts for this 3-dimensional structure and its control on water.

The shape of the distribution of the topographic index was similar for all three landscapes (Fig. 6), due to the common structure shared by all landscapes: ridgelines, hillslopes, and channels. The driest regions of each landscape were the ridgelines, and the topographic index tended to increase on hillslopes towards the channels (Figs. 3a, 4a, and 5a). However, the mean, median, and range of the topographic index differed for each landscape.

The landslide-dominated landscape was the driest of the three landscapes and the creep-dominated landscape was the wettest. The lower topographic index values on the landslide-dominated landscape are due to steeper slopes than the other two landscapes. The higher topographic index values of the creep-dominated landscape are attributable to both lower slope gradients and greater median contributing area than the other two landscapes. Although the creep-dominated landscape has convex hilltops and therefore greater divergence than the other landscapes, the mean length of the steepest descent transects (i.e. those that followed flow paths) were longer and was likely the cause of the greater median contributing area. Thus, hillslope points near the channel were driest on the landslide-dominated landscape, wetter on the overland flow-dominated landscape, and wettest on the creep-dominated landscape. The same pattern applied to hillslopes and ridgelines of the three landscapes.

47

Soil moisture was sampled using transects laid from channel to ridgeline, a method used by some ecologists to generate gradients for plant tolerance curves (Whittaker 1956, Racine 1971), an approach that is comparable to categorical methods also used (Whittaker 1956, 1960, 1967). It has been shown that transects from channel to ridgeline do not consider landscape curvature or hillslope length and therefore do not give consistent moisture gradients. These transects often intersect flow paths that have converged and/or diverged with other paths, each of varying lengths, and, as a result, soil moisture along them is likely to fluctuate in a non-linear way (Figs. 8 and 9). A path of steepest ascent was also shown to inconsistently define the moisture gradient because it preferentially seeks out high elevations whereas flow paths seek out low elevations (Figs. 9 and 10).

Transects taken using a path of steepest descent do follow flow paths, and therefore contributing area tended to increase towards the channel and gave more consistent moisture gradients than the other two transect methods. As a result, moisture gradients obtained by steepest descent transects were not as variable. However, flow path divergence means that contributing area can decrease as well as increase along one flow path towards the channel and potentially cause decreases in soil moisture. Furthermore, slope gradient is also variable, adding to fluctuations in soil moisture (Figs. 3b, 4b, 5b, and Appendix A).

Studies sometimes average transects or categories to construct tolerance curves (Whittaker 1967). For transects, this assumes that soil moisture values are comparable at similar distances upslope. However, variable hillslope lengths, curvature, and slope gradients make this unlikely. For example, consider transects taken on two hillslopes with

parallel flow and equal slope gradients but different lengths. Topographic index values will differ at the same distance from the channel because one hillslope has a greater contributing area to that point than the other. Alternatively two hillslopes with parallel flow and same lengths but different slope gradients will differ in their ability to hold water and therefore will also differ in their topographic indexes. Furthermore, rates of change of the topographic index along transects in the above examples will differ. Convergence, divergence, and variable slope gradients on hillslopes may introduce further variation. As a result, it is very unlikely that conditions would be such that transects from two different hillslopes could be considered to have equal representations of the environmental gradient. Normalizing transects does little to resolve this variation (Figs. 13, 14, and 15).

As a consequence of different topographic index values and rates of change of the values along transects, plant tolerance curves differed from transect to transect for all three transect methods (Figs. 13, 14, and 15). However, the steepest descent method did tend to produce tolerance curves most similar to the original curve (Fig. 2) distributed on the landscapes. Where the topographic index fluctuated, so too did plant abundance, and multimodality resulted in the tolerance curves. Different index values on different transects but at the same distance from the channel resulted in different modes (Figs. 8,10, 11, 13, 14, and 15). Furthermore, different rates of change of the topographic index influenced skew in the tolerance curves (Figs. 8,10, 11, 13, 14, and 15).

The most notable effect the three different landscapes had on the tolerance curves was through the range of the topographic index represented on each landscape. The landslide-dominated landscape had the lowest topographic index values of the three

49

landscapes (Fig. 6), and covered the full range of values for which the mesic plant species occurred. The overland flow dominated landscape was wetter than the landslide-dominated landscape, and lacked the driest values of the mesic species range. The creep-dominated landscape, the wettest of the three, had only the wetter half of the mesic species range. This resulted in complete tolerance curves on the landslide-dominated landscape (Fig. 16g, h, i), nearly complete curves on the overland flow dominated landscape (Fig. 16d, e, f), and partial curves for the creep-dominated landscape (Fig. 16a, b, c).

A mesic plant was used in the present study; however, the conclusions are applicable to all plant types. Since plant abundance is primarily determined by soil moisture (e.g., Curtis and McIntosh 1951, Whittaker 1956, Waring and Major 1964, Bridge and Johnson 2000, Zinko et al. 2005, and many others), the location of any plant will be dependent in part on the structure of the landscape as determined by the geomorphic processes that played a role in its development. Using transects or categories will result in tolerance curves that have variable modes, ranges, and skew from one transect to the next because the 1-dimensional definition of the soil moisture gradient is inconsistent with the processes of water movement. Since soil moisture is determined by processes that act in 3-dimensions, a similarity index such as the topographic index should result in better agreement of tolerance curves than traditional 1-dimensional transects or categories when extended to actual landscapes.

In order to accurately define plant tolerance curves, we must first accurately define and understand the gradient. While sampling via transects that define the soil moisture gradient by distance from channel and lumping them together will provide a

50

tolerance curve, the curve is unlikely to apply in a different landscape. For example, the complete curves from the landslide-dominated landscape will not accurately predict the plant's distribution and abundance on the runoff or creep-dominated landscapes if the same assumptions of decrease in moisture from channel to ridgeline are applied because these two landscapes are not as dry. The differences in the soil moisture patterns on these landscapes are due to the different imprints on the landscapes created by the differing dominant geomorphic processes.

We should seek to understand the processes creating the gradient. The moisture gradient is not simply wet to dry from channel to ridge because water moves downhill. Landscapes are complex structures and hillslope curvature and lengths dependent on geomorphic processes dictate where water will collect and how much, while slope gradient will dictate the capacity for water to remain at any one point. Defining the gradient by using a topographic index that considers these variations makes sites directly comparable, that are not so using transect or categorical methods.

In the geomorphological literature efforts are being made to understand the link between vegetation and geomorphic processes. Vegetation provides added resistance to erosion (e.g., Thornes 1990) and has been incorporated into CHILD in terms of growth and removal impacting the critical shear stress for erosion (Collins et al. 2004). By increasing the critical shear stress necessary for erosion, vegetation results in landscapes of greater relief that are steeper and have lower drainage densities (i.e. longer hillslopes) (Collins et al. 2004).

When vegetation is incorporated into the diffusion equation for soil creep, inhibiting the rate of movement, and pore-pressure landsliding is a dominant process,

51

hillslopes steepen and a lower contributing area is necessary for failure, resulting in

greater channel initiation and drainage density (Istanbulluoglu and Bras 2005). As in the

present simulations, landscapes with less vegetation tend to be overland flow-dominated.

Disturbances by overland flow, landsliding and fires that remove vegetation increase

drainage density by increasing the ability of effective shear stress to overcome critical

shear stress and decrease relief as opposed to situations where vegetation remains

constant (Istanbulluoglu and Bras 2005).

Taking the development of vegetation a step further, vegetation was recently

incorporated into CHILD (not present in the version used in this study) in terms of

logistic population growth (Collins and Bras 2010). Growth rate is determined by relating

the vegetation's physiology, as represented by a single exponent, to soil moisture, as

approximated by an index that incorporates the topographical variables of slope and area,

as well as precipitation. In this case, an increase in precipitation in dry landscapes

increases vegetation and through an increase in critical shear stress, decreases drainage

density. However, in wet landscapes, the increase in precipitation does little to increase

vegetation, but does increase overland flow which subsequently decreases drainage

density (Collins and Bras 2010).

Collins and Bras (2010) do consider the effect of water stress on plant populations

as influenced by topography and landscape development, however, like the other studies

above, the focus is on the implications of vegetation in geomorphic processes and the

effects on landscape development. The implications of the landscape for plant

distribution and abundance have only been marginally considered to date. Hack and

Goodlett (1960) first implicated the role of topography in determining soil moisture via

contributing areas and related this to vegetation patterns. Zinko et al. (2005) more recently showed that the topographic index was related to plant species richness.

There is a clear relationship between topography and vegetation, and this has implications for plant species distributions, and communities. By taking a more interdisciplinary approach it is possible to better understand the process controls on plant communities and how these communities influence the shape of their landscapes.

Conclusion

Different geomorphic processes result in different patterns of slope gradients, hillslope lengths, and hillslope curvatures that create unique patterns of soil moisture. As a consequence of the controls of topography on soil moisture, plant abundance differs on landscapes with differing geomorphologies. Hillslopes within a landscape also have different lengths, curvatures, and slope gradients, and as a result, soil moisture sampled by transects that approximate soil moisture using distance are not directly comparable. While a transect method that considers the structure of topography and its influence on soil moisture defines the soil moisture gradient better than those that do not, transects are one dimensional and cannot fully represent the three dimensional structure of landscapes. Therefore, gradient methods using transects or categories will inconsistently define the soil moisture gradient and resultant plant tolerance curves will differ in shape. A similarity index that considers the shape of the landscape such as the topographic index of Kirkby (1975) allows for direct comparison of one location to another and best defines the soil moisture gradient.

REFERENCES

Anderson, R. S. 1994. Evolution of the Santa Cruz Mountains, California, through tectonic growth and geomorphic decay. Journal of Geophysical Research **99**:161-120.

Aryal, S. K., E. M. O'Loughlin, and R. G. Mein. 2002. A similarity approach to predict landscape saturation in catchments. Water Resources Research **38**:14.

Austin, M. P. 1987. Models for the analysis of species' response to environmental gradients. Vegetatio **69**:35-45.

Austin, M. P., R. B. Cunningham, and P. M. Fleming. 1984. New approaches to direct gradient analysis using environmental scalars and statistical curve-fitting procedures. Vegetatio **55**:11-27.

Benda, L., and T. Dunne. 1997. Stochastic forcing of sediment supply to channel networks from landsliding and debris flow. Water Resources Research **33**:2849-2863.

Beven, K., and J. Freer. 2001. A dynamic TOPMODEL. Hydrological Processes **15**:1993-2011.

Beven, K. J. 2001. Rainfall-Runoff Modelling - the Primer. John Wiley & Sons, West Sussex.

Black, T. A., and D. R. Montgomery. 1991. Sediment transport by burrowing mammals, Marin County, California. Earth Surface Processes and Landforms **16**:163-172.

Bogaart, P. W., and M. Guardiola. 2007. The hsB toolkit in MATLAB.

Bogaart, P. W., and P. A. Troch. 2006. Curvature distribution within hillslopes and catchments and its effect on the hydrological response. Hydrology and Earth System Sciences **10**:925-936.

Braun, J., and M. Sambridge. 1997. Modelling landscape evolution on geological time scales: a new method based on irregular spatial discretization. Basin Research **9**:27-52.

Bridge, S. R. J., and E. A. Johnson. 2000. Geomorphic Principles of Terrain Organization and Vegetation Gradients. Journal of Vegetation Science **11**:57-70.

Collins, D. B. G., and R. L. Bras. 2010. Climatic and ecological controls of equilibrium drainage density, relief, and channel concavity in dry lands. Water Resour. Res. **46**:W04508.

Collins, D. B. G., R. L. Bras, and G. E. Tucker. 2004. Modeling the effects of vegetation-erosion coupling on landscape evolution. Journal of Geophysical Research **109**:F03004.

Costa-Cabral, M. C., and S. J. Burges. 1994. Digital Elevation Model Networks (DEMON): A model of flow over hillslopes for computation of contributing and dispersal areas. Water Resources Research **30**:1681-1692.

Culling, W. E. H. 1960. Analytical theory of erosion. Journal of Geology **68**:336-344.

Culling, W. E. H. 1963. Soil Creep and the Development of Hillside Slopes. The Journal of Geology **71**:127-161.

Curtis, J. T., and R. P. McIntosh. 1951. An Upland Forest Continuum in the Prairie-Forest Border Region of Wisconsin. Ecology **32**:476-496.

Davis, W. M. 1892. The Convex Profile of Bad-Land Divides. Science **20**:245.

Davison, C. 1889. On the creep of the soil-cap through the action of frost. Geological Magazine **6**:255.

Dawes, W. R., and D. Short. 1994. The significance of topology for modeling the surface hydrology of fluvial landscapes. Water Resources Research **30**:1045-1055.

Dietrich, W. E., and D. R. Montgomery. 1998. Hillslopes, Channels, and Landscape Scale. Pages 30-60 *in* G. Sposito, editor. Scale Dependence and Scale Invariance in Hydrology. Cambridge University Press, New York.

Eagleson, P. S. 1978. Climate, Soil, and Vegetation .2. Distribution of Annual Precipitation Derived from Observed Storm Sequences. Water Resources Research **14**:713-721.

Fleming, R. W., and A. M. Johnson. 1975. Rates of seasonal creep of silty clay soil. Quarterly Journal of Engineering Geology **8**:1-29.

Gauch, H. G. J. 1982. Multivariate Analysis in Community Ecology. Cambridge University Press, Cambridge, UK.

Gilbert, G. K. 1909. The convexity of hilltops. The Journal of Geology **17**:344-350.

Grayson, R. B., A. W. Western, and F. H. S. Chiew. 1997. Preferred states in spatial soil moisture patterns: Local and nonlocal controls. Water Resources Research **33**:2897-2908.

Hack, J. T., and J. C. Goodlett. 1960. Geomorphology and forest ecology of a mountain region in the central Appalachians. U. S. Geological Survey Professional Paper **347**.

Harmon, R. S., and W. W. I. Doe, editors. 2001. Landscape Erosion and Evolution Modeling. Kluwer Academic /Plenum Publishers, New York.

Hjerdt, K. N., J. J. McDonnell, J. Seibert, and A. Rodhe. 2004. A new topographic index to quantify downslope controls on local drainage. Water Resour. Res. **40**:W05602.

Horton, R. E. 1933. The role of infiltration in the hydrologic cycle. Transactions of the American Geophysical Union **14**:446-460.

Horton, R. E. 1945. Erosional Development of Streams and Their Drainage Basins - Hydrophysical Approach to Quantitative Morphology. Geological Society of America Bulletin **56**:275-370.

Howard, A. D. 1994. A detachment-limited model of drainage basin evolution. Water Resources Research **30**:2261-2285.

Istanbulluoglu, E., and R. L. Bras. 2005. Vegetation-modulated landscape evolution: Effects of vegetation on landscape processes, drainage density, and topography. Journal of Geophysical Research **110**.

Kirkby, M. J. 1975. Hydrograph Modelling Strategies. Pages 69-90 *in* R. Peel, M. Chisholm, and P. Haggett, editors. Processes in Physical and Human Geography. Heinemann Educational Books Ltd., London.

Kirkby, M. J., and R. J. Chorley. 1967. Throughflow, Overland Flow and Erosion. Hydrological Sciences Journal **12**:5 - 21.

Lancaster, S. T., S. K. Hayes, and G. E. Grant. 2003. Effects of wood on debris flow runout in small mountain watersheds. Water Resources Research **39**.

Leopold, L. B., and T. J. Maddock. 1953. The Hydraulic Geometry of Stream Channels and Some Physiographic Implications. Geological Survey Professional Paper 252.

Martin, Y. 2000. Modelling hillslope evolution: linear and nonlinear transport relations. Geomorphology **34**:1-21.

McKean, J. A., W. E. Dietrich, R. C. Finkel, J. R. Southon, and M. W. Caffee. 1993. Quantification of Soil Production and Downslope Creep Rates from Cosmogenic Be-10 Accumulations on a Hillslope Profile. Geology **21**:343-346.

McNamara, J. P., A. D. Ziegler, S. H. Wood, and J. B. Vogler. 2006. Channel head locations with respect to geomorphologic thresholds derived from a digital elevation model: A case study in northern Thailand. Forest Ecology and Management **224**:147-156.

Minchin, P. R. 1989. Montane vegetation of the Mt. Field massif, Tasmania: a test of some hypotheses about properties of community patterns. Vegetatio **83**:97-110.

Moeyersons, J. 1975. An experimental study of pluvial processes on granite gruss. Catena **2**:289-308.

Montgomery, D. R., and W. E. Dietrich. 1988. Where do channels begin? Nature **336**:232-234.

Montgomery, D. R., and W. E. Dietrich. 1989. Source Areas, Drainage Density, and Channel Initiation. Water Resources Research **25**:1907-1918.

Montgomery, D. R., and W. E. Dietrich. 1992. Channel Initiation and the Problem of Landscape Scale. Science **255**:826-830.

Montgomery, D. R., and W. E. Dietrich. 1994. Landscape Dissection and Drainage Area-Slope Thresholds.*in* M. J. Kirkby, editor. Process Models and Theoretical Geomorphology. John Wiley & Sons Ltd.

Montgomery, D. R., and E. Foufoula-Georgiou. 1993. Channel Network Source Representation Using Digital Elevation Models. Water Resources Research **29**:3925-3934.

O'Callaghan, J. F., and D. M. Mark. 1984. The extraction of drainage networks from digital elevation data. Computer Vision, Graphics, and Image Processing **28**:323-344.

O'Loughlin, E. M. 1981. Saturation regions in catchments and their relations to soil and topographic properties. Journal of Hydrology **53**:229-246.

O'Loughlin, E. M. 1986. Prediction of Surface Saturation Zones in Natural Catchments by Topographic Analysis. Water Resources Research **22**:794-804.

Oksanen, J., and P. R. Minchin. 2002. Continuum theory revisited: what shape are species responses along ecological gradients? Ecological Modelling **157**:119-129.

Pelletier, J. D. 2008. Quantitative Modeling of Earth Surface Processes. Cambridge University Press, New York.

Racine, C. H. 1971. Reproduction of Three Species of Oak in Relation to Vegetational and Environmental Gradients in Southern Blue Ridge. Bulletin of the Torrey Botanical Club **98**:297-310.

Roering, J. J., P. Almond, P. Tonkin, and J. McKean. 2002. Soil transport driven by biological processes over millennial time scales. Pages 1115-1118.

Roering, J. J., J. W. Kirchner, and W. E. Dietrich. 1999. Evidence for nonlinear, diffusive sediment transport on hillslopes and implications for landscape morphology. Water Resources Research **35**:853-870.

Small, E. E., R. S. Anderson, and G. S. Hancock. 1999. Estimates of the rate of regolith production using 10Be and 26Al from an alpine hillslope. Geomorphology **27**:131-150.

Smith, R. L., and T. M. Smith. 2001. Ecology and Field Biology. Sixth edition. Benjamin Cummings, United States of America.

Smithson, P., K. Addison, and K. Atkinson. 2002. Fundamentals of the Physical Environment. Third edition. Routledge, New York.

Tarboton, D. G. 1989. The Analysis of River Basins and Channel Networks using Digital Terrain Data. PhD. Massachusetts Institute of Technology, Cambridge, Massachusetts.

Tarboton, D. G. 1997. A new method for the determination of flow directions and upslope areas in grid digital elevation models. Water Resources Research **33**:309-319.

Thornes, J. B., editor. 1990. Vegetation and erosion: processes and environments. John Wiley and Sons, Chichester.

Troch, P. A., C. Paniconi, and E. Emiel van Loon. 2003. Hillslope-storage Boussinesq model for subsurface flow and variable source areas along complex hillslopes: 1. Formulation and characteristic response. Water Resources Research **39**:doi:10.1029/2002WR001728.

Tsukamoto, Y., and T. Ohta. 1988. Runoff process on a steep forested slope. Journal of Hydrology **102**:165-178.

Tucker, G. E., and R. L. Bras. 1998. Hillslope processes, drainage density, and landscape morphology. Water Resources Research **34**:2751-2764.

Tucker, G. E., and R. L. Bras. 2000. A stochastic approach to modeling the role of rainfall variability in drainage basin evolution. Water Resources Research **36**:1953-1964.

Tucker, G. E., S. T. Lancaster, N. M. Gasparini, and R. L. Bras. 2001. The Channel-Hillslope Integrated Landscape Development (CHILD) Model. Pages 349-388 *in* R. S. Harmon and W. W. Doe, editors. Landscape Erosion and Evolution Modeling. Kluwer Academic/ Plenum Publishers, New York.

Tucker, G. E., and R. L. Slingerland. 1994. Erosional Dynamics, Flexural Isostasy, and Long-Lived Escarpments - a Numerical Modeling Study. Journal of Geophysical Research-Solid Earth **99**:12229-12243.

Waring, R. H., and J. Major. 1964. Some vegetation of the California Coastal Region in Relation to Gradients of Moisture, Nutrients, Light, and Temperature. Ecological Monographs **34**:167-215.

Warntz, W. 1975. Stream ordering and contour mapping. Journal of Hydrology **25**:209-227.

Werner, C. 1988. Formal Analysis of Ridge and Channel Patterns in Maturely Eroded Terrain. Annals of the Association of American Geographers **78**:253-270.

Werner, C. 1991. Several Duality Theorems for Interlocking Ridge and Channel Networks. Water Resources Research **27**:3237-3247.

Whittaker, R. H. 1956. Vegetation of the Great Smoky Mountains. Ecological Monographs **26**:1-80.

Whittaker, R. H. 1960. Vegetation of the Siskiyou Mountains, Oregon and California. Ecological Monographs **30**:279-338.

Whittaker, R. H. 1967. Gradient analysis of vegetation. Biological Reviews of the Cambridge Philosophical Society **49**:207-264.

Willgoose, G. 1994. A Statistic for Testing the Elevation Characteristics of Landscape Simulation-Models. Journal of Geophysical Research-Solid Earth **99**:13987-13996.

Willgoose, G., R. L. Bras, and I. Rodríguez-Iturbe. 1991a. A Physical Explanation of an Observed Link Area-Slope Relationship. Water Resources Research **27**:1697-1702.

Willgoose, G., R. L. Bras, and I. Rodríguez-Iturbe. 1991b. Results from a new model of river basin evolution. Earth Surface Processes and Landforms **16**:237-254.

Wu, W., and R. C. Sidle. 1995. A Distributed Slope Stability Model for Steep Forested Basins. Water Resources Research **31**:2097-2110.

Yoo, K., R. Amundson, A. M. Heimsath, and W. E. Dietrich. 2005. Process-based model linking pocket gopher (*Thomomys bottae*) activity to sediment transport and soil thickness. Geology **33**:917-920.

Zinko, U., J. Seibert, M. Dynesius, and C. Nilsson. 2005. Plant species numbers predicted by a topography-based groundwater flow index. Ecosystems **8**:430-441.

APPENDIX A
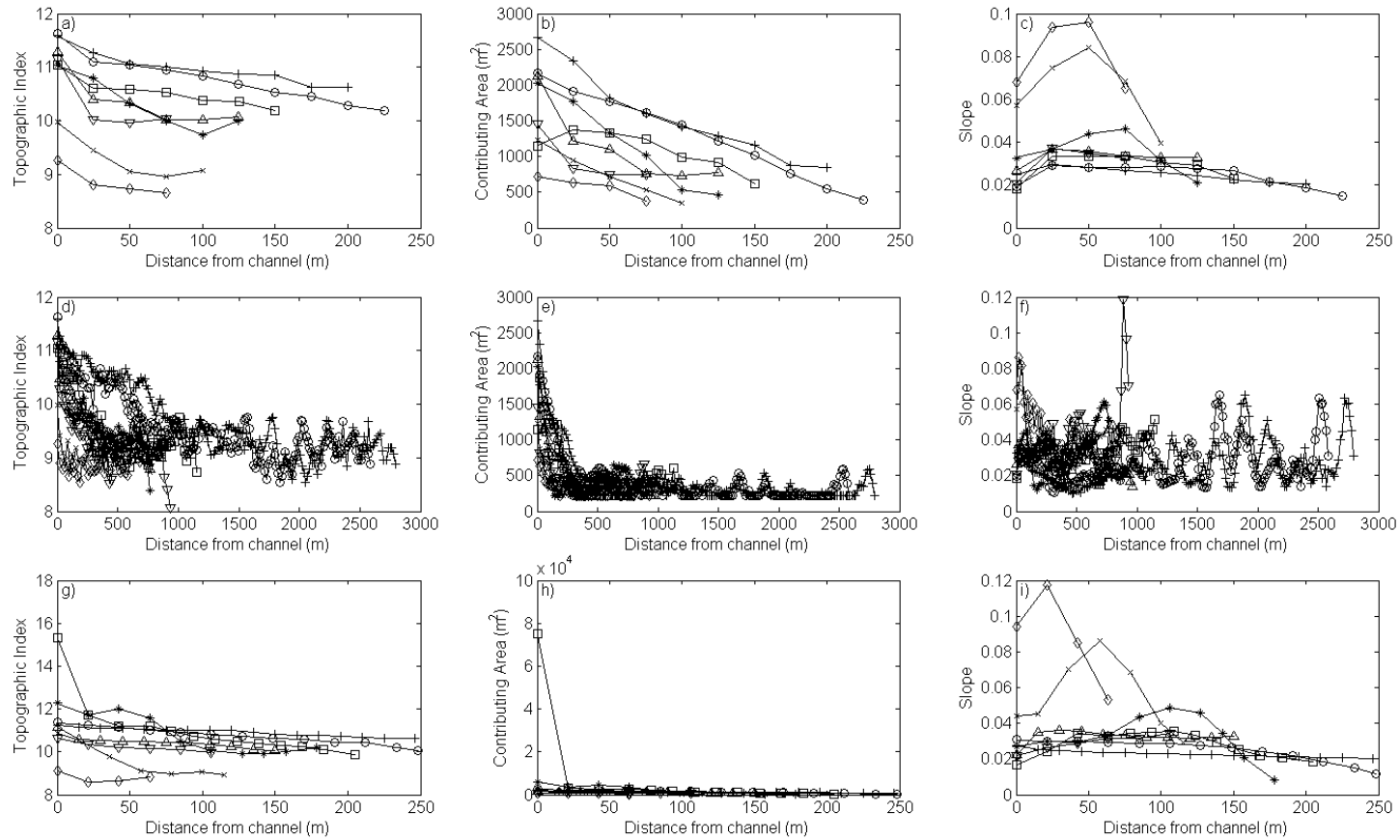
Figure A1. Creep-dominated landscape divergent-convex hillslopes topographic index, contributing area, and slope as a function of distance from the channel for a) - c) channel to ridgeline transects, d) - f) ascent transects, and g) - i) descent transects. The same symbol indicates data obtained from the same transect within each of the three sampling methods.
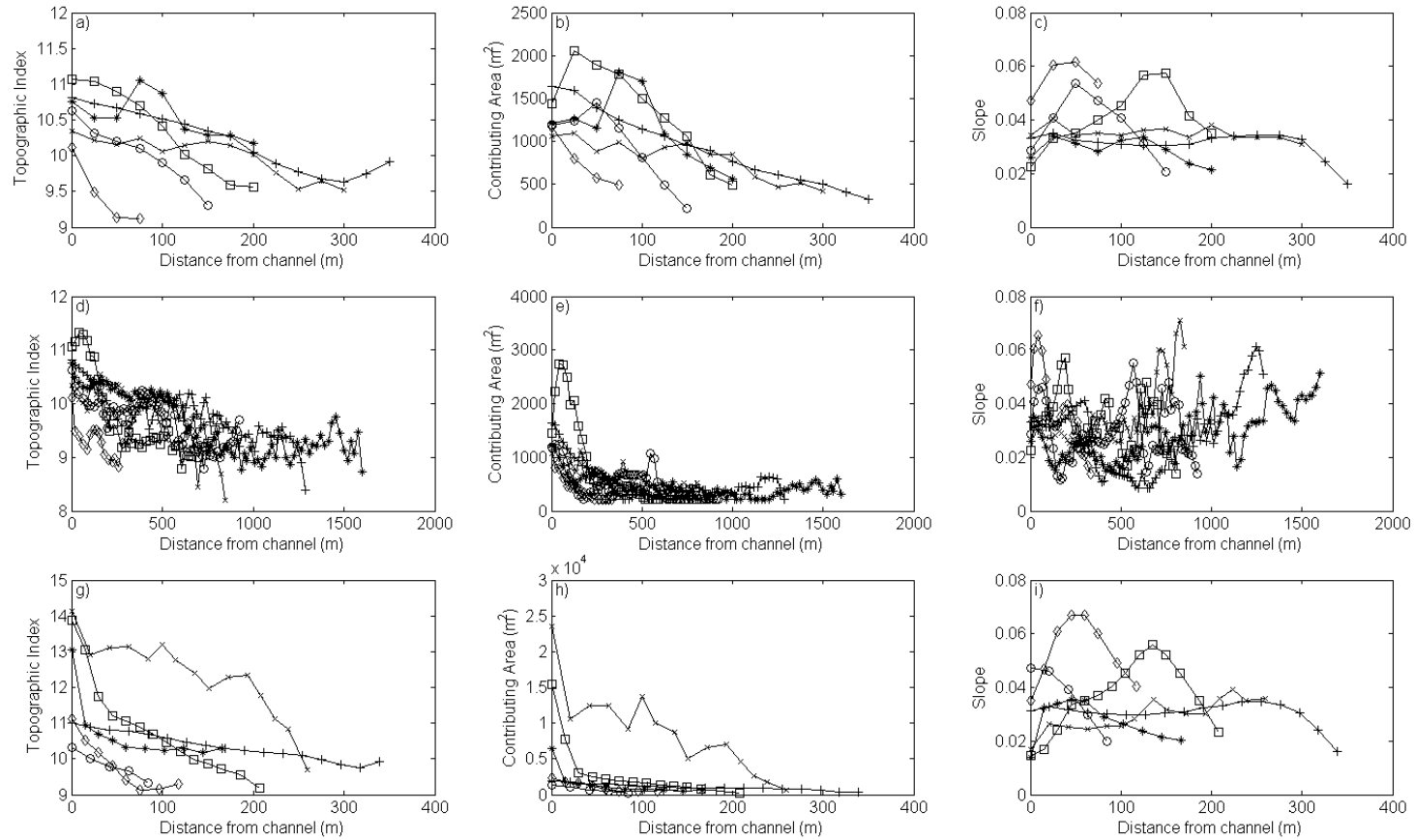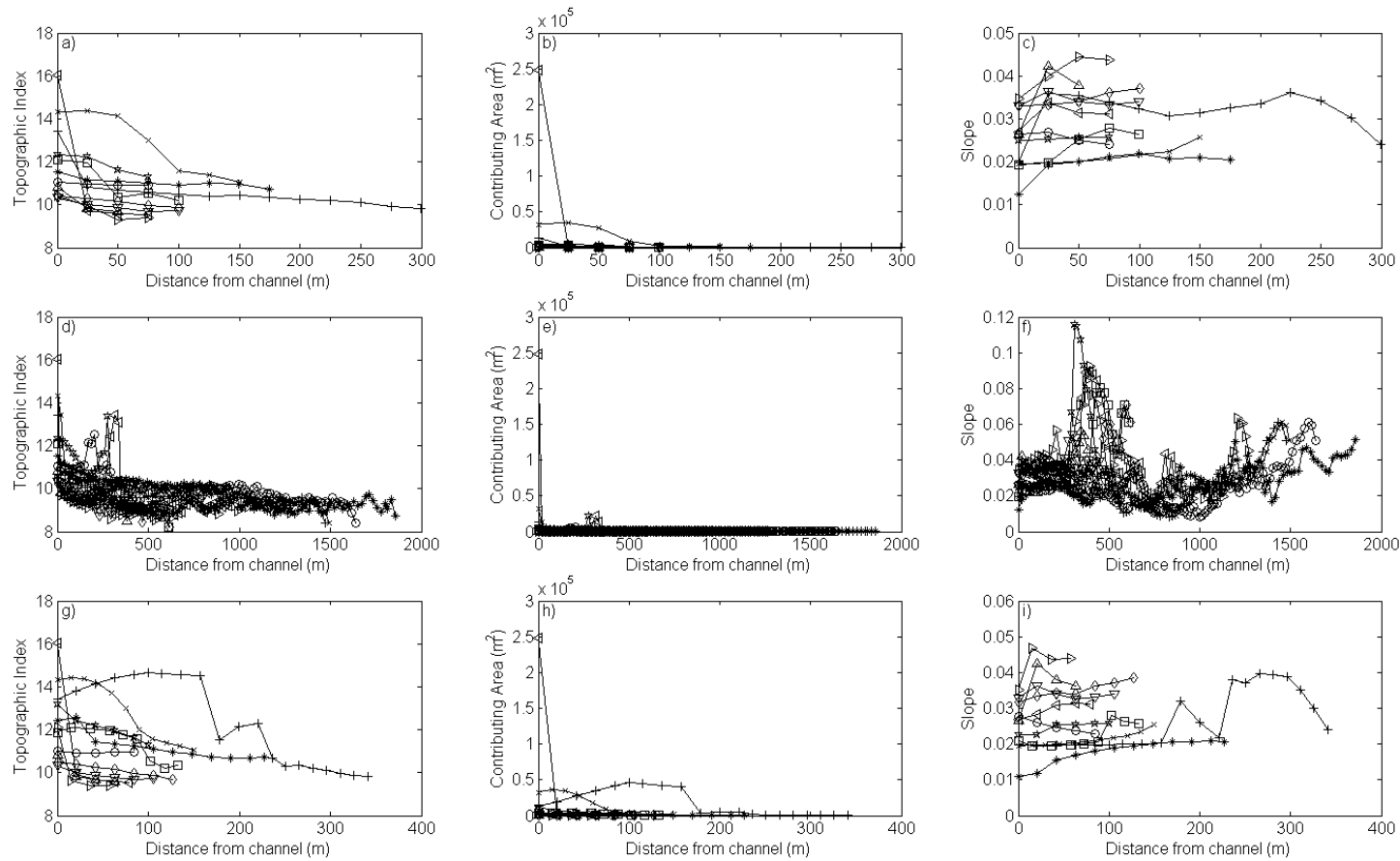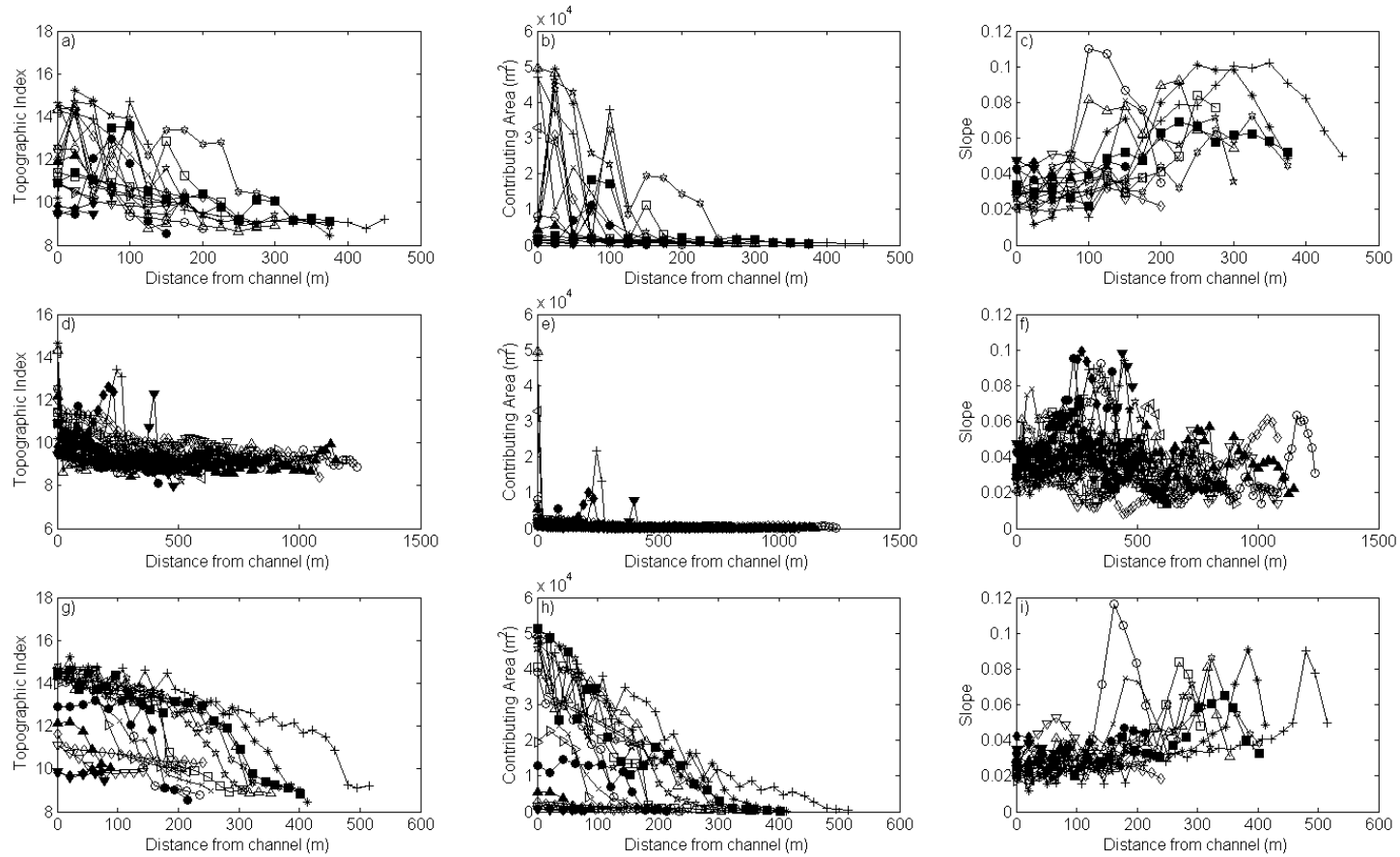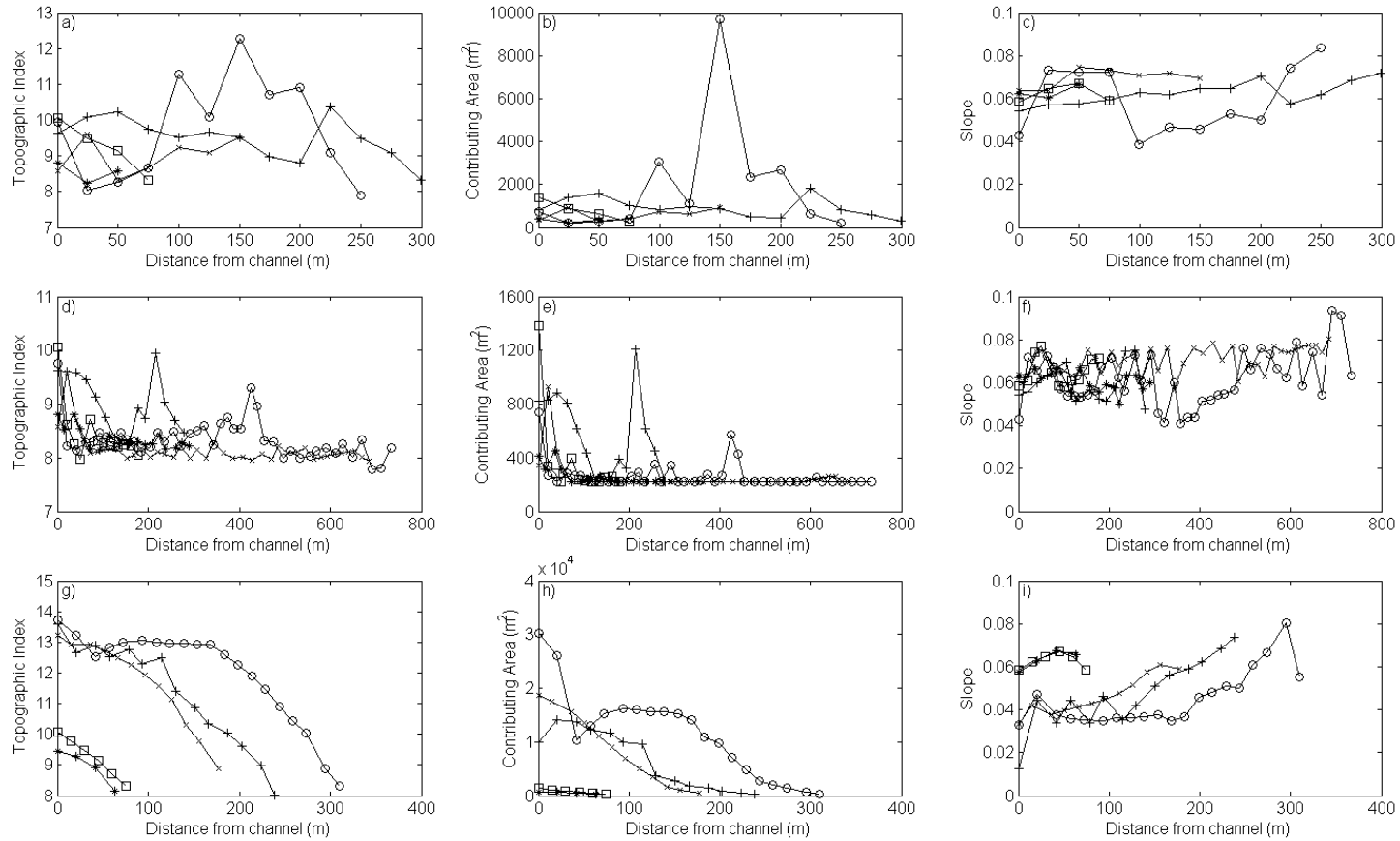
Figure A2. Creep-dominated landscape divergent-planar hillslopes topographic index, contributing area, and slope as a function of distance from the channel for a) - c) channel to ridgeline transects, d) - f) ascent transects, and g) - i) descent transects. The same symbol indicates data obtained from the same transect within each of the three sampling methods.
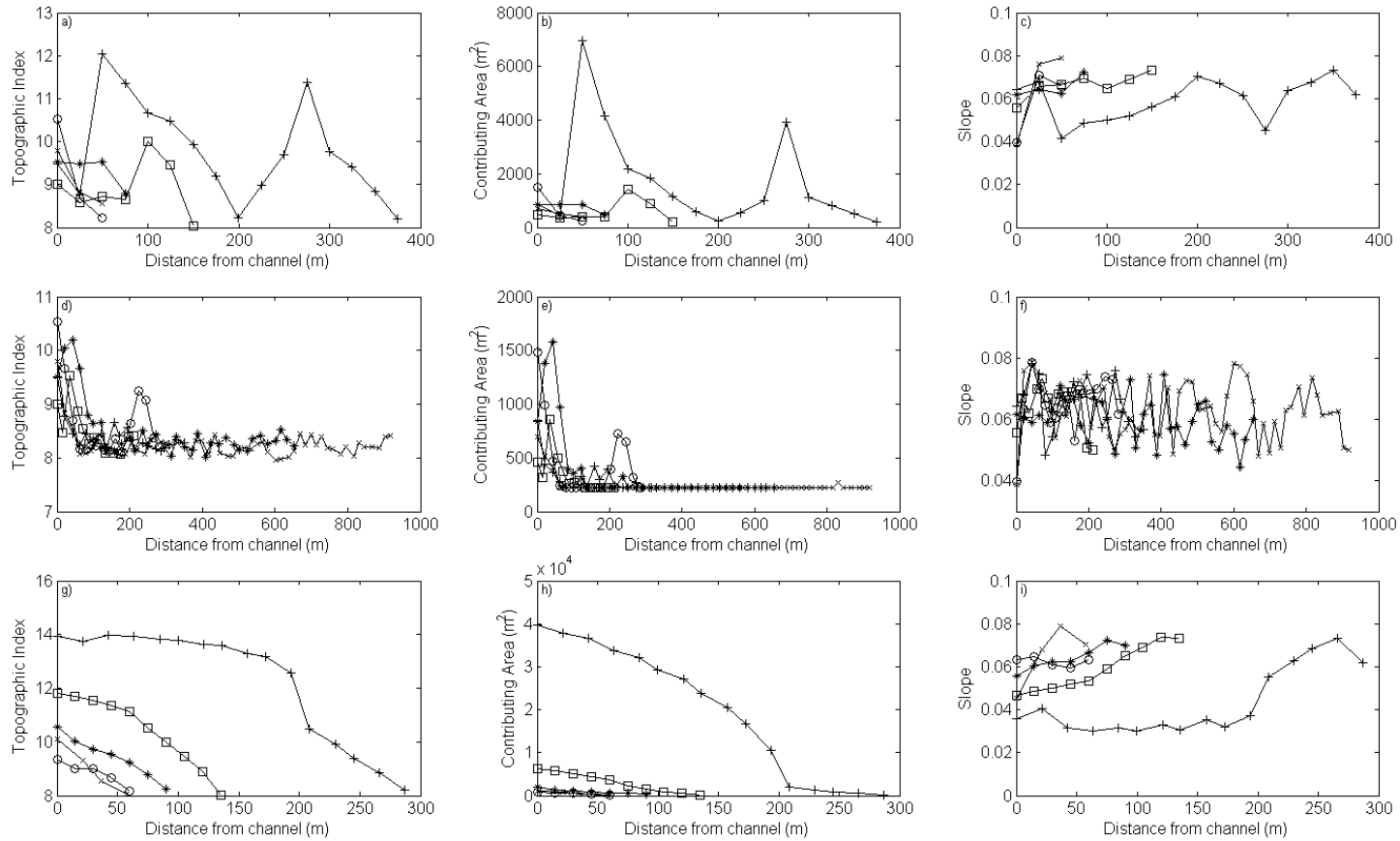
61
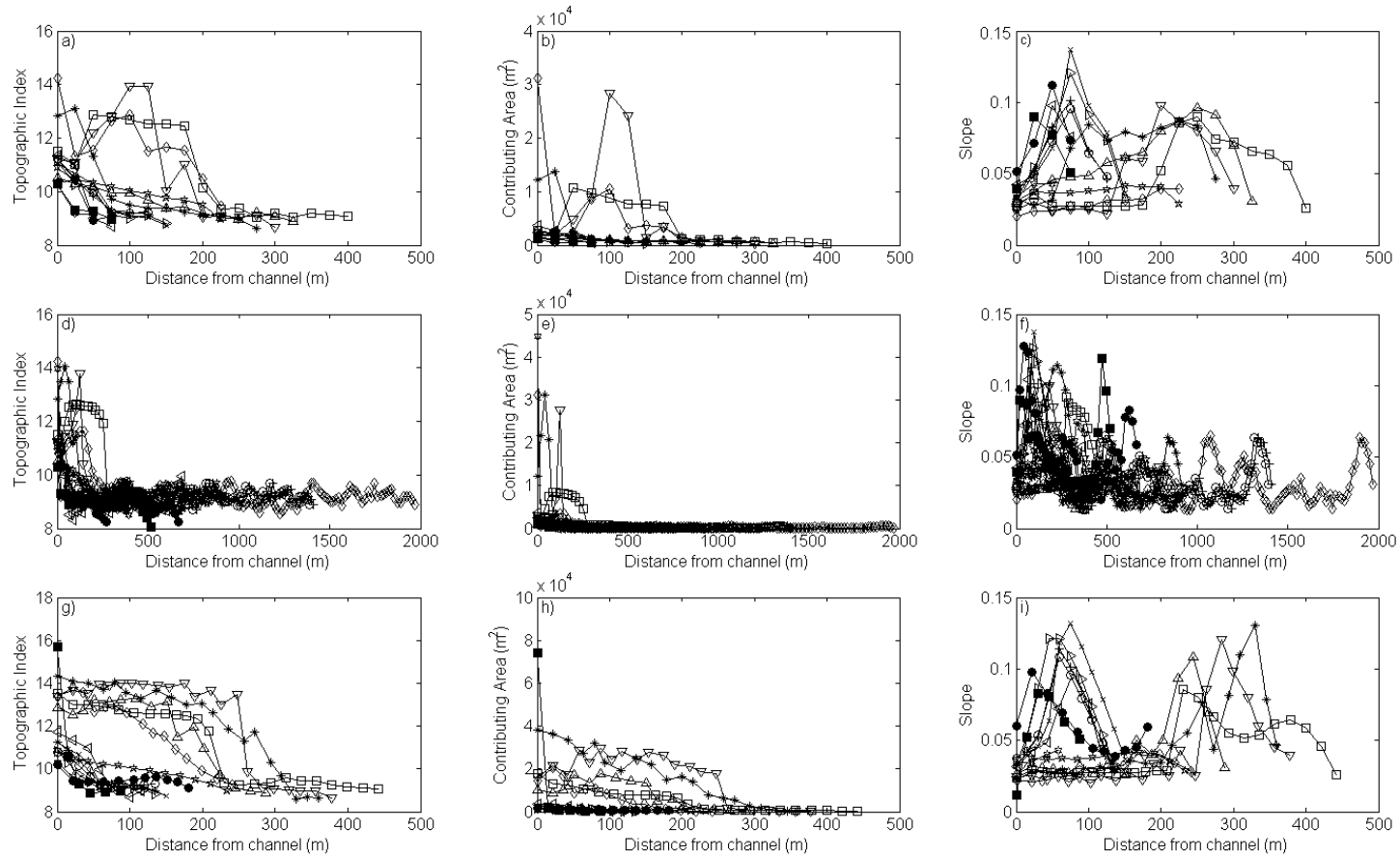
Figure A3. Creep-dominated landscape divergent-concave hillslopes topographic index, contributing area, and slope as a function of distance from the channel for a) - c) channel to ridgeline transects, d) - f) ascent transects, and g) - i) descent transects. The same symbol indicates data obtained from the same transect within each of the three sampling methods.
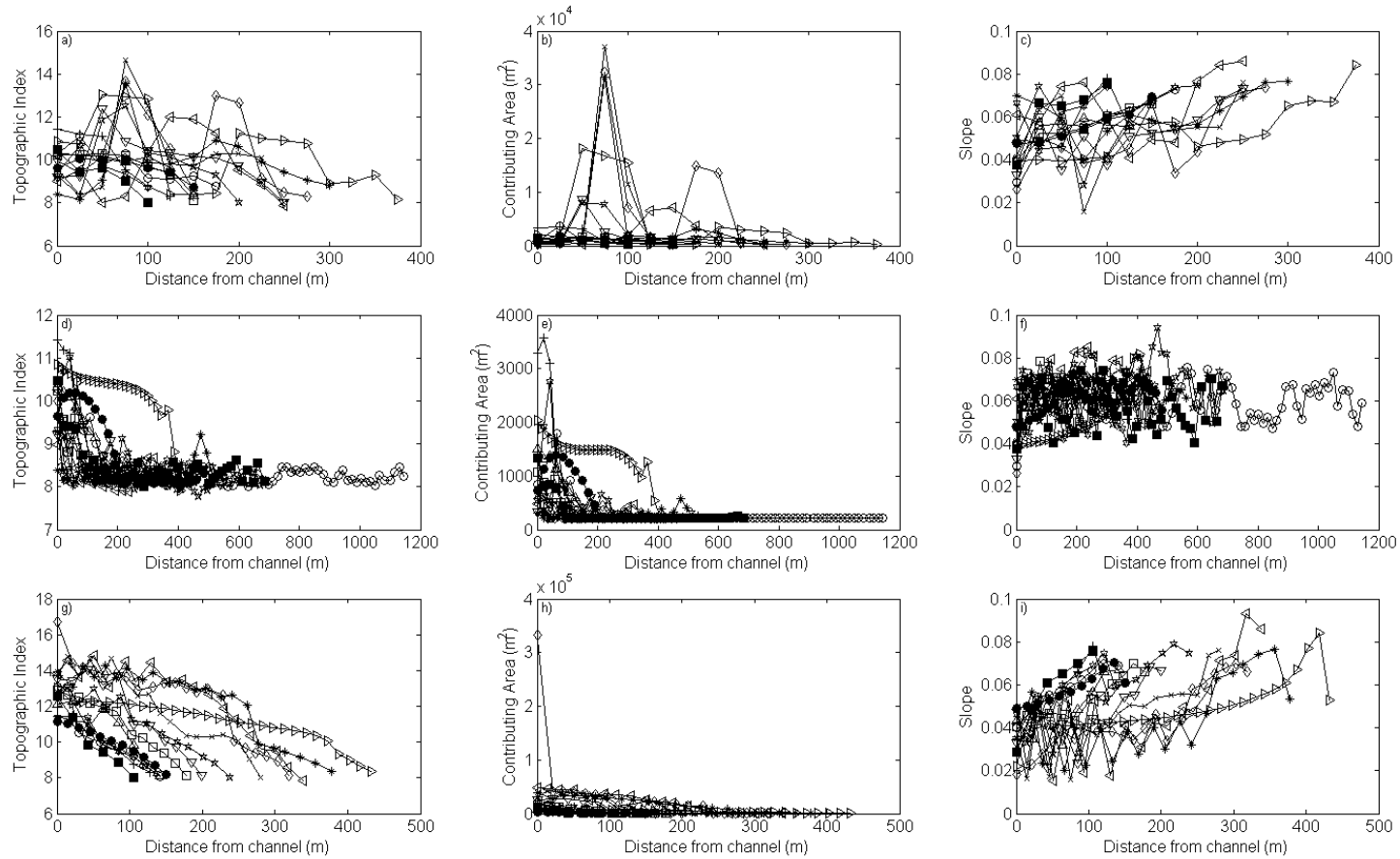
62
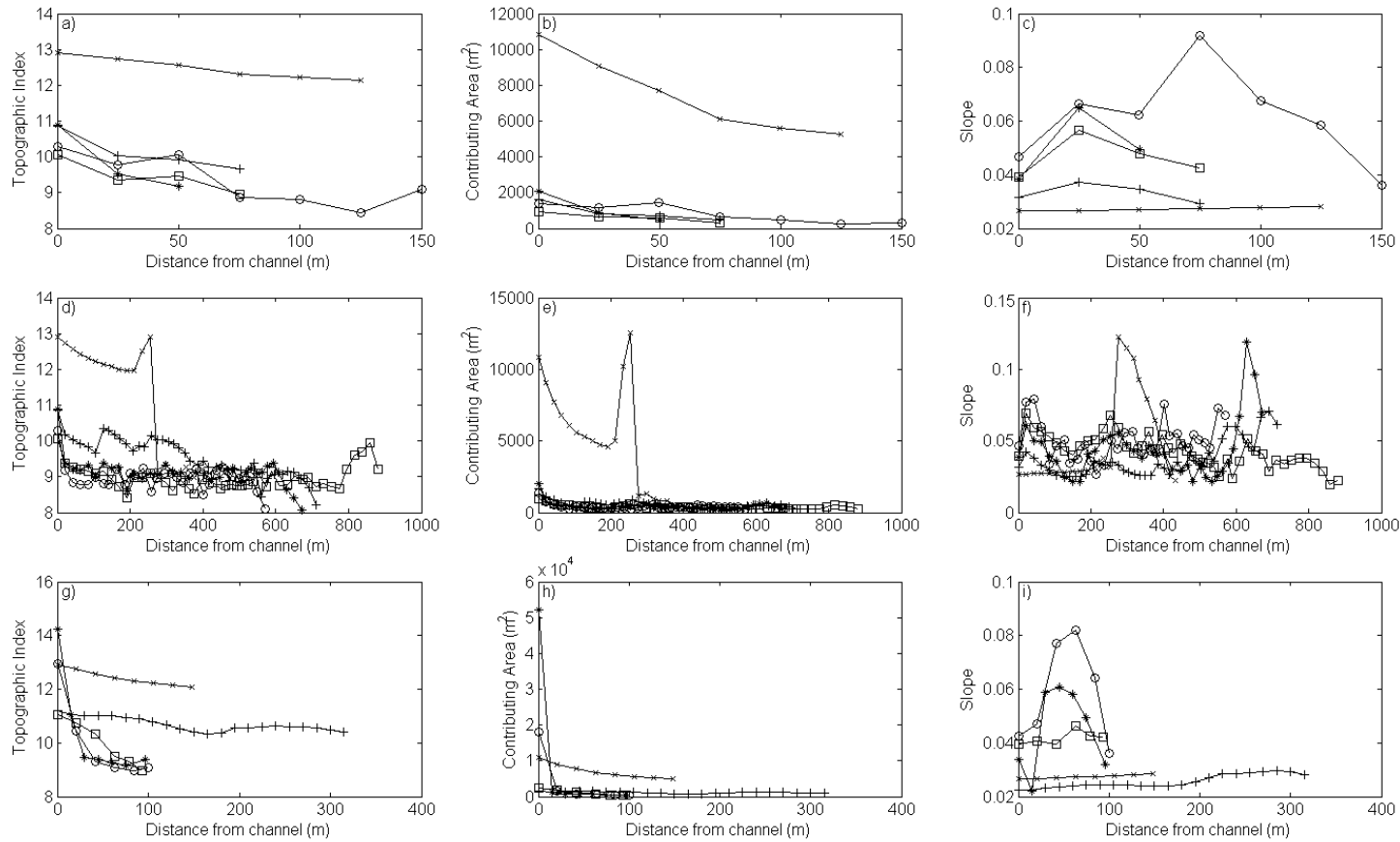
Figure A4. Creep-dominated landscape parallel-convex hillslopes topographic index, contributing area, and slope as a function of distance from the channel for a) - c) channel to ridgeline transects, d) - f) ascent transects, and g) - i) descent transects. The same symbol indicates data obtained from the same transect within each of the three sampling methods.
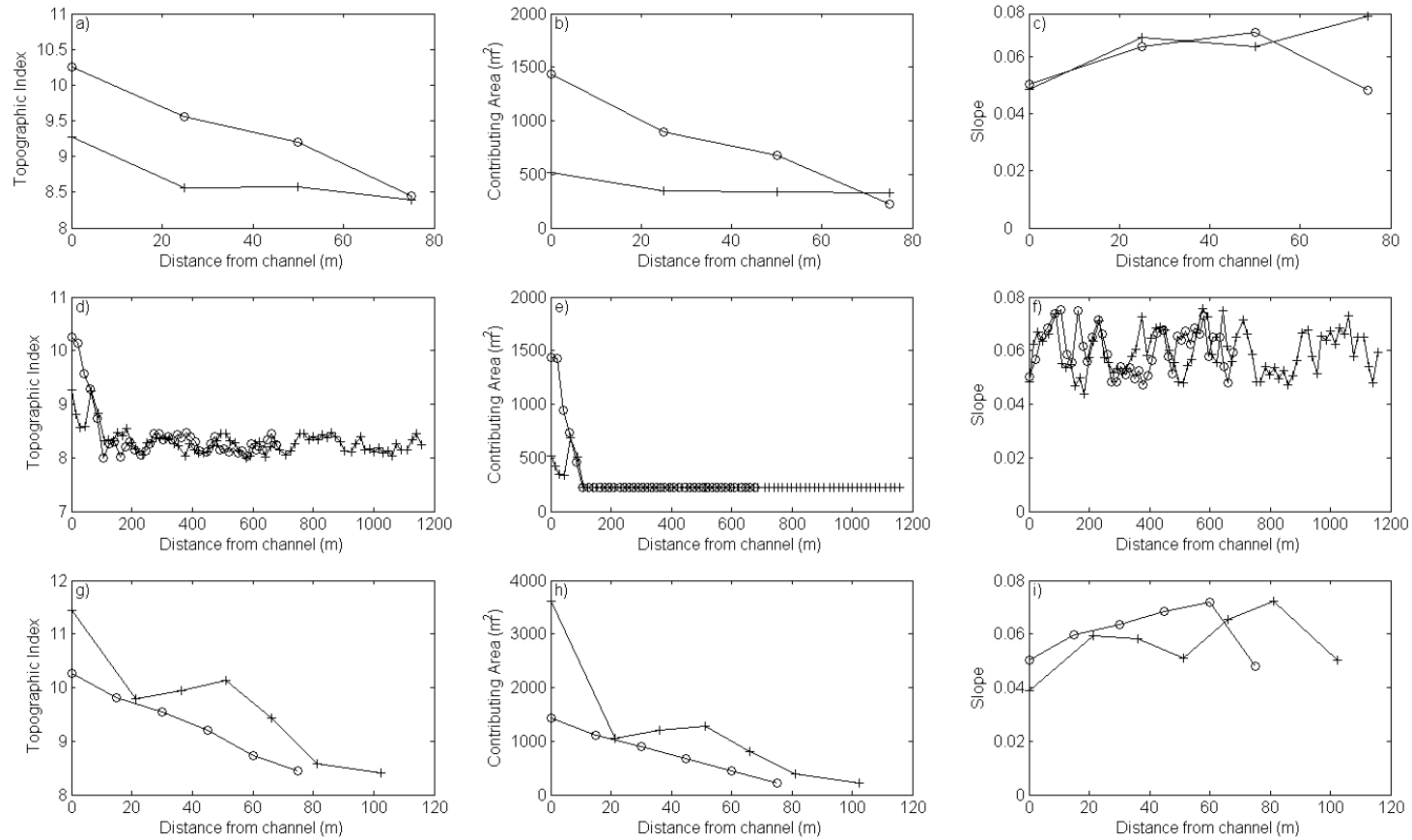
63
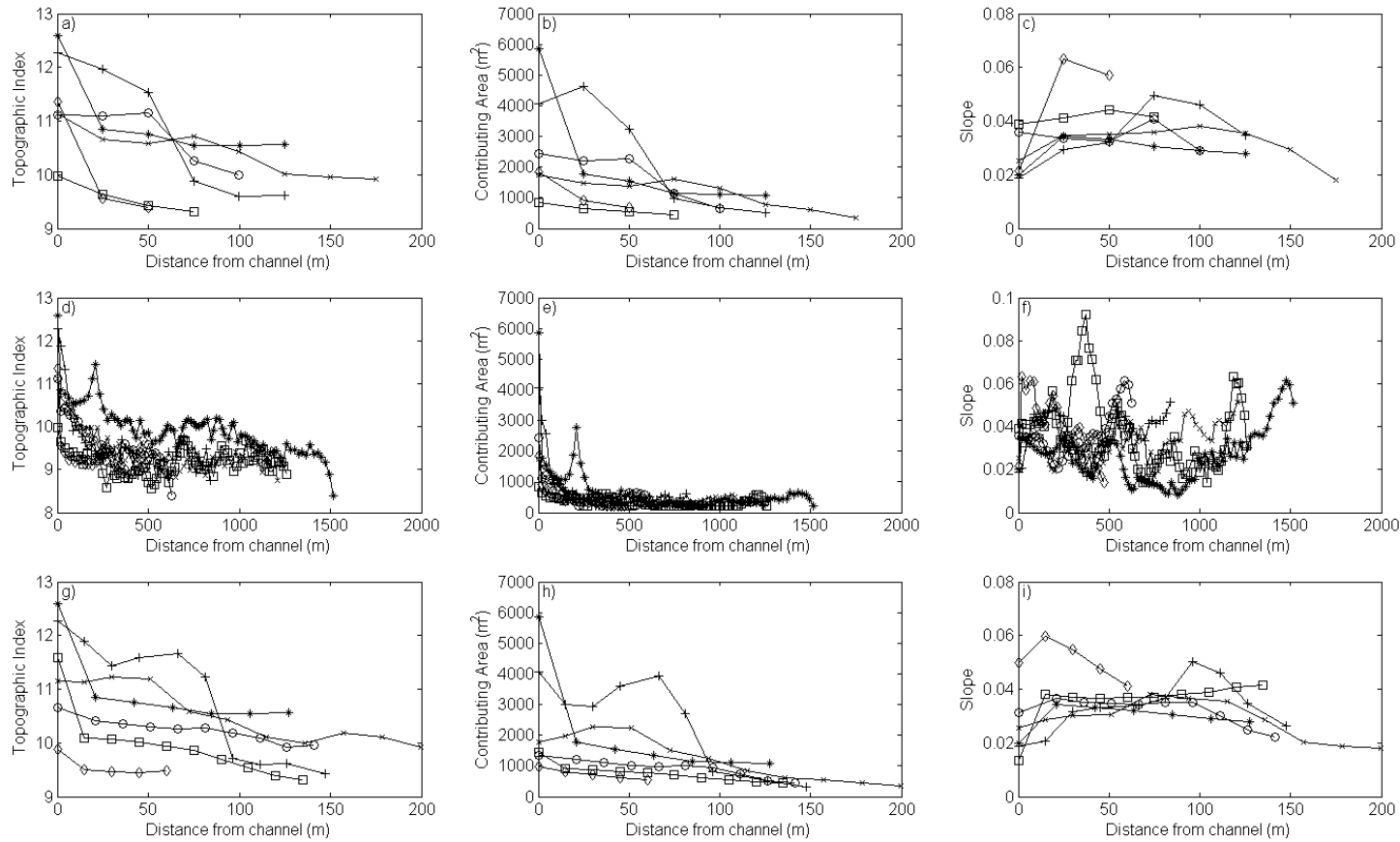
Figure A5. Creep-dominated landscape parallel-planar hillslopes topographic index, contributing area, and slope as a function of distance from the channel for a) - c) channel to ridgeline transects, d) - f) ascent transects, and g) - i) descent transects. The same symbol indicates data obtained from the same transect within each of the three sampling methods.
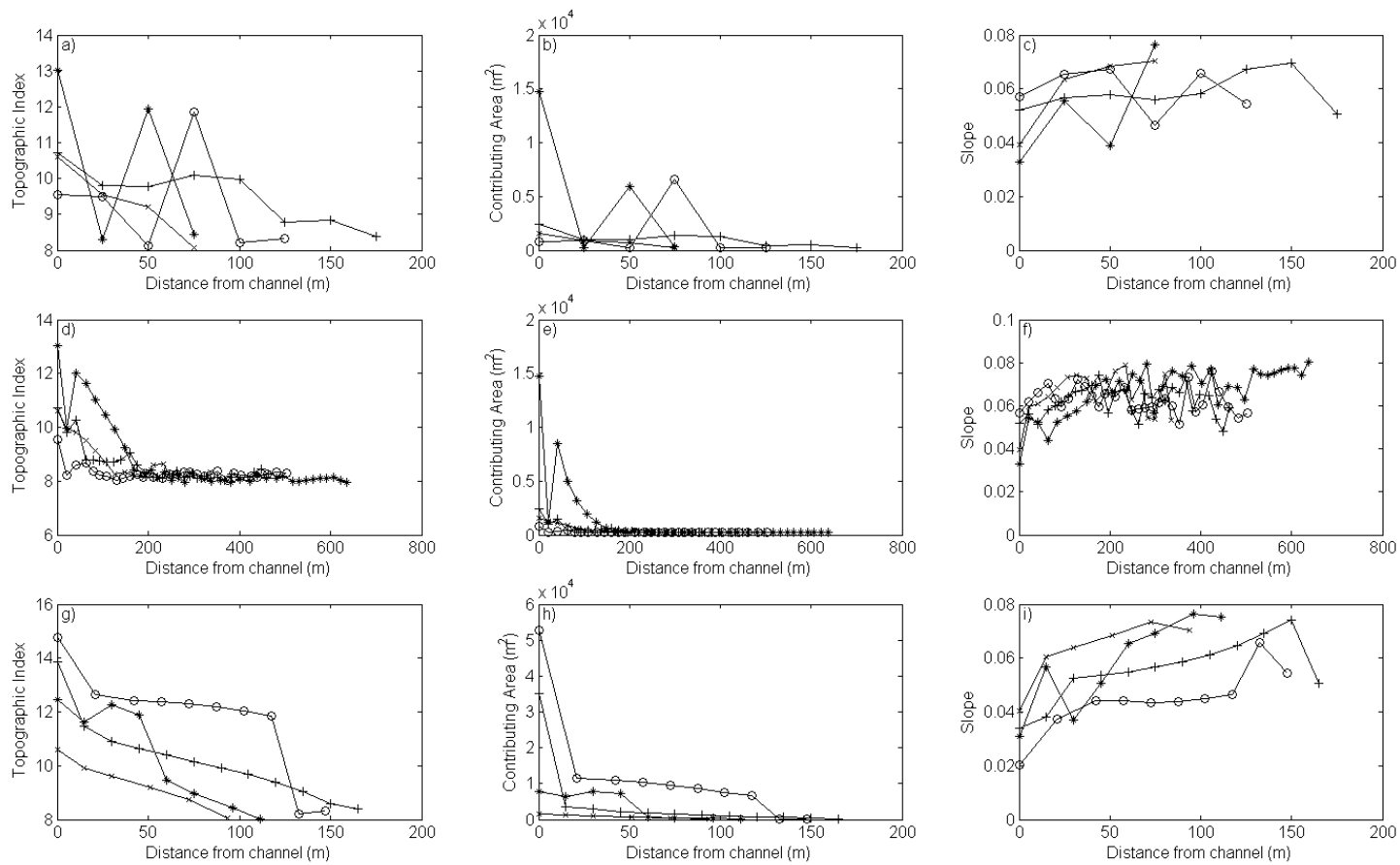
64
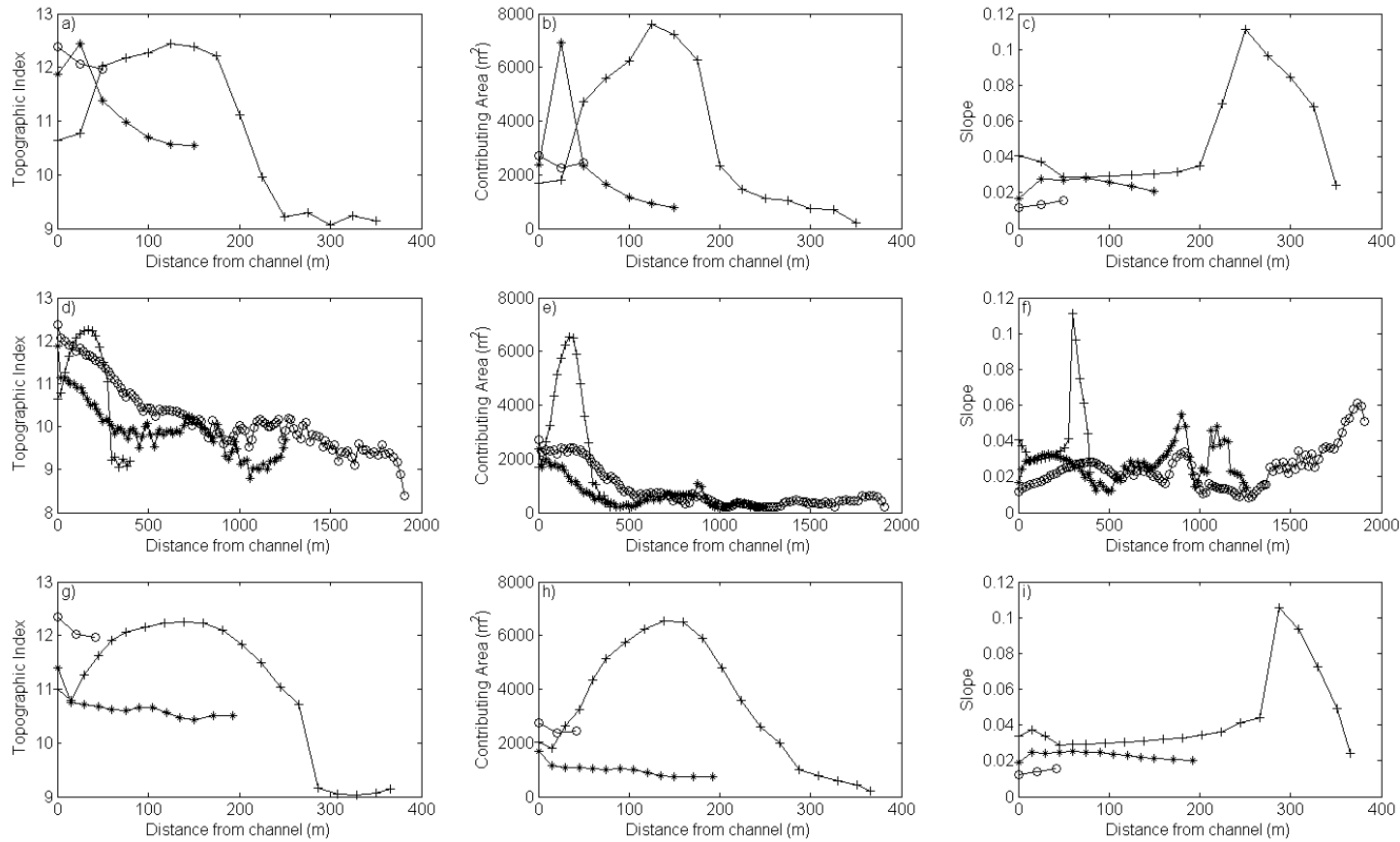
Figure A6. Creep-dominated landscape parallel-concave hillslopes topographic index, contributing area, and slope as a function of distance from the channel for a) - c) channel to ridgeline transects, d) - f) ascent transects, and g) - i) descent transects. The same symbol indicates data obtained from the same transect within each of the three sampling methods.
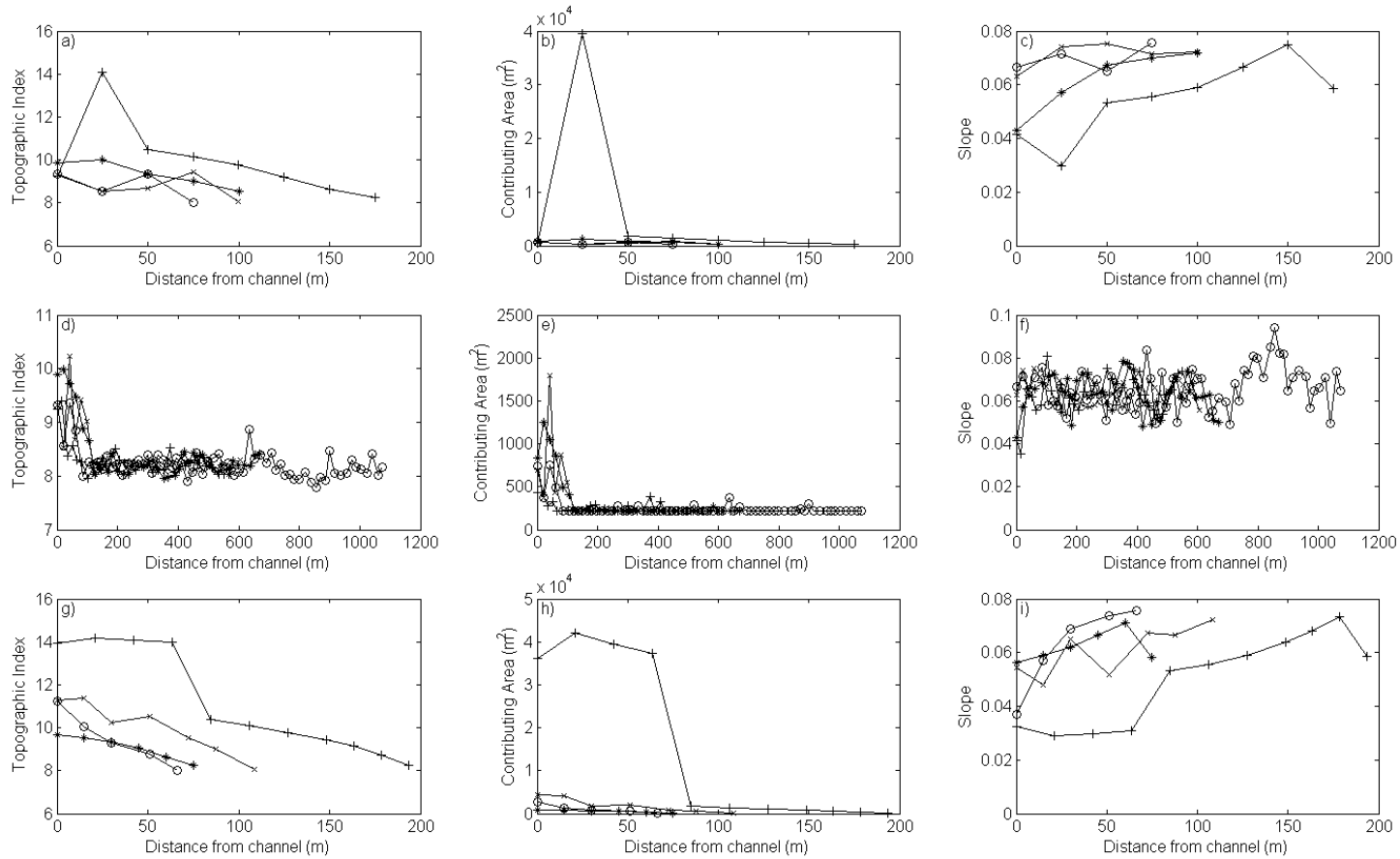
65
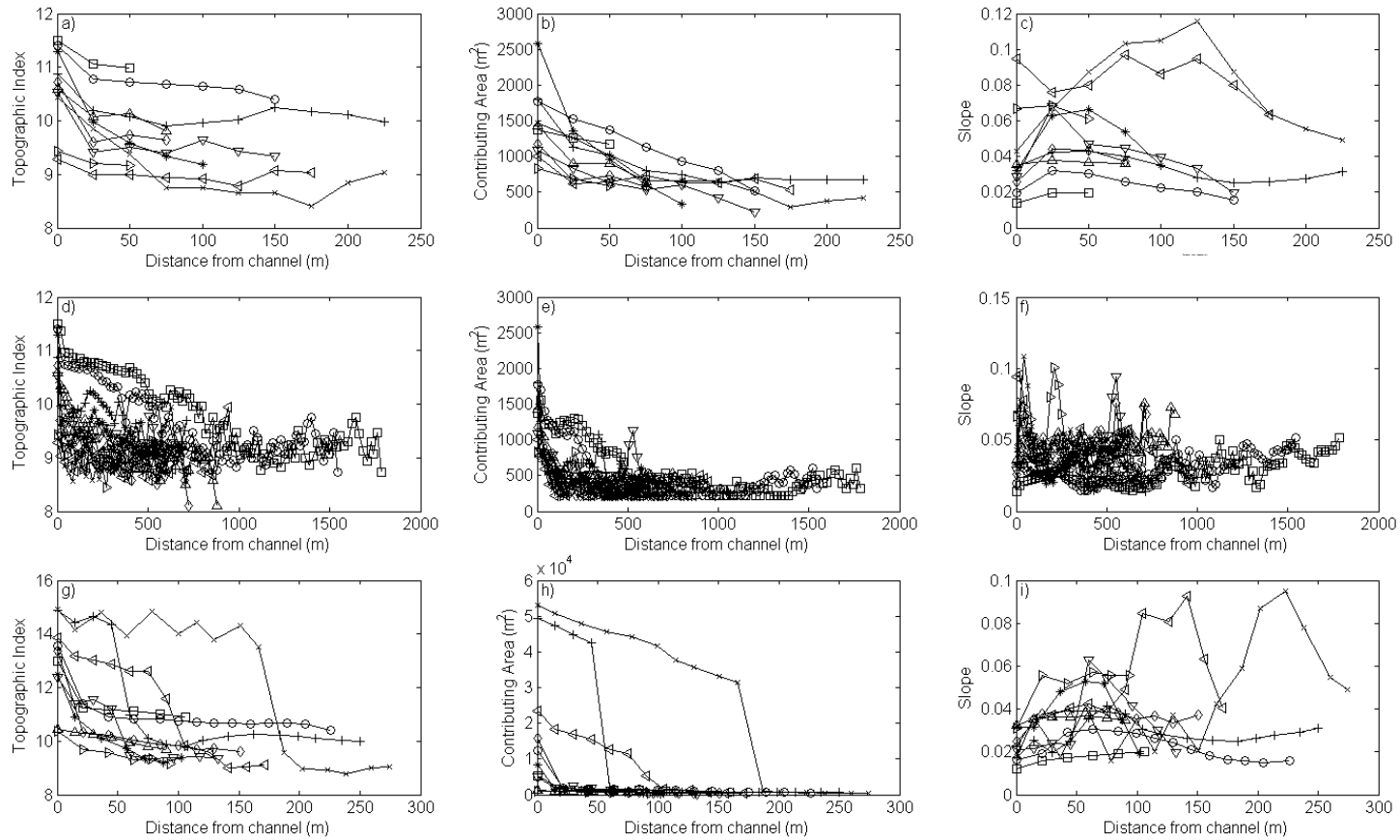
Figure A7. Creep-dominated landscape convergent-convex hillslopes topographic index, contributing area, and slope as a function of distance from the channel for a) - c) channel to ridgeline transects, d) - f) ascent transects, and g) - i) descent transects. The same symbol indicates data obtained from the same transect within each of the three sampling methods.
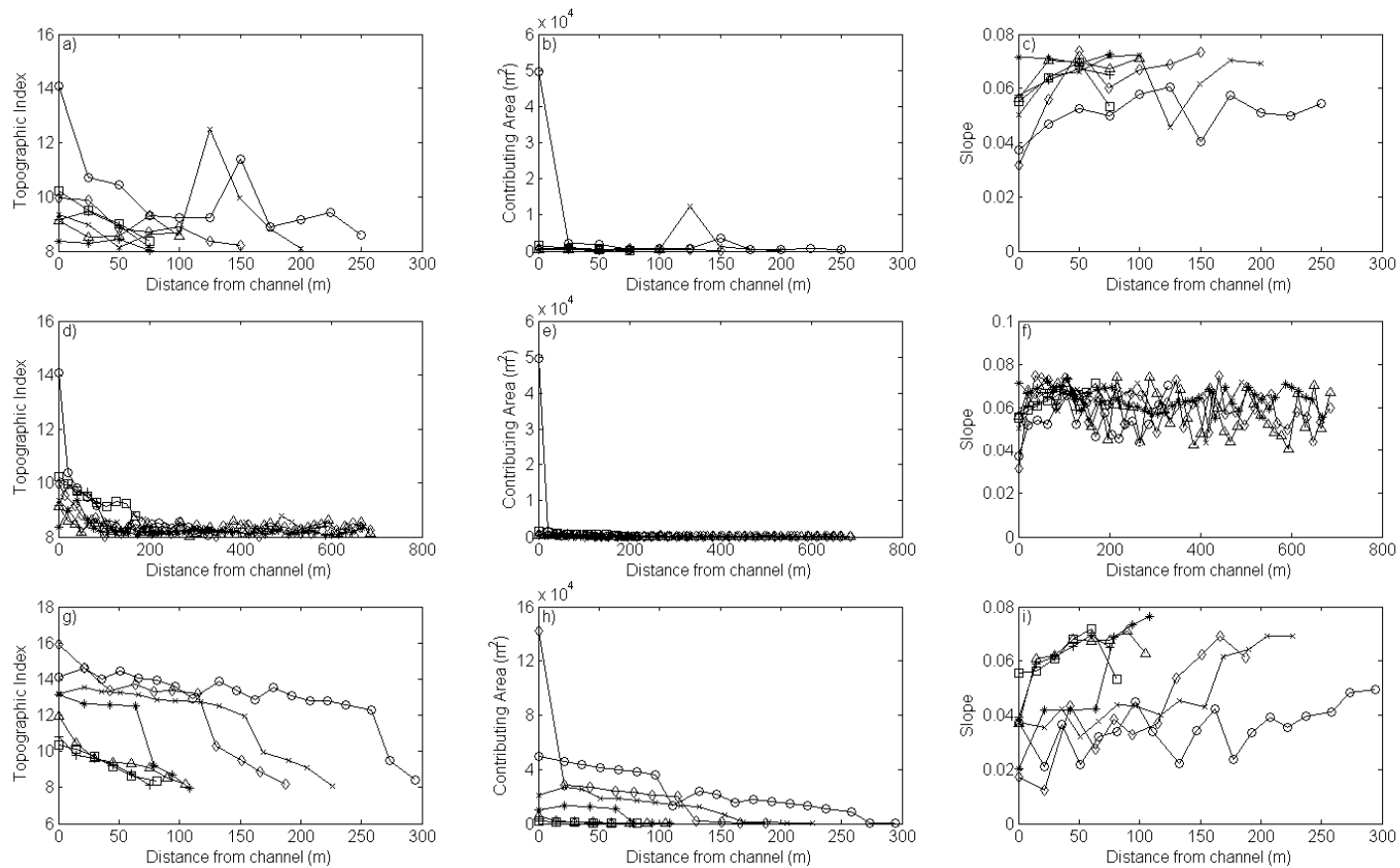
66

Figure A8. Creep-dominated landscape convergent-planar hillslopes topographic index, contributing area, and slope as a function of distance from the channel for a) - c) channel to ridgeline transects, d) - f) ascent transects, and g) - i) descent transects. The same symbol indicates data obtained from the same transect within each of the three sampling methods.
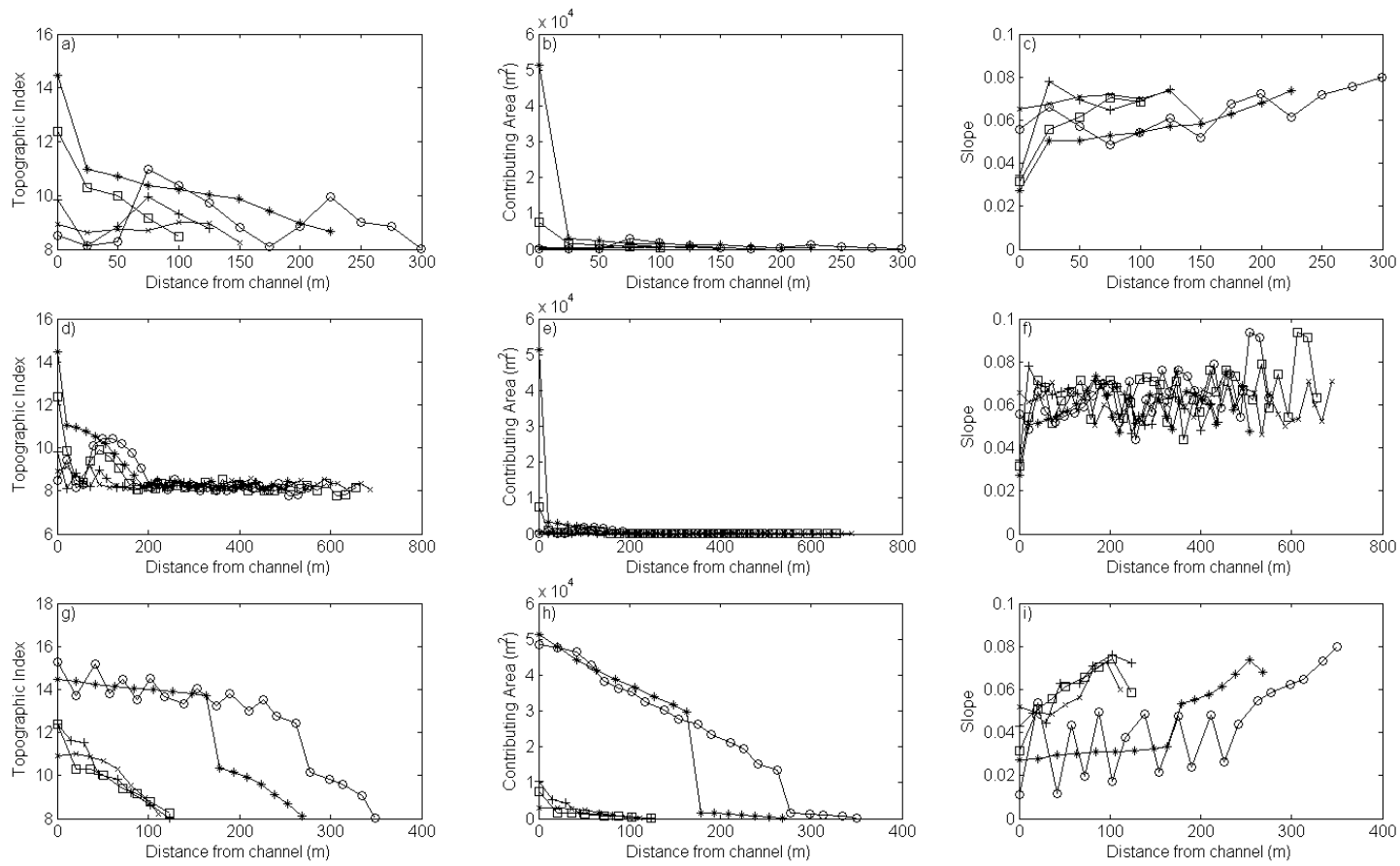
67

Figure A9. Creep-dominated landscape convergent-concave hillslopes topographic index, contributing area, and slope as a function of distance from the channel for a) - c) channel to ridgeline transects, d) - f) ascent transects, and g) - i) descent transects. The same symbol indicates data obtained from the same transect within each of the three sampling methods.

68

Figure A10. Overland flow-dominated landscape divergent-convex hillslopes topographic index, contributing area, and slope as a function of distance from the channel for a) - c) channel to ridgeline transects, d) - f) ascent transects, and g) - i) descent transects. The same symbol indicates data obtained from the same transect within each of the three sampling methods.
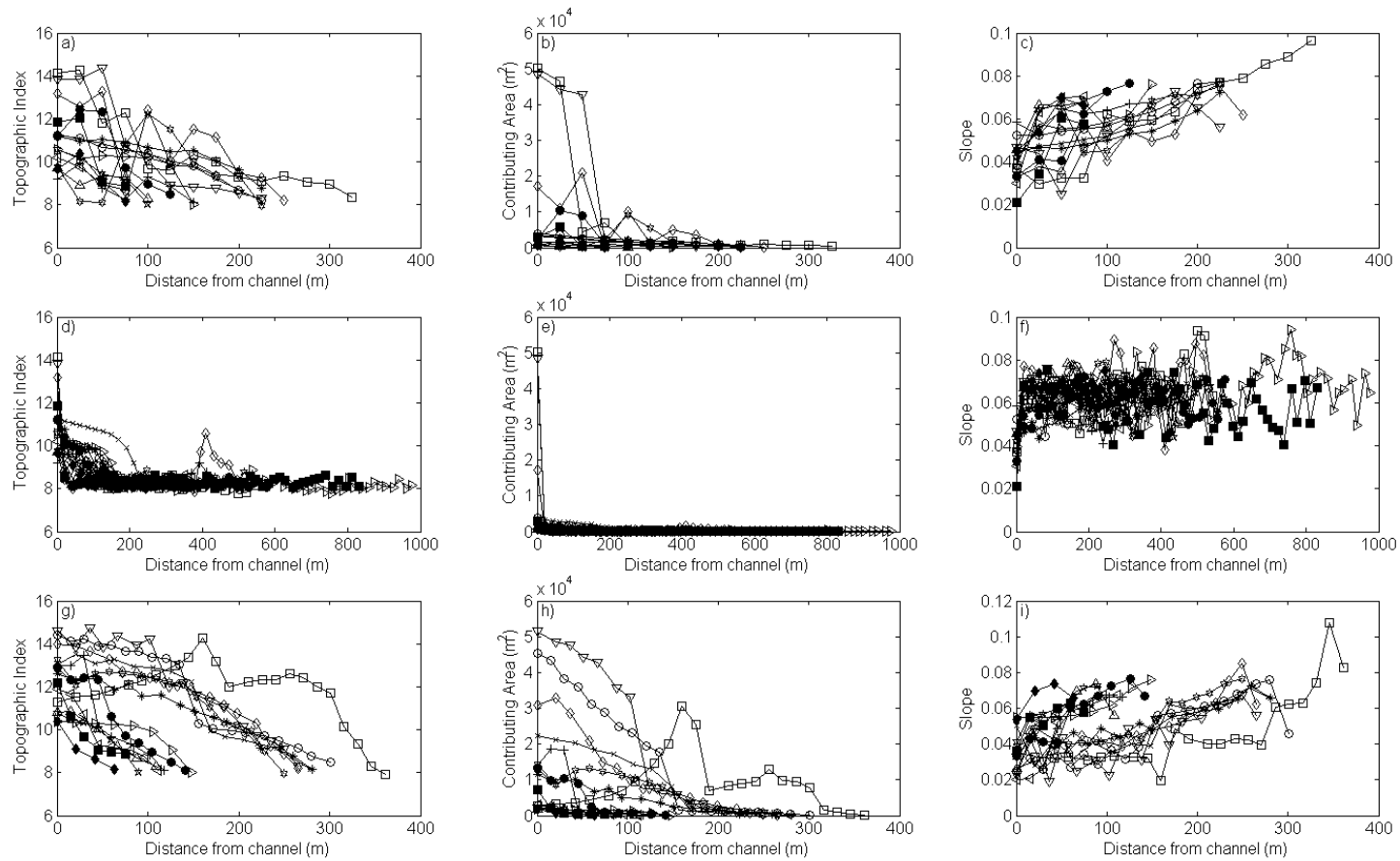
69

Figure A11. Overland flow-dominated landscape divergent-planar hillslopes topographic index, contributing area, and slope as a function of distance from the channel for a) - c) channel to ridgeline transects, d) - f) ascent transects, and g) - i) descent transects. The same symbol indicates data obtained from the same transect within each of the three sampling methods.

70

Figure A12. Overland flow-dominated landscape divergent-concave hillslopes topographic index, contributing area, and slope as a function of distance from the channel for a) - c) channel to ridgeline transects, d) - f) ascent transects, and g) - i) descent transects. The same symbol indicates data obtained from the same transect within each of the three sampling methods.
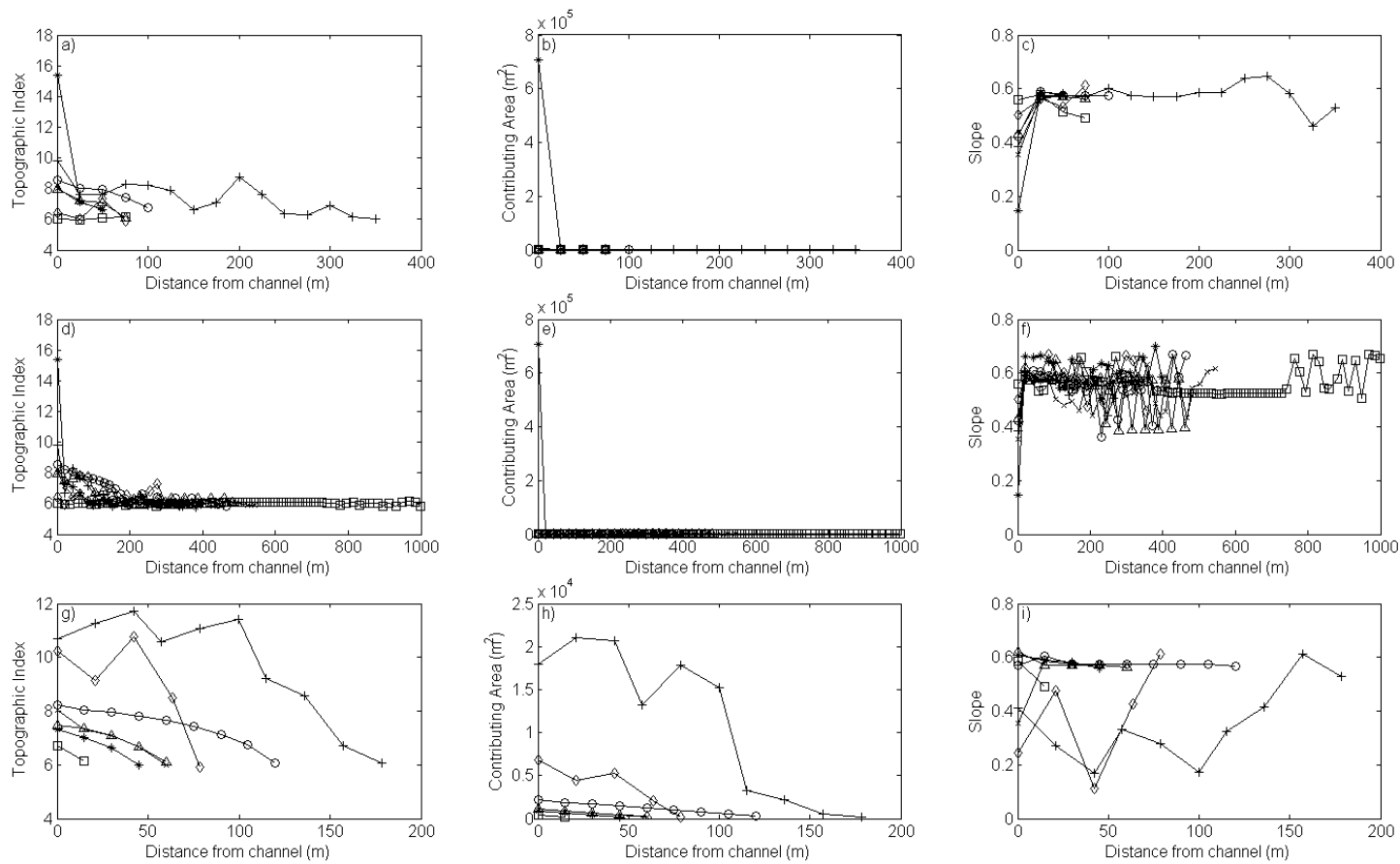
71

Figure A13. Overland flow-dominated landscape parallel-convex hillslopes topographic index, contributing area, and slope as a function of distance from the channel for a) - c) channel to ridgeline transects, d) - f) ascent transects, and g) - i) descent transects. The same symbol indicates data obtained from the same transect within each of the three sampling methods.
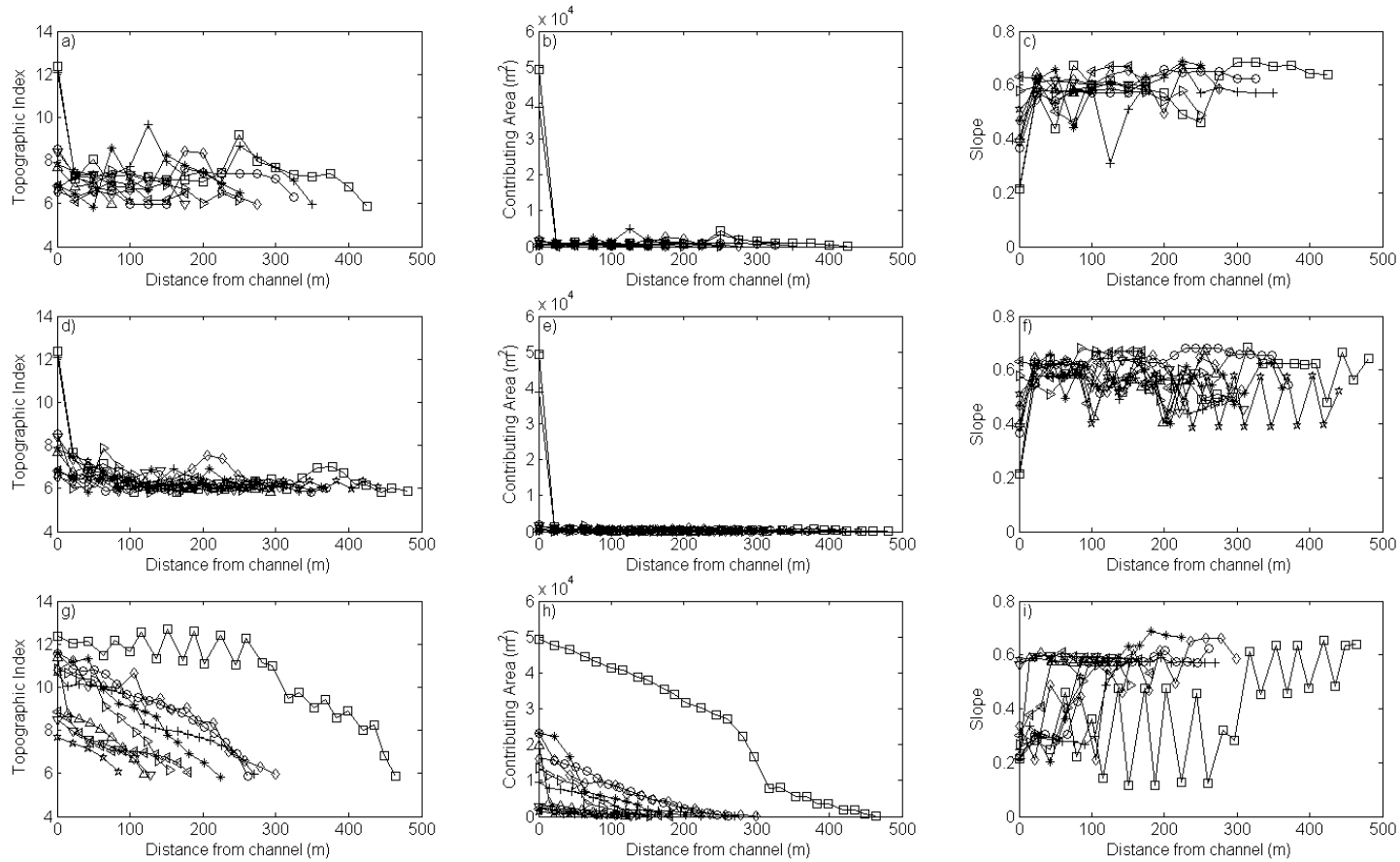
Figure A14. Overland flow-dominated landscape parallel-planar hillslopes topographic index, contributing area, and slope as a function of distance from the channel for a) - c) channel to ridgeline transects, d) - f) ascent transects, and g) - i) descent transects. The same symbol indicates data obtained from the same transect within each of the three sampling methods.
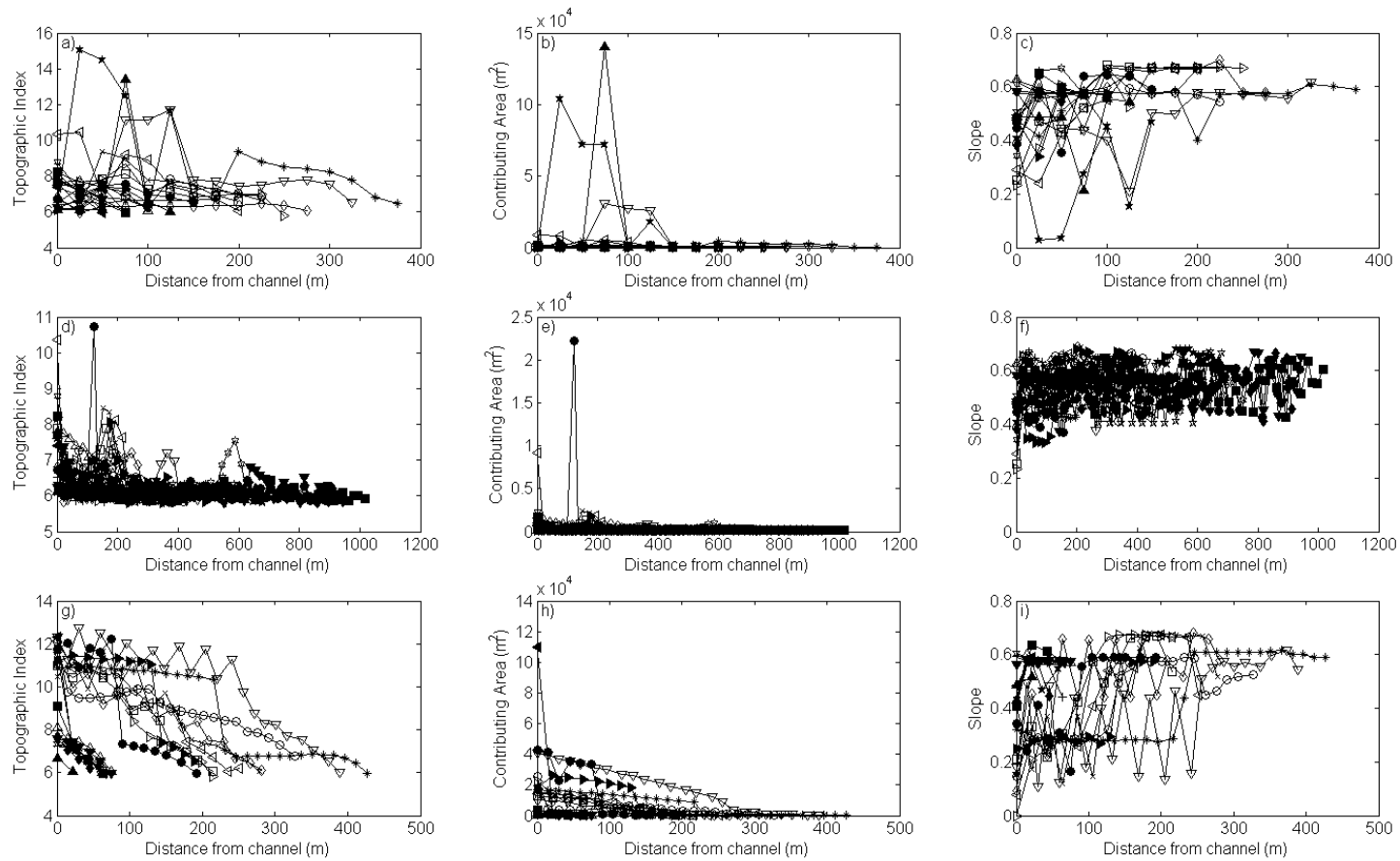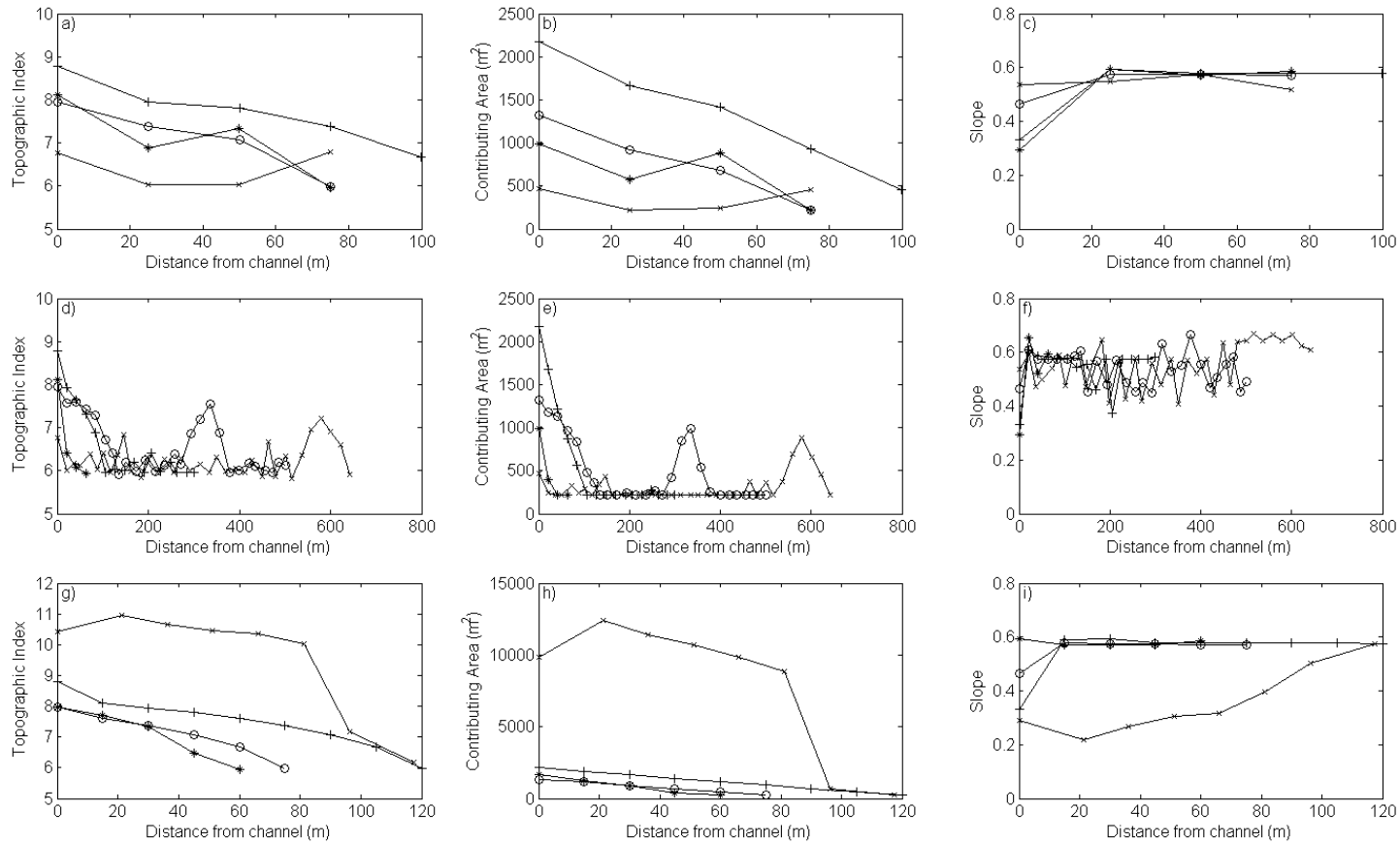
73

Figure A15. Overland flow-dominated landscape parallel-concave hillslopes topographic index, contributing area, and slope as a function of distance from the channel for a) - c) channel to ridgeline transects, d) - f) ascent transects, and g) - i) descent transects. The same symbol indicates data obtained from the same transect within each of the three sampling methods.

74

Figure A16. Overland flow-dominated landscape convergent-convex hillslopes topographic index, contributing area, and slope as a function of distance from the channel for a) - c) channel to ridgeline transects, d) - f) ascent transects, and g) - i) descent transects. The same symbol indicates data obtained from the same transect within each of the three sampling methods.
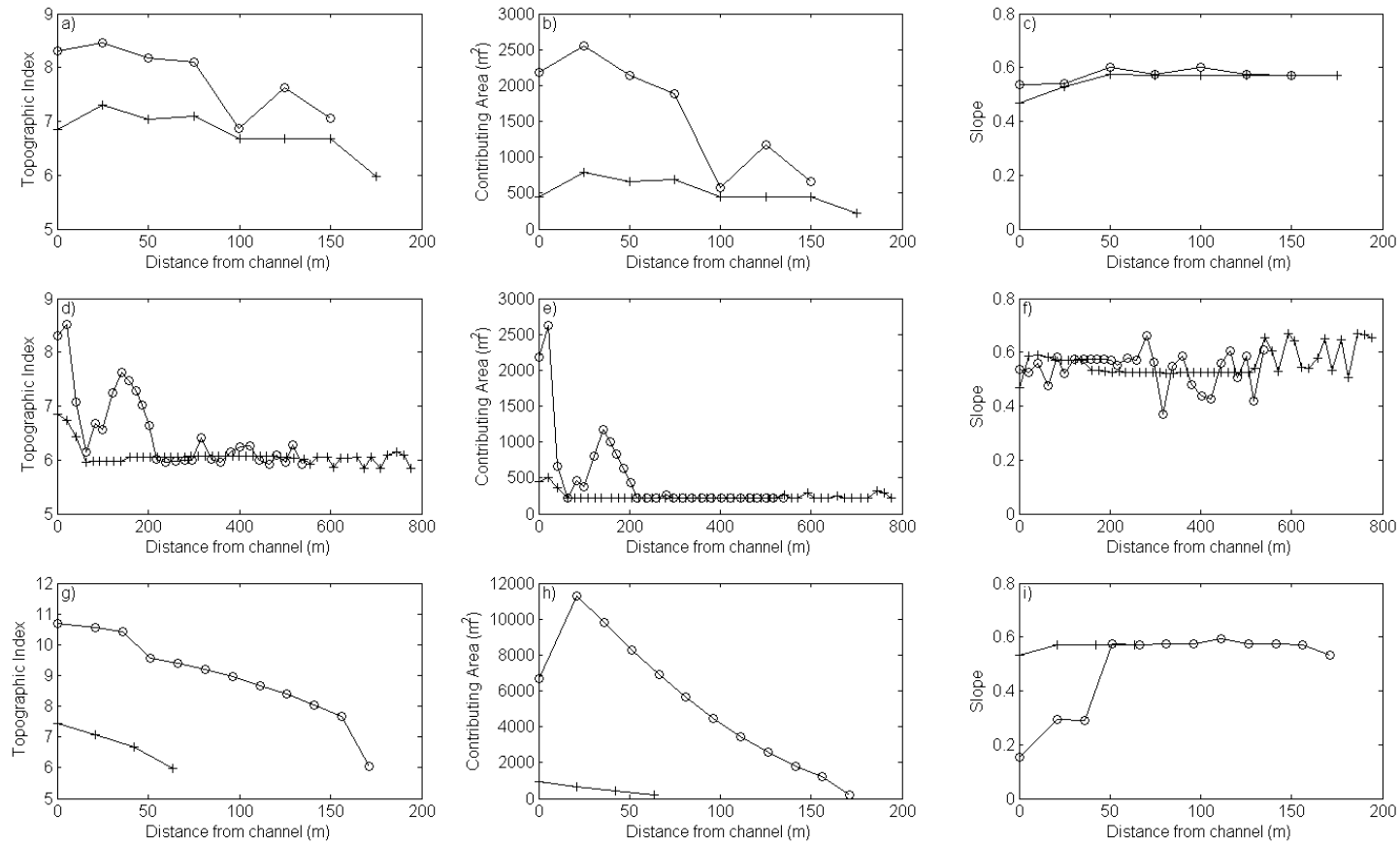
Figure A17. Overland flow-dominated landscape convergent-planar hillslopes topographic index, contributing area, and slope as a function of distance from the channel for a) - c) channel to ridgeline transects, d) - f) ascent transects, and g) - i) descent transects. The same symbol indicates data obtained from the same transect within each of the three sampling methods.
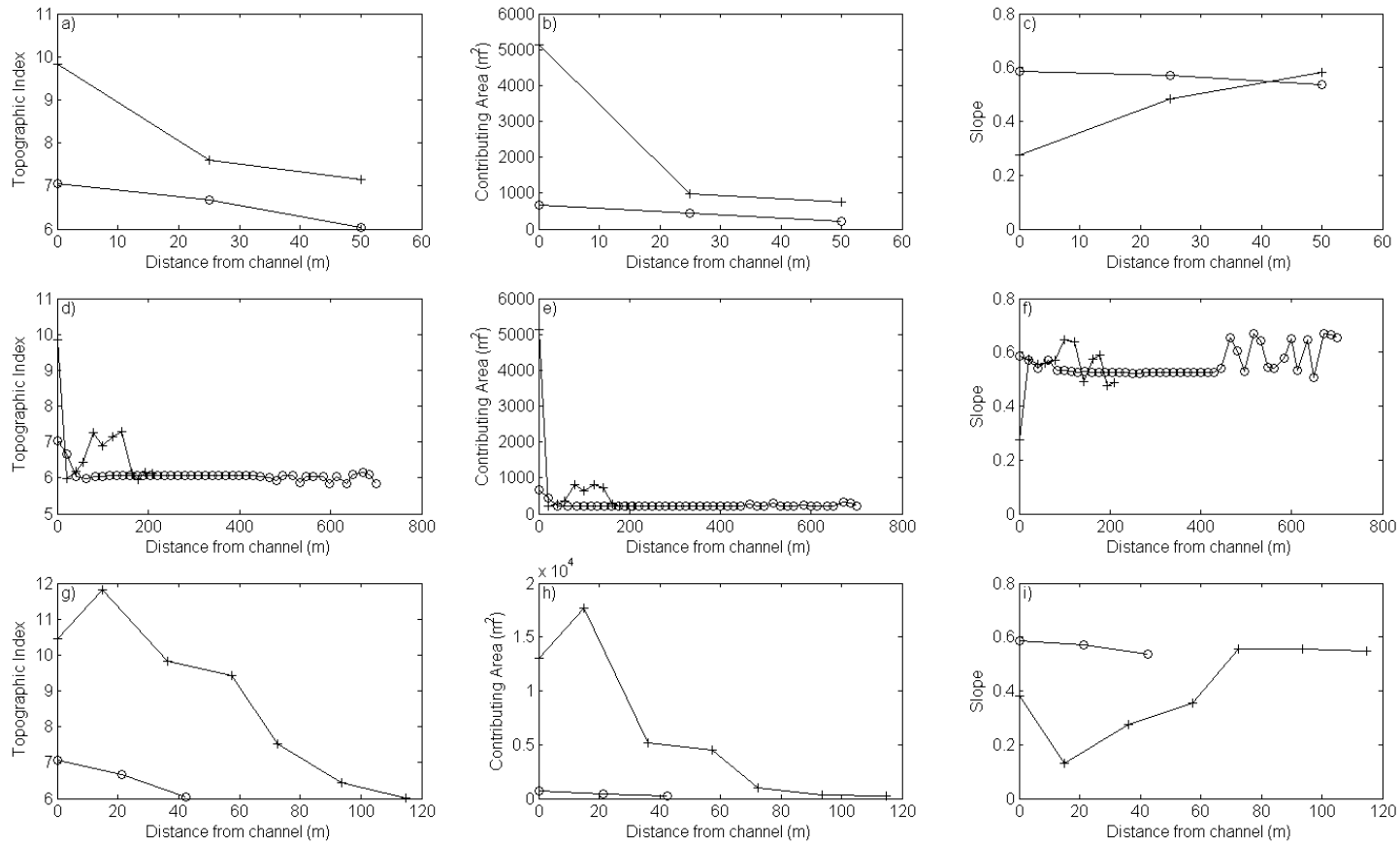
76

Figure A18. Overland flow-dominated landscape convergent-concave hillslopes topographic index, contributing area, and slope as a function of distance from the channel for a) - c) channel to ridgeline transects, d) - f) ascent transects, and g) - i) descent transects. The same symbol indicates data obtained from the same transect within each of the three sampling methods.
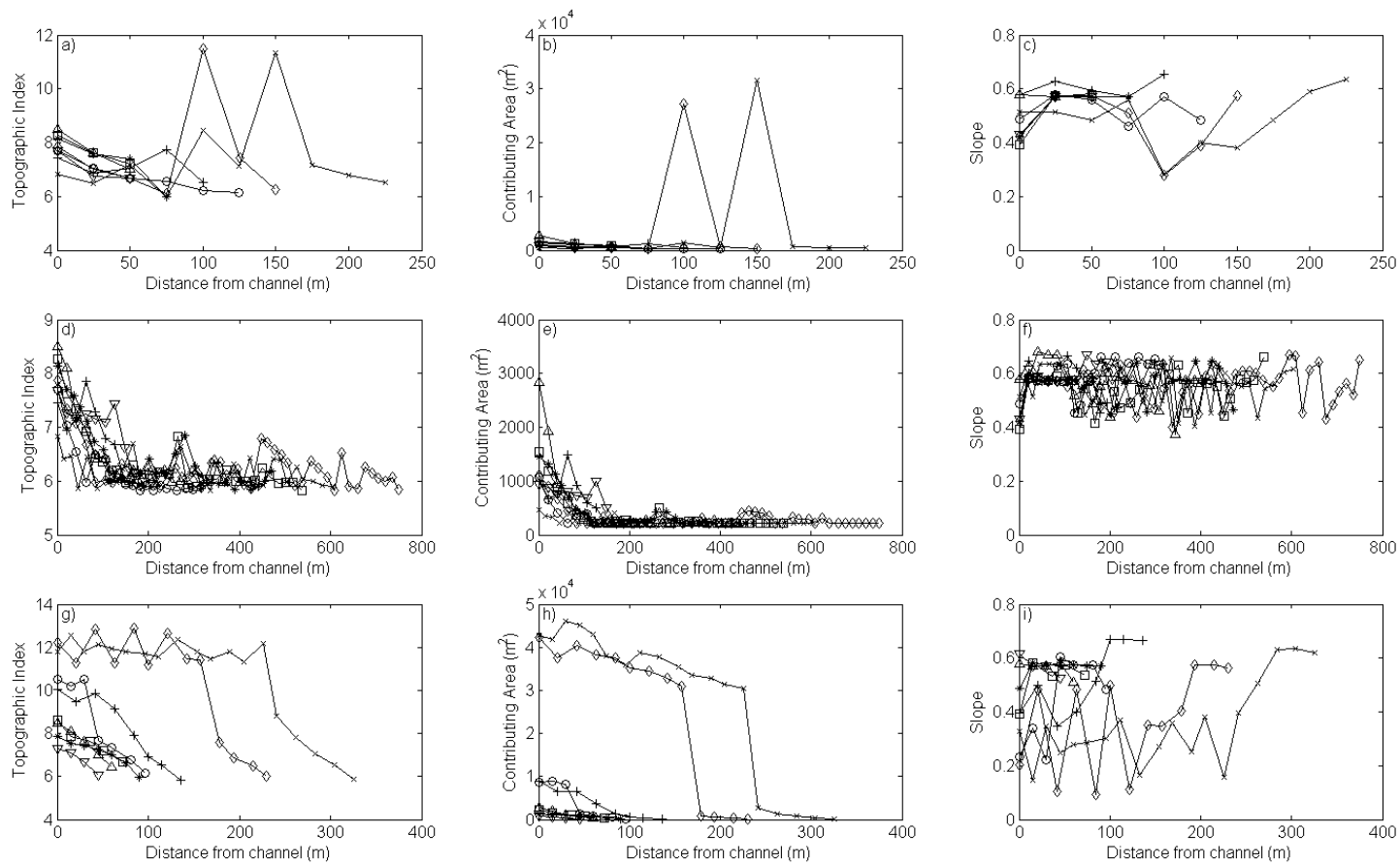
77

Figure A19. Landslide-dominated landscape divergent-convex hillslopes topographic index, contributing area, and slope as a function of distance from the channel for a) - c) channel to ridgeline transects, d) - f) ascent transects, and g) - i) descent transects. The same symbol indicates data obtained from the same transect within each of the three sampling methods.
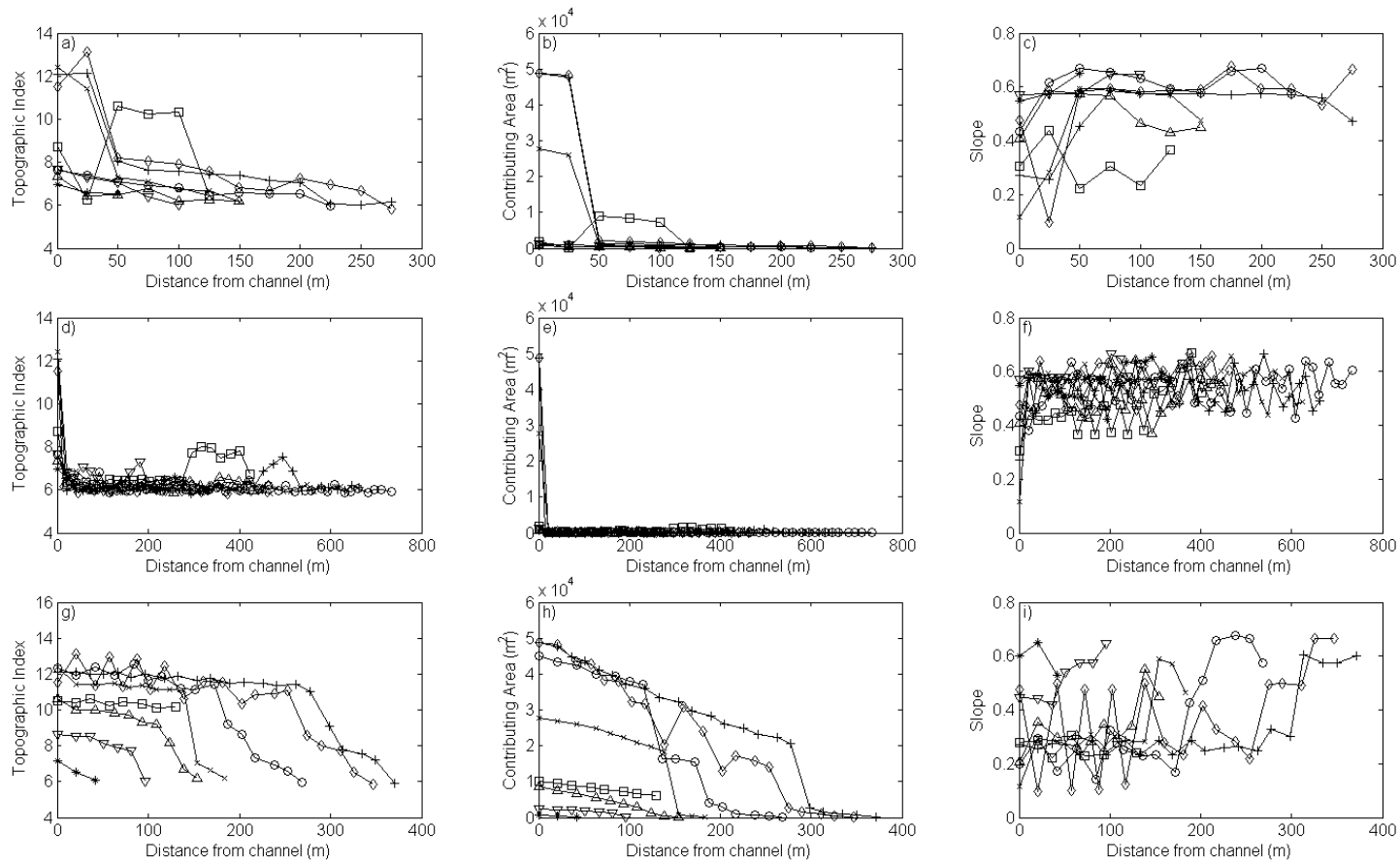
Figure A20. Landslide-dominated landscape divergent-planar hillslopes topographic index, contributing area, and slope as a function of distance from the channel for a) - c) channel to ridgeline transects, d) - f) ascent transects, and g) - i) descent transects. The same symbol indicates data obtained from the same transect within each of the three sampling methods.

79

Figure A21. Landslide-dominated landscape divergent-concave hillslopes topographic index, contributing area, and slope as a function of distance from the channel for a) - c) channel to ridgeline transects, d) - f) ascent transects, and g) - i) descent transects. The same symbol indicates data obtained from the same transect within each of the three sampling methods.
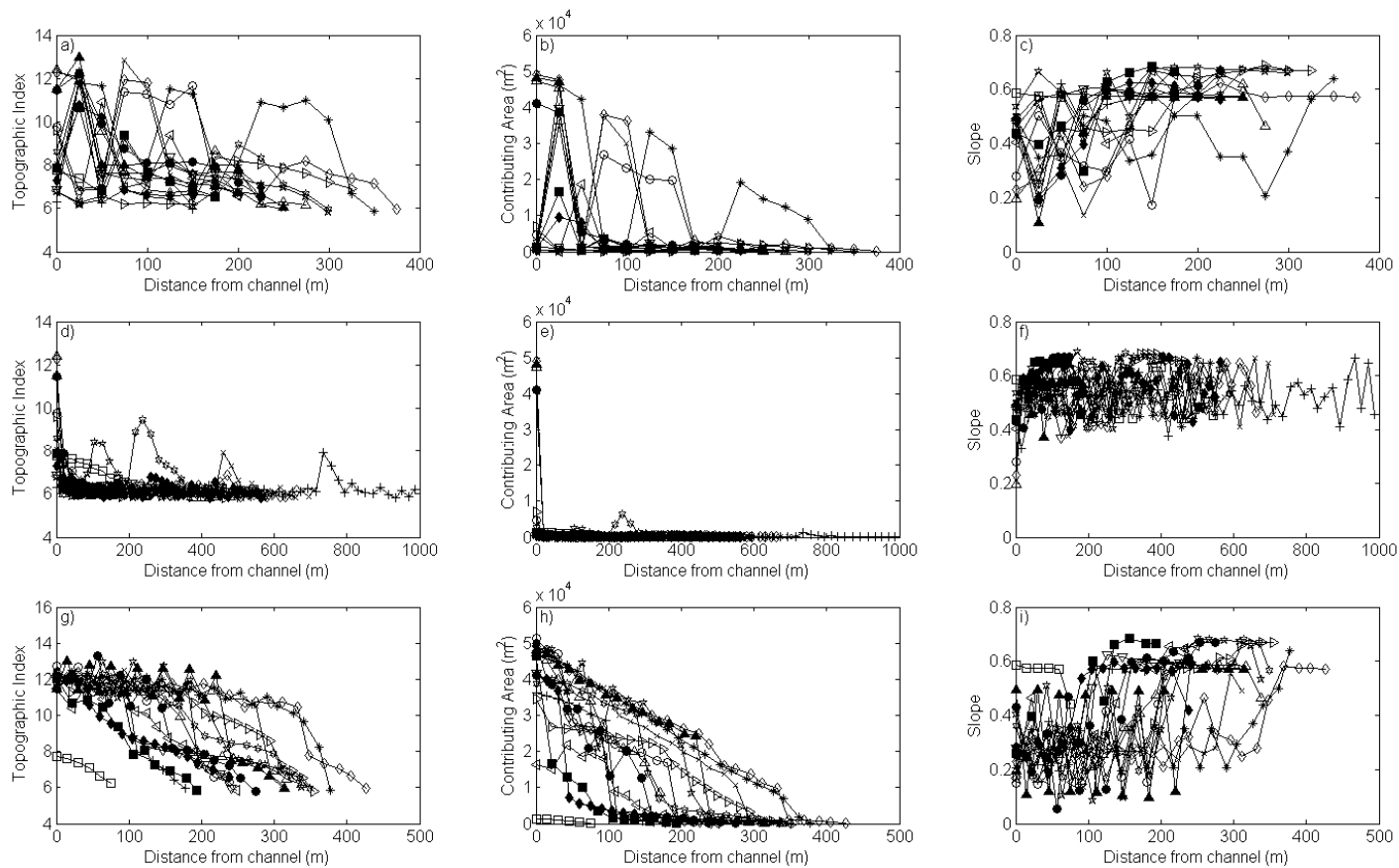
80

Figure A22. Landslide-dominated landscape parallel-convex hillslopes topographic index, contributing area, and slope as a function of distance from the channel for a) - c) channel to ridgeline transects, d) - f) ascent transects, and g) - i) descent transects. The same symbol indicates data obtained from the same transect within each of the three sampling methods.

81

Figure A23. Landslide-dominated landscape parallel-planar hillslopes topographic index, contributing area, and slope as a function of distance from the channel for a) - c) channel to ridgeline transects, d) - f) ascent transects, and g) - i) descent transects. The same symbol indicates data obtained from the same transect within each of the three sampling methods.

82

Figure A24. Landslide-dominated landscape parallel-concave hillslopes topographic index, contributing area, and slope as a function of distance from the channel for a) - c) channel to ridgeline transects, d) - f) ascent transects, and g) - i) descent transects. The same symbol indicates data obtained from the same transect within each of the three sampling methods.

Figure A25. Landslide-dominated landscape convergent-convex hillslopes topographic index, contributing area, and slope as a function of distance from the channel for a) - c) channel to ridgeline transects, d) - f) ascent transects, and g) - i) descent transects. The same symbol indicates data obtained from the same transect within each of the three sampling methods.

84

Figure A26. Landslide-dominated landscape convergent-planar hillslopes topographic index, contributing area, and slope as a function of distance from the channel for a) - c) channel to ridgeline transects, d) - f) ascent transects, and g) - i) descent transects. The same symbol indicates data obtained from the same transect within each of the three sampling methods.

85

Figure A27. Landslide-dominated landscape convergent-concave hillslopes topographic index, contributing area, and slope as a function of distance from the channel for a) - c) channel to ridgeline transects, d) - f) ascent transects, and g) - i) descent transects. The same symbol indicates data obtained from the same transect within each of the three sampling methods.

86

APPENDIX B
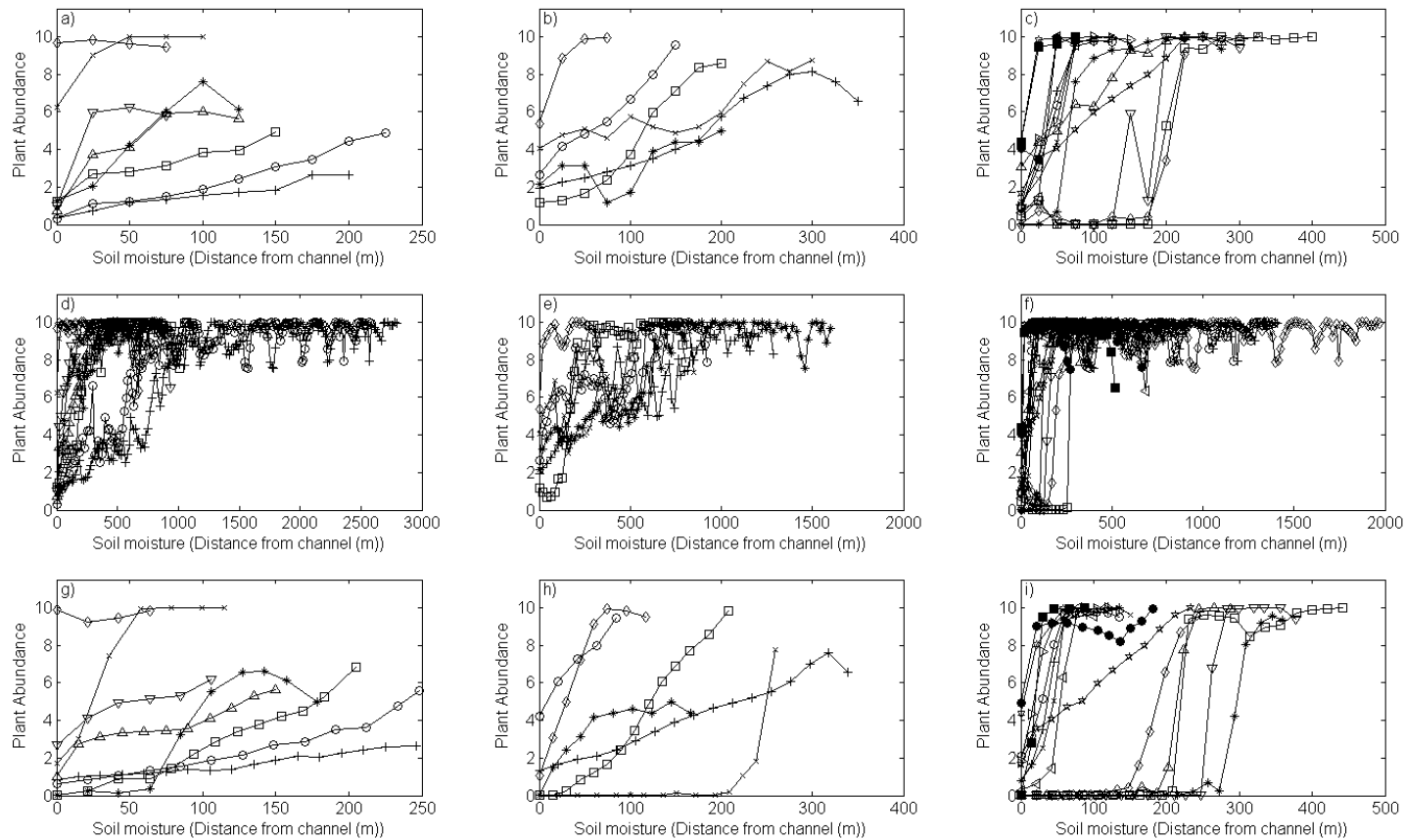
Figure B1. Creep-dominated landscape divergent-convex (left), divergent-planar (middle), and divergent-concave (right) hillslope plant tolerance curves where soil moisture is approximated by distance from the channel (wet) to the ridgeline (dry) for a) - c) channel to ridgeline transects, d) - f) ascent transects, and g) - i) descent transects. The same symbol indicates data obtained from the same hillslope (ex. divergent-convex) for each of the three sampling methods (i.e. channel to ridgeline, ascent and descent).
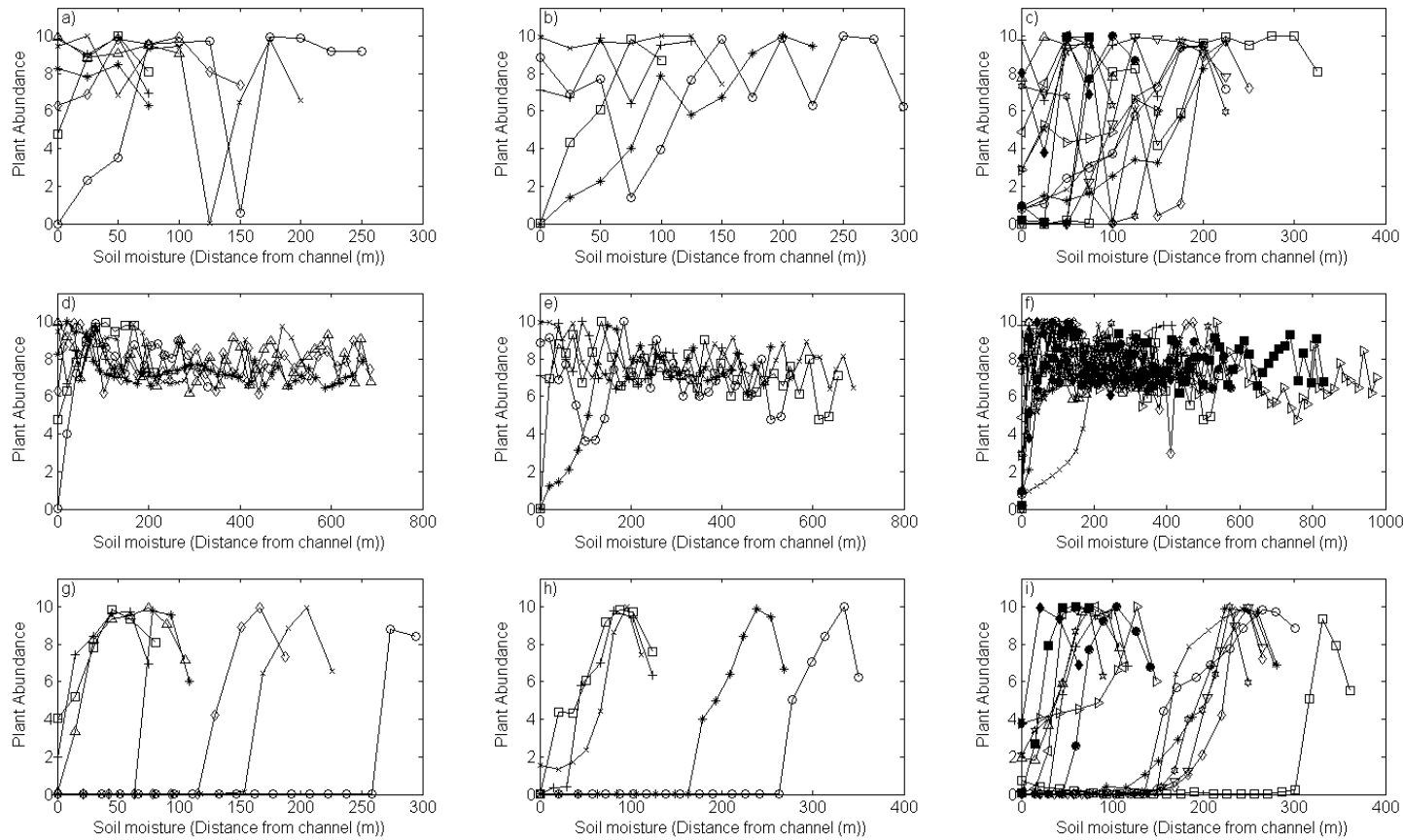
88
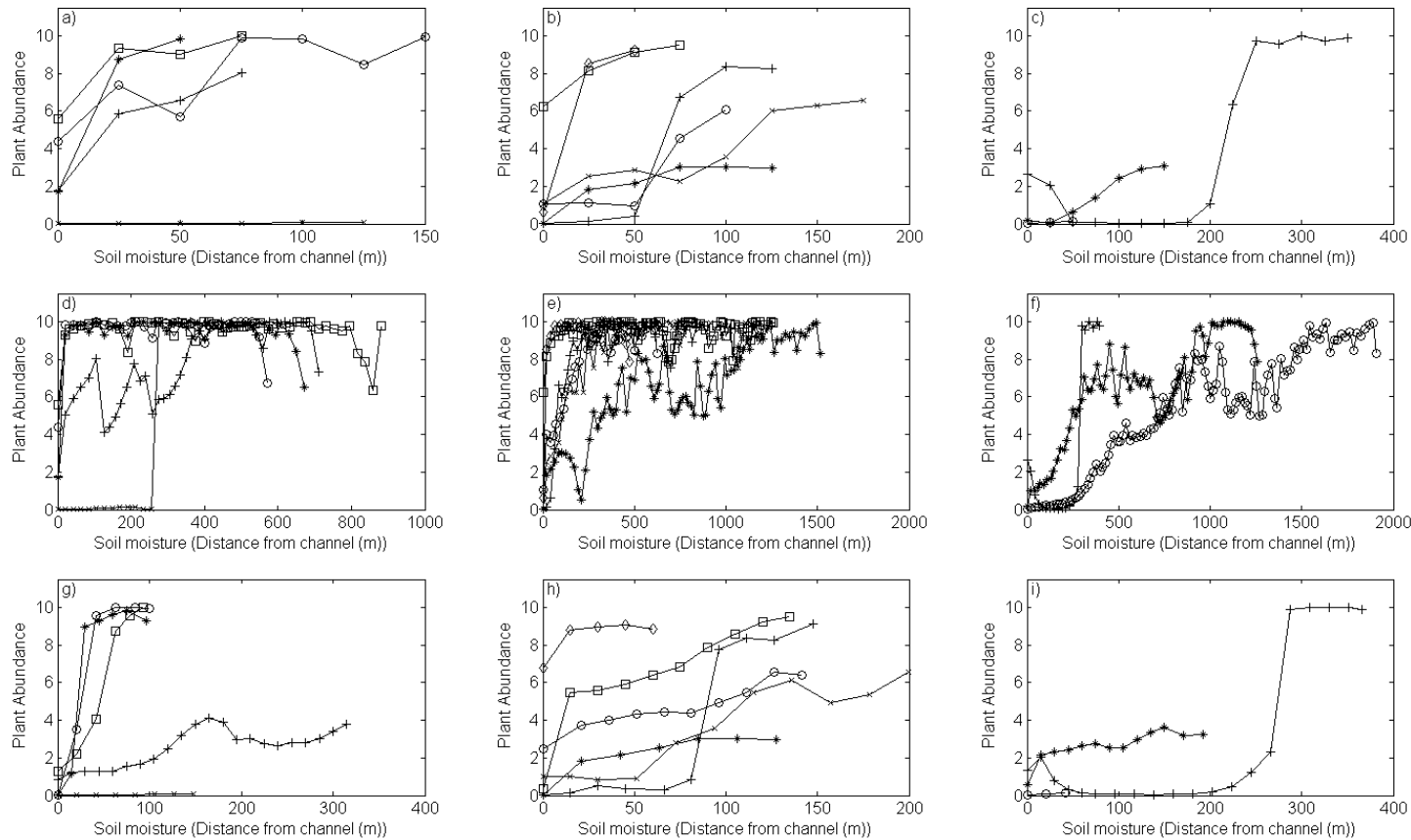
Figure B2. Creep-dominated landscape parallel-convex (left), parallel-planar (middle), and parallel-concave (right) hillslope plant tolerance curves where soil moisture is approximated by distance from the channel (wet) to the ridgeline (dry) for a) - c) channel to ridgeline transects, d) - f) ascent transects, and g) - i) descent transects. The same symbol indicates data obtained from the same hillslope (ex. parallel-convex) for each of the three sampling methods (i.e. channel to ridgeline, ascent and descent).

89
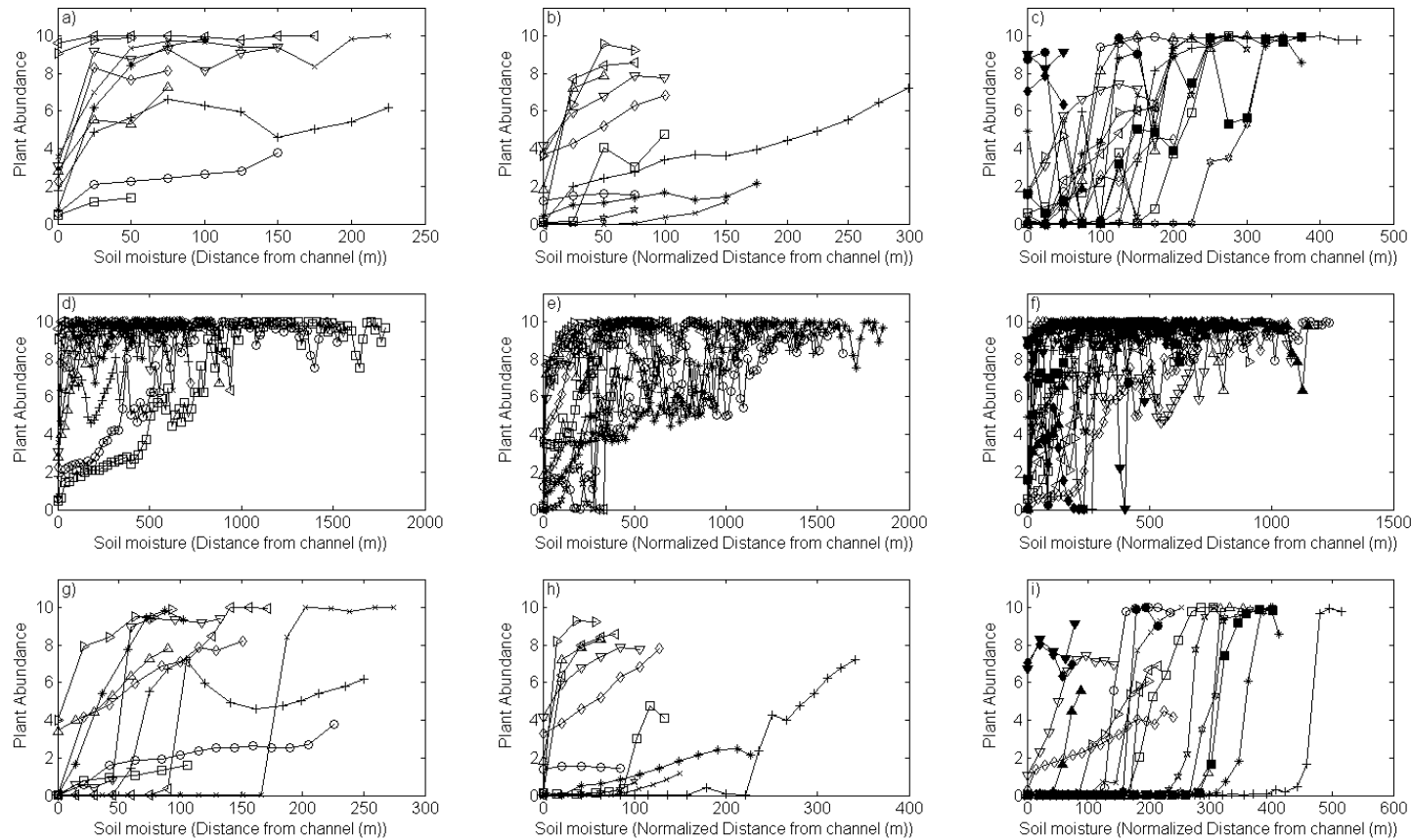
Figure B3. Creep-dominated landscape convergent-convex (left), convergent-planar (middle), and convergent-concave (right) hillslope plant tolerance curves where soil moisture is approximated by distance from the channel (wet) to the ridgeline (dry) for a) - c) channel to ridgeline transects, d) - f) ascent transects, and g) - i) descent transects. The same symbol indicates data obtained from the same hillslope (ex. convergent-convex) for each of the three sampling methods (i.e. channel to ridgeline, ascent and descent).
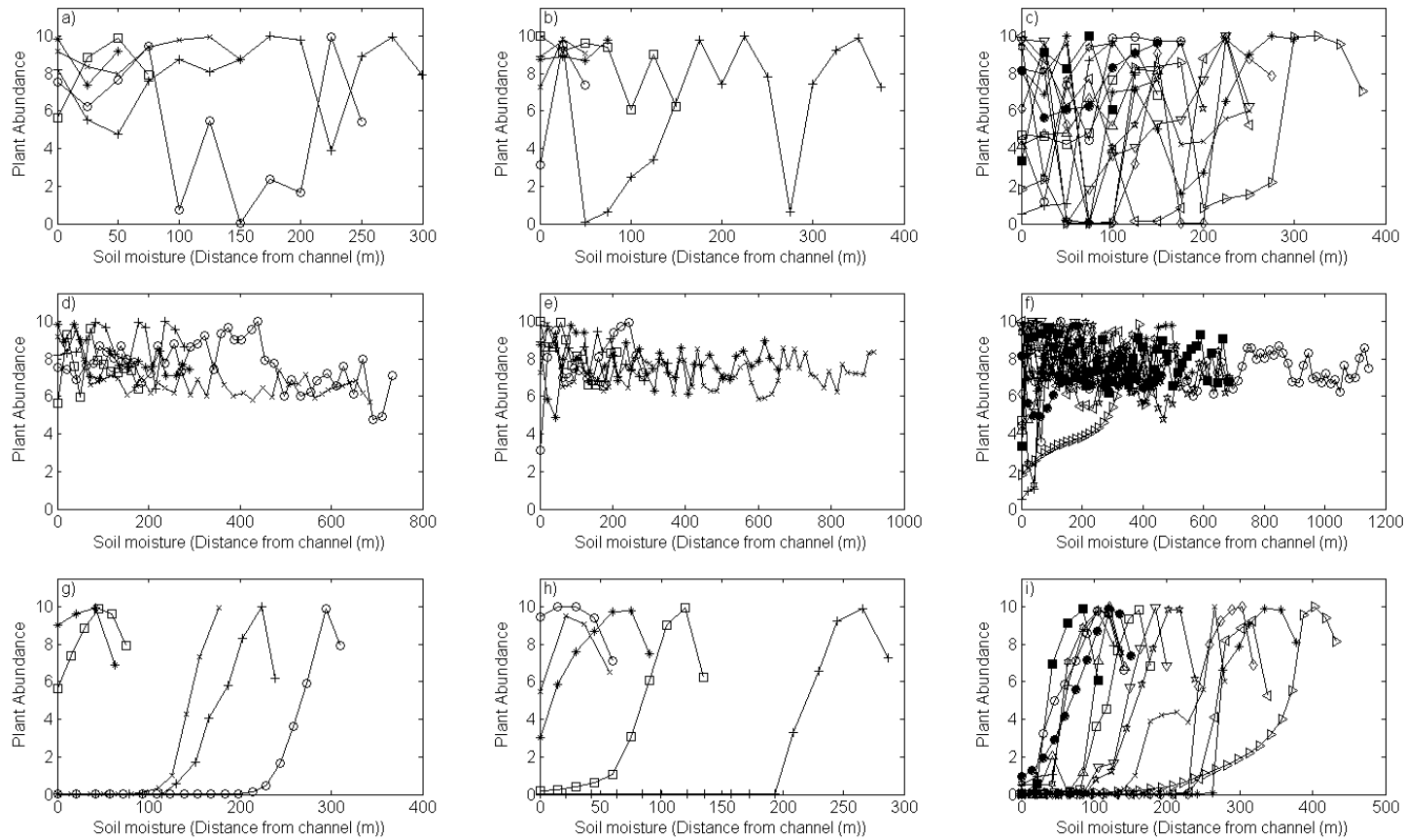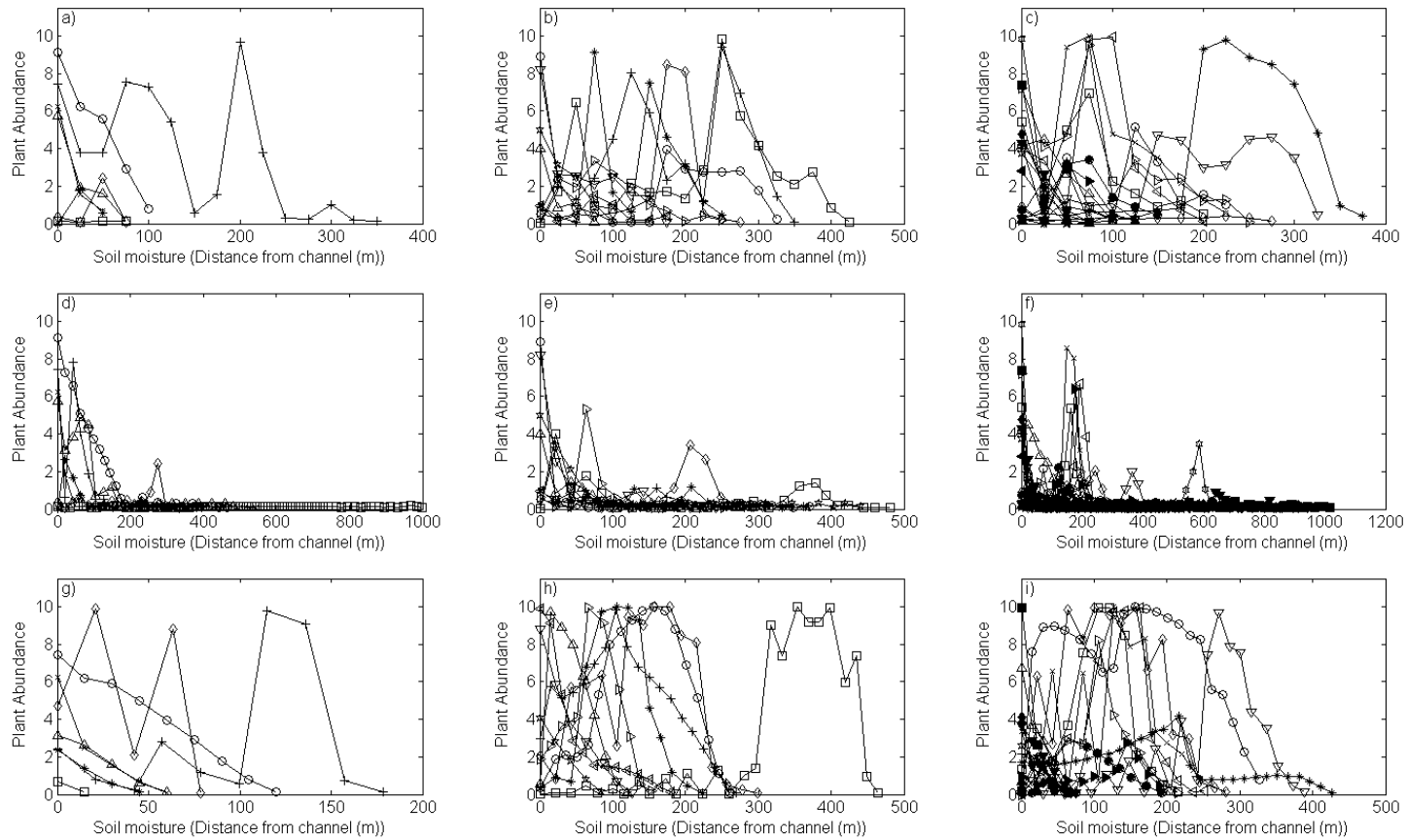
Figure B4. Overland flow-dominated landscape divergent-convex (left), divergent-planar (middle), and divergent-concave (right) hillslope plant tolerance curves where soil moisture is approximated by distance from the channel (wet) to the ridgeline (dry) for a) - c) channel to ridgeline transects, d) - f) ascent transects, and g) - i) descent transects. The same symbol indicates data obtained from the same hillslope (ex. divergent-convex) for each of the three sampling methods (i.e. channel to ridgeline, ascent and descent).
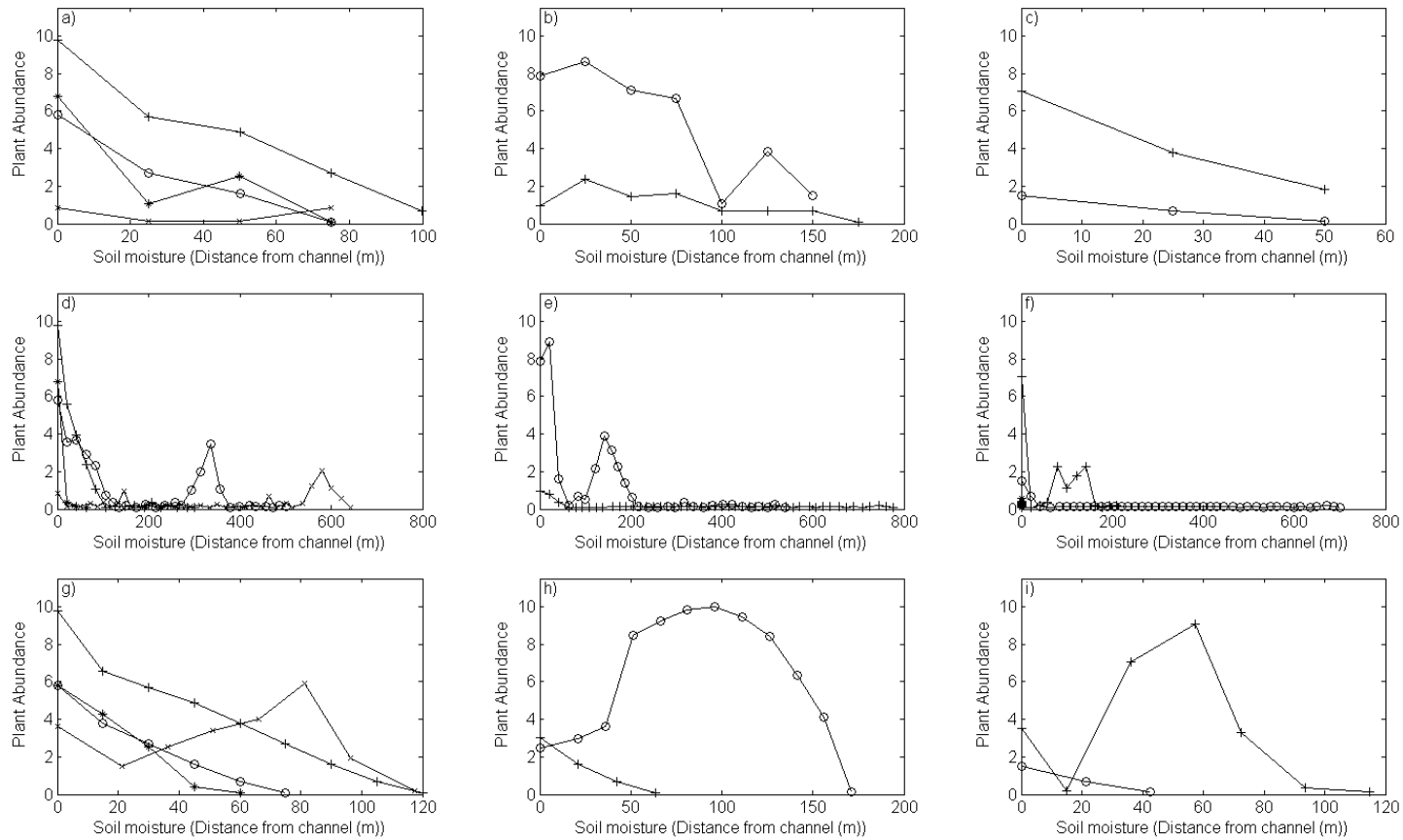
91
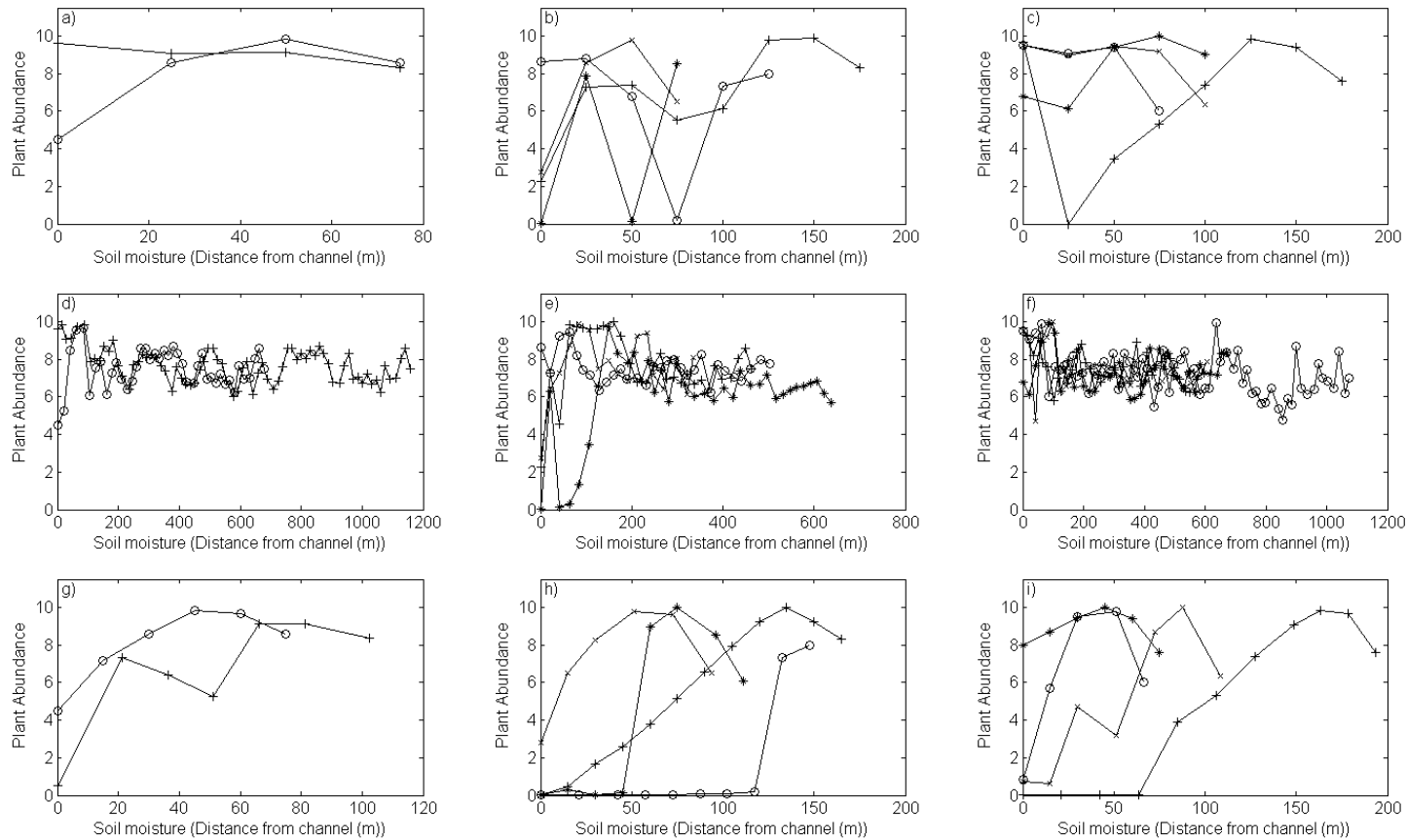
Figure B5. Overland flow-dominated landscape parallel-convex (left), parallel-planar (middle), and parallel-concave (right) hillslope plant tolerance curves where soil moisture is approximated by distance from the channel (wet) to the ridgeline (dry) for a) - c) channel to ridgeline transects, d) - f) ascent transects, and g) - i) descent transects. The same symbol indicates data obtained from the same hillslope (ex. parallel-convex) for each of the three sampling methods (i.e. channel to ridgeline, ascent and descent).
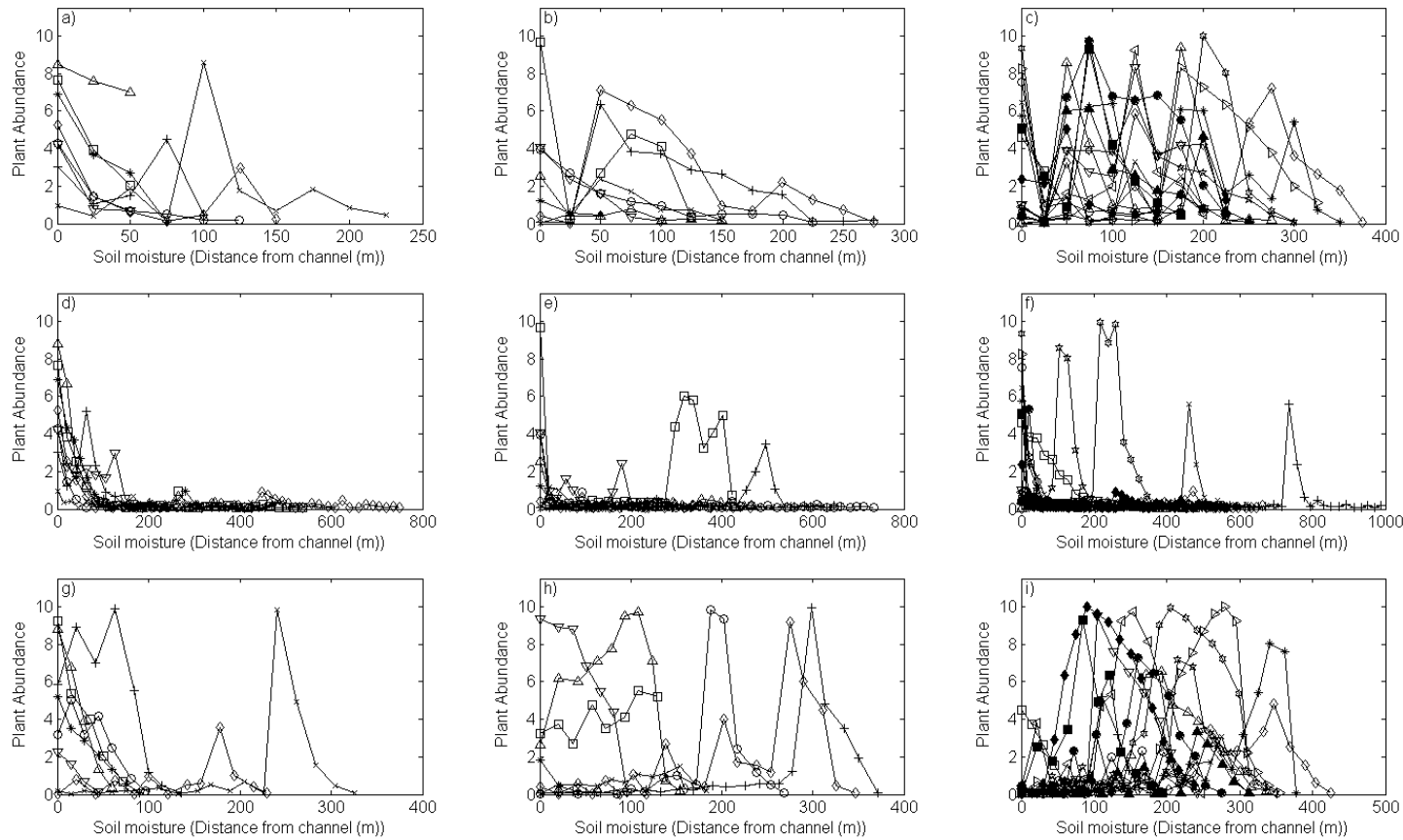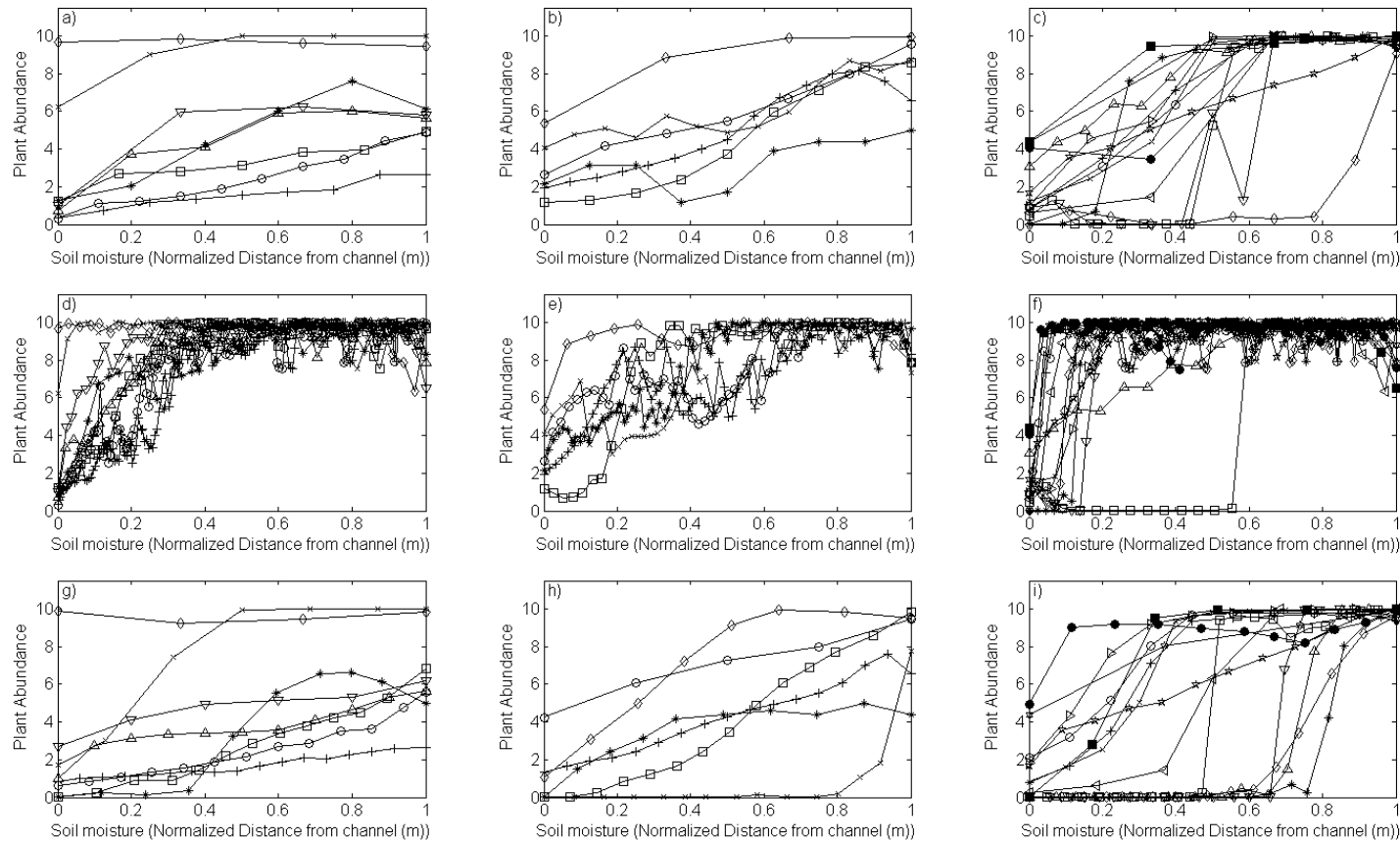
Figure B6. Overland flow-dominated landscape convergent-convex (left), convergent-planar (middle), and convergent-concave (right) hillslope plant tolerance curves where soil moisture is approximated by distance from the channel (wet) to the ridgeline (dry) for a) - c) channel to ridgeline transects, d) - f) ascent transects, and g) - i) descent transects. The same symbol indicates data obtained from the same hillslope (ex. convergent-convex) for each of the three sampling methods (i.e. channel to ridgeline, ascent and descent).
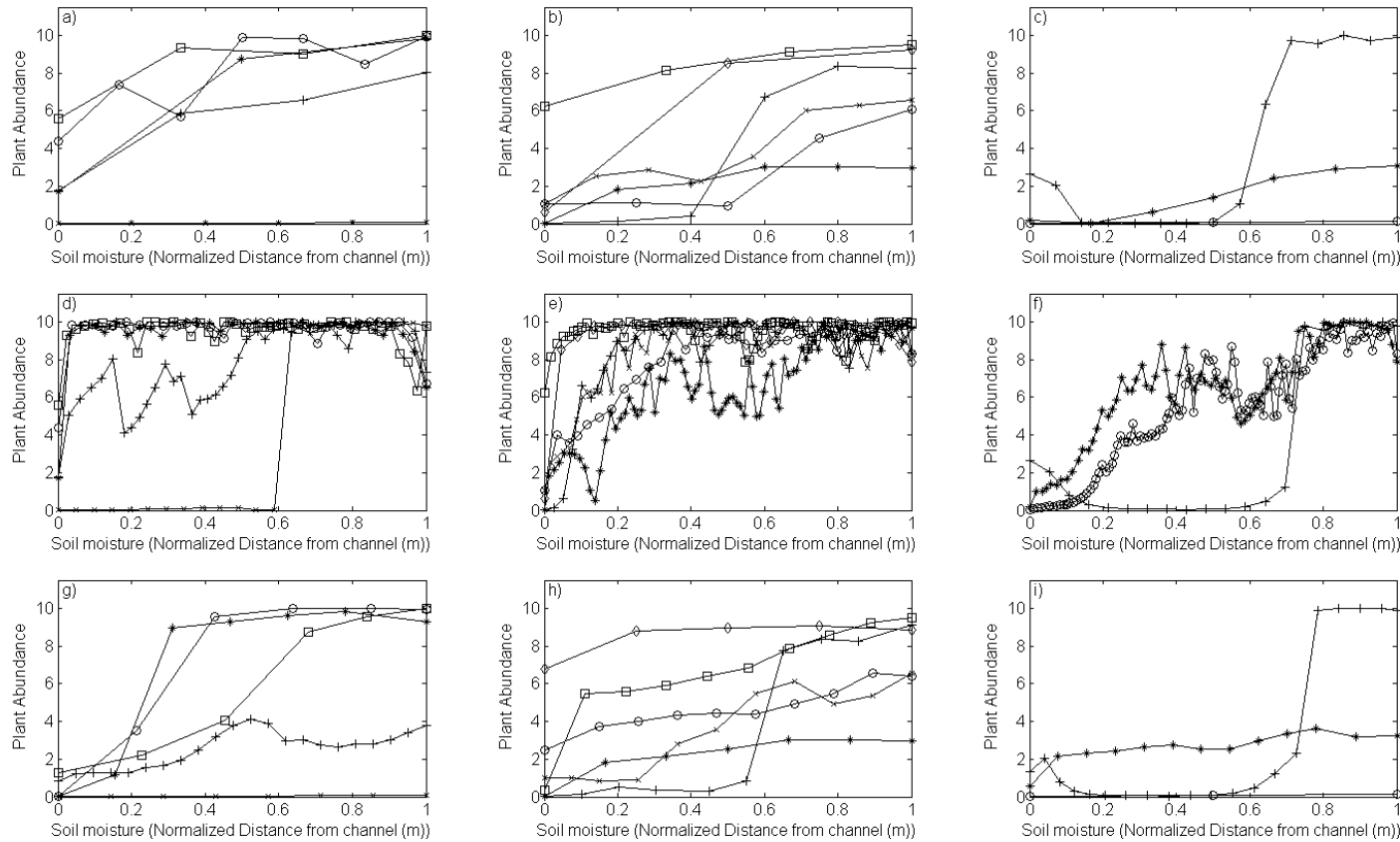
Figure B7. Landslide-dominated landscape divergent-convex (left), divergent-planar (middle), and divergent-concave (right) hillslope plant tolerance curves where soil moisture is approximated by distance from the channel (wet) to the ridgeline (dry) for a) - c) channel to ridgeline transects, d) - f) ascent transects, and g) - i) descent transects. The same symbol indicates data obtained from the same hillslope (ex. divergent-convex) for each of the three sampling methods (i.e. channel to ridgeline, ascent and descent).
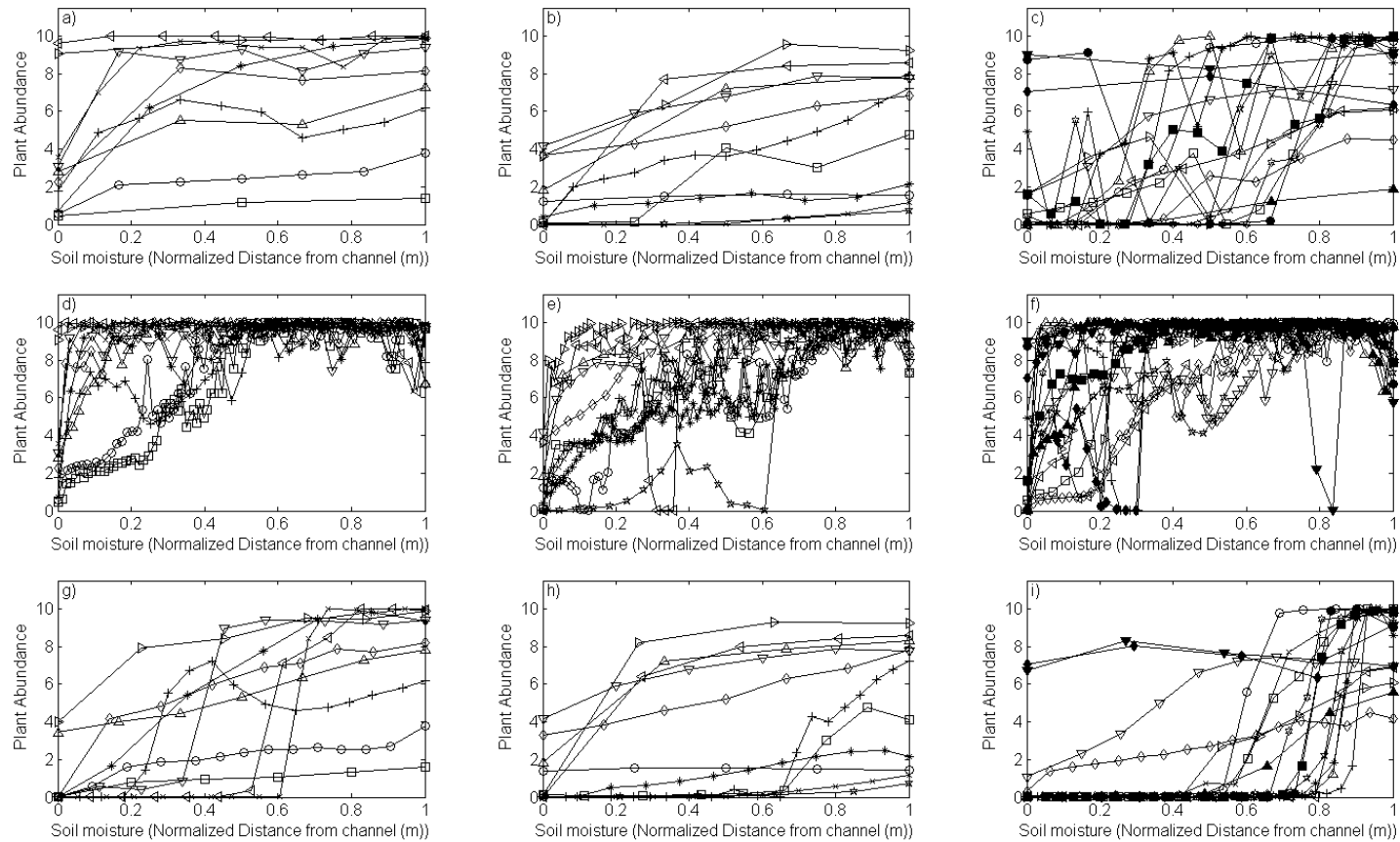
Figure B8. Landslide-dominated landscape parallel-convex (left), parallel-planar (middle), and parallel-concave (right) hillslope plant tolerance curves where soil moisture is approximated by distance from the channel (wet) to the ridgeline (dry) for a) - c) channel to ridgeline transects, d) - f) ascent transects, and g) - i) descent transects. The same symbol indicates data obtained from the same hillslope (ex. parallel-convex) for each of the three sampling methods (i.e. channel to ridgeline, ascent and descent).
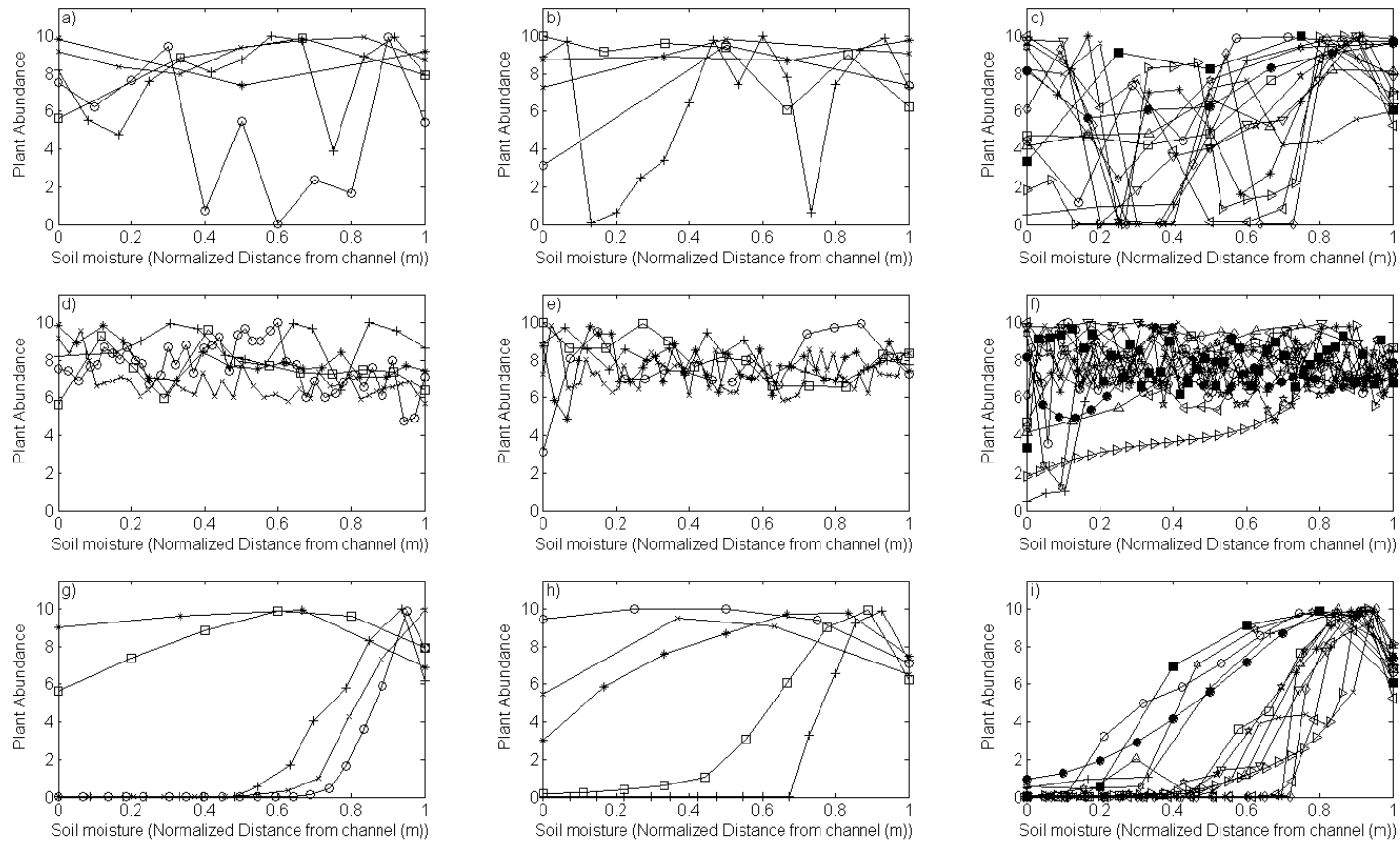
Figure B9. Landslide-dominated landscape convergent-convex (left), convergent-planar (middle), and convergent-concave (right) hillslope plant tolerance curves where soil moisture is approximated by distance from the channel (wet) to the ridgeline (dry) for a) - c) channel to ridgeline transects, d) - f) ascent transects, and g) - i) descent transects. The same symbol indicates data obtained from the same hillslope (ex. convergent-convex) for each of the three sampling methods (i.e. channel to ridgeline, ascent and descent).
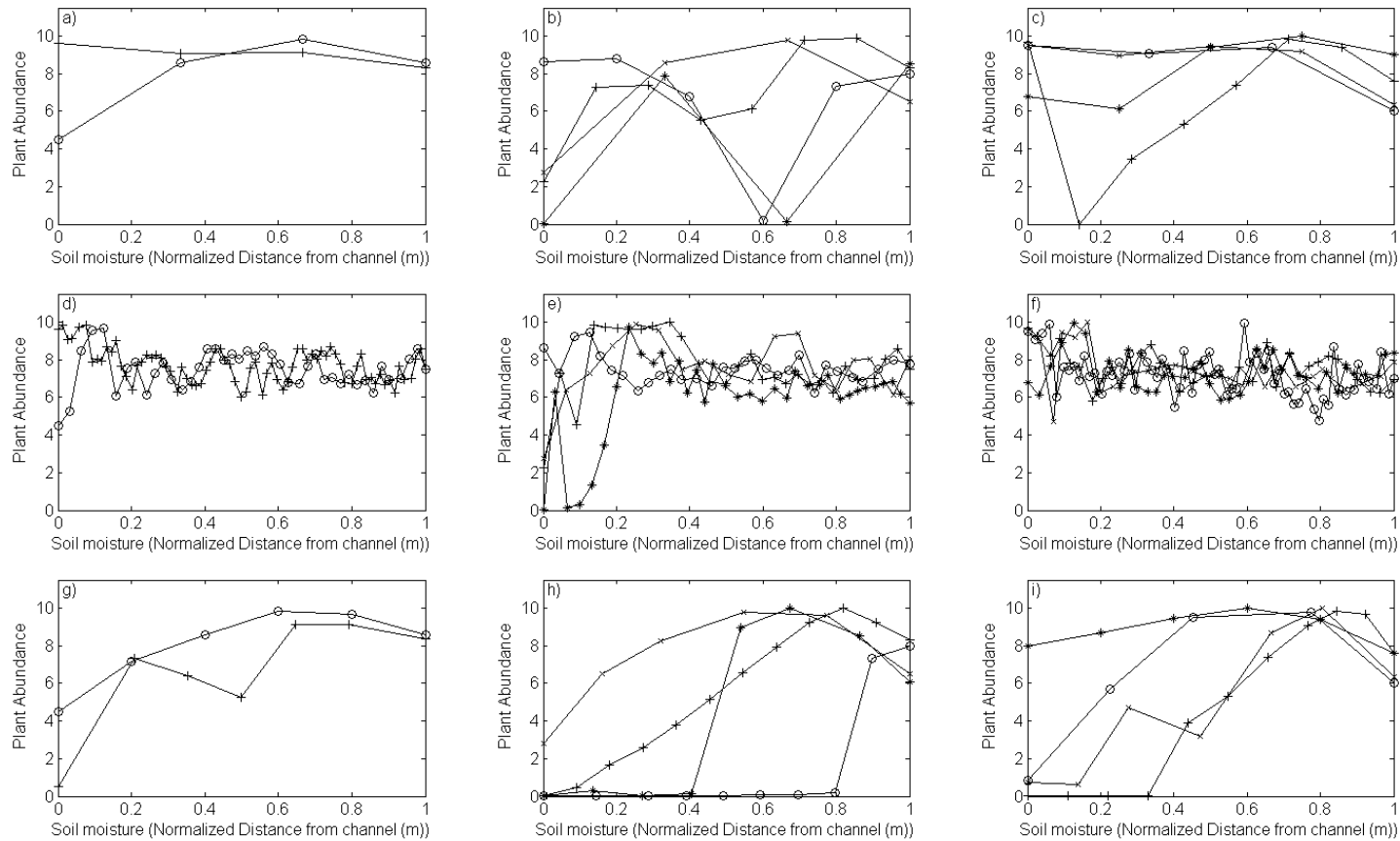
Figure B10. Creep-dominated landscape divergent-convex (left), divergent-planar (middle), and divergent-concave (right) hillslope plant tolerance curves where soil moisture is approximated by normalized distance from the channel (wet) to the ridgeline (dry) for a) - c) channel to ridgeline transects, d) - f) ascent transects, and g) - i) descent transects. The same symbol indicates data obtained from the same hillslope (ex. divergent-convex) for each of the three sampling methods (i.e. channel to ridgeline, ascent and descent).

97

Figure B11. Creep-dominated landscape parallel-convex (left), parallel-planar (middle), and parallel-concave (right) hillslope plant tolerance curves where soil moisture is approximated by normalized distance from the channel (wet) to the ridgeline (dry) for a) - c) channel to ridgeline transects, d) - f) ascent transects, and g) - i) descent transects. The same symbol indicates data obtained from the same hillslope (ex. parallel-convex) for each of the three sampling methods (i.e. channel to ridgeline, ascent and descent).
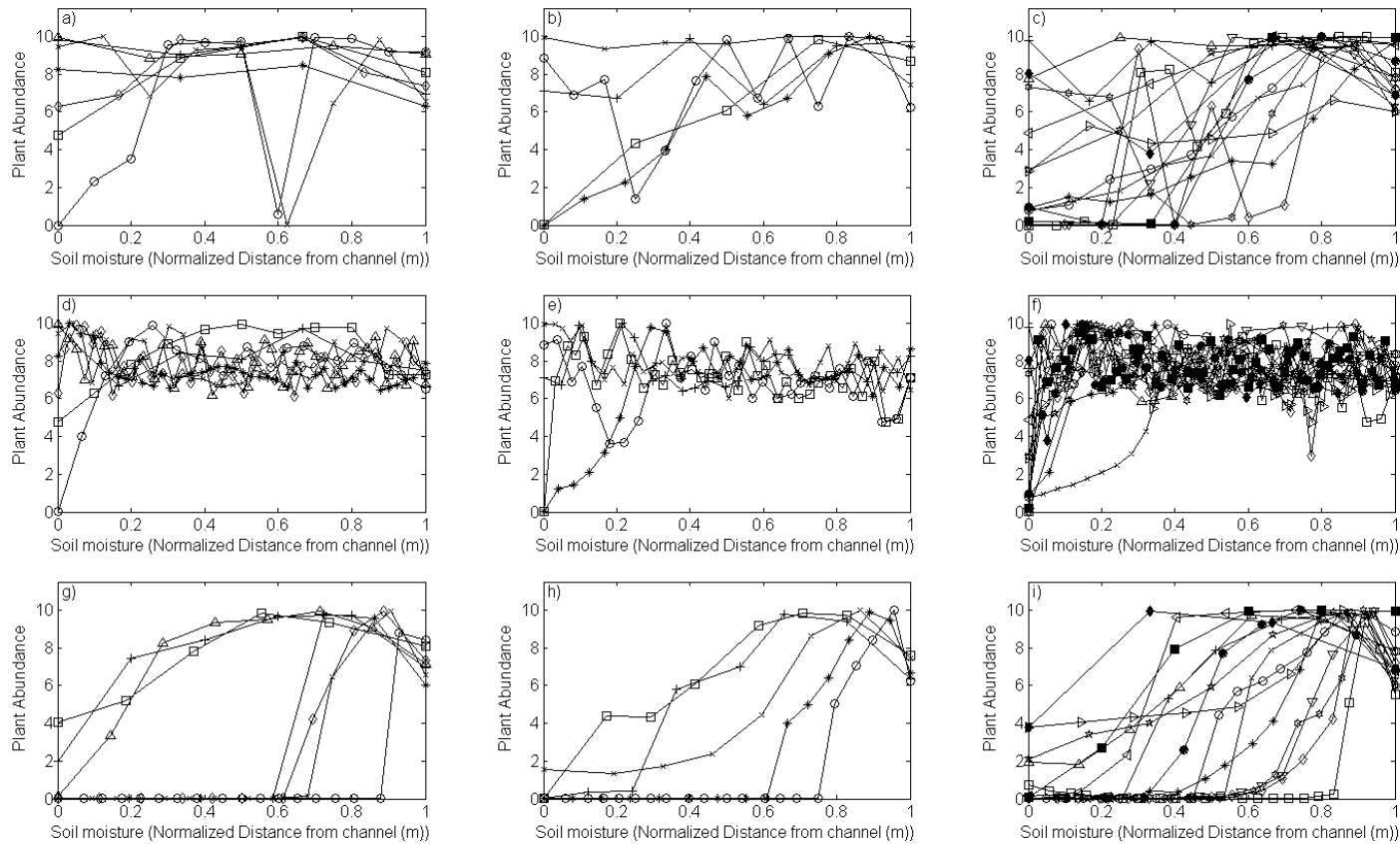
Figure B12. Creep-dominated landscape convergent-convex (left), convergent-planar (middle), and convergent-concave (right) hillslope plant tolerance curves where soil moisture is approximated by normalized distance from the channel (wet) to the ridgeline (dry) for a) - c) channel to ridgeline transects, d) - f) ascent transects, and g) - i) descent transects. The same symbol indicates data obtained from the same hillslope (ex. convergent-convex) for each of the three sampling methods (i.e. channel to ridgeline, ascent and descent).
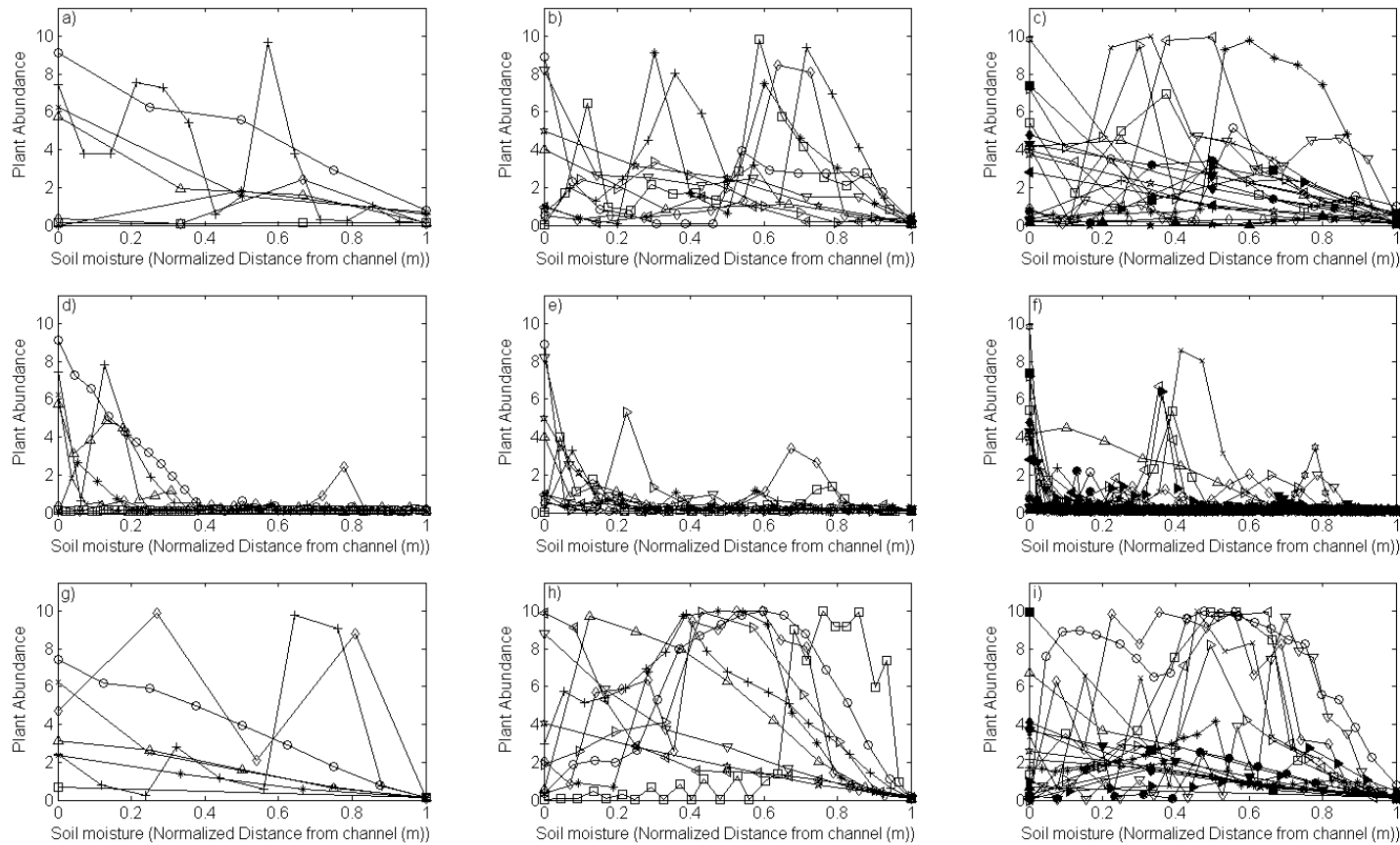
Figure B13. Overland flow-dominated landscape divergent-convex (left), divergent-planar (middle), and divergent-concave (right) hillslope plant tolerance curves where soil moisture is approximated by normalized distance from the channel (wet) to the ridgeline (dry) for a) - c) channel to ridgeline transects, d) - f) ascent transects, and g) - i) descent transects. The same symbol indicates data obtained from the same hillslope (ex. divergent-convex) for each of the three sampling methods (i.e. channel to ridgeline, ascent and descent).
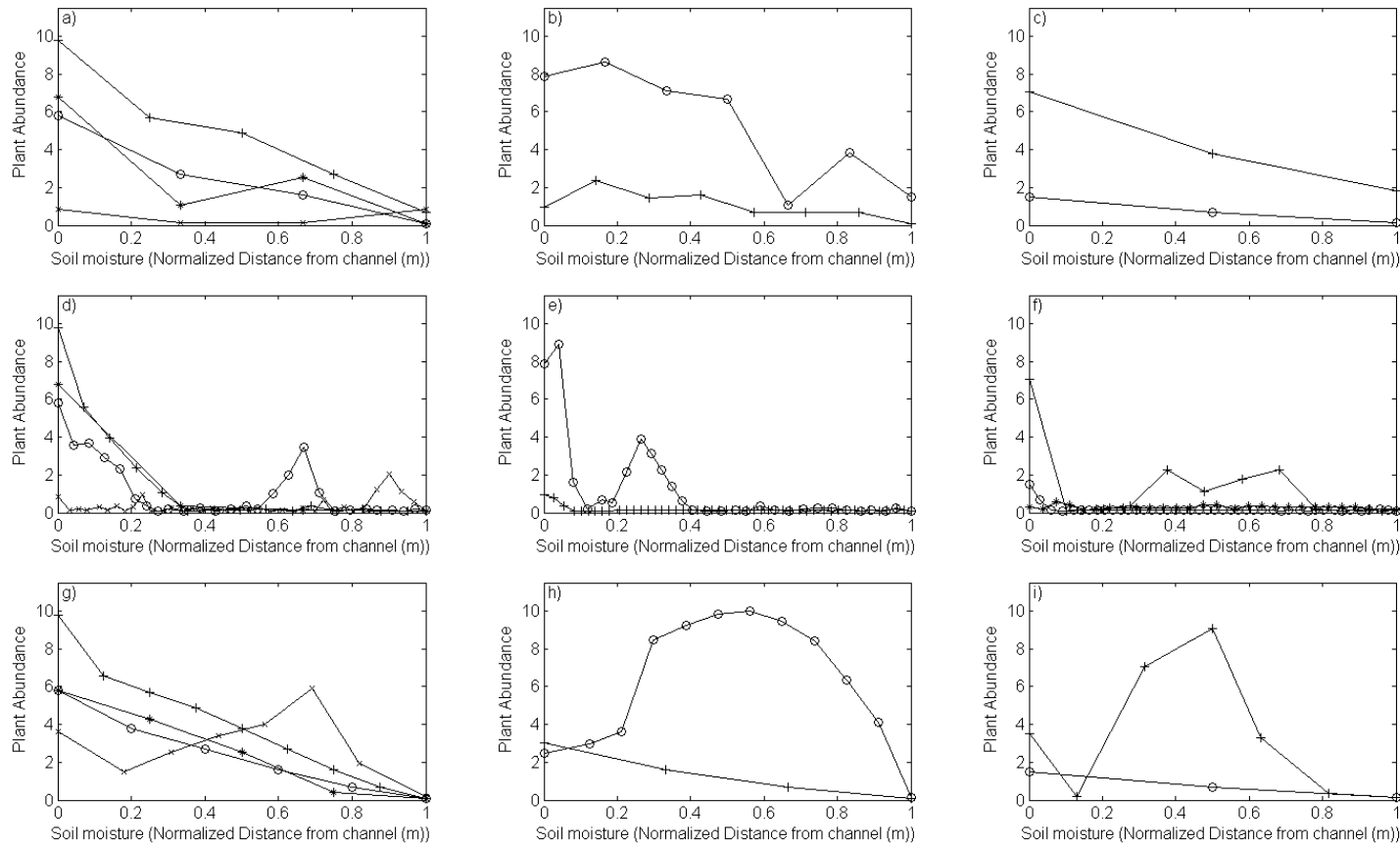
Figure B14. Overland flow-dominated landscape parallel-convex (left), parallel-planar (middle), and parallel-concave (right) hillslope plant tolerance curves where soil moisture is approximated by normalized distance from the channel (wet) to the ridgeline (dry) for a) - c) channel to ridgeline transects, d) - f) ascent transects, and g) - i) descent transects. The same symbol indicates data obtained from the same hillslope (ex. parallel-convex) for each of the three sampling methods (i.e. channel to ridgeline, ascent and descent).
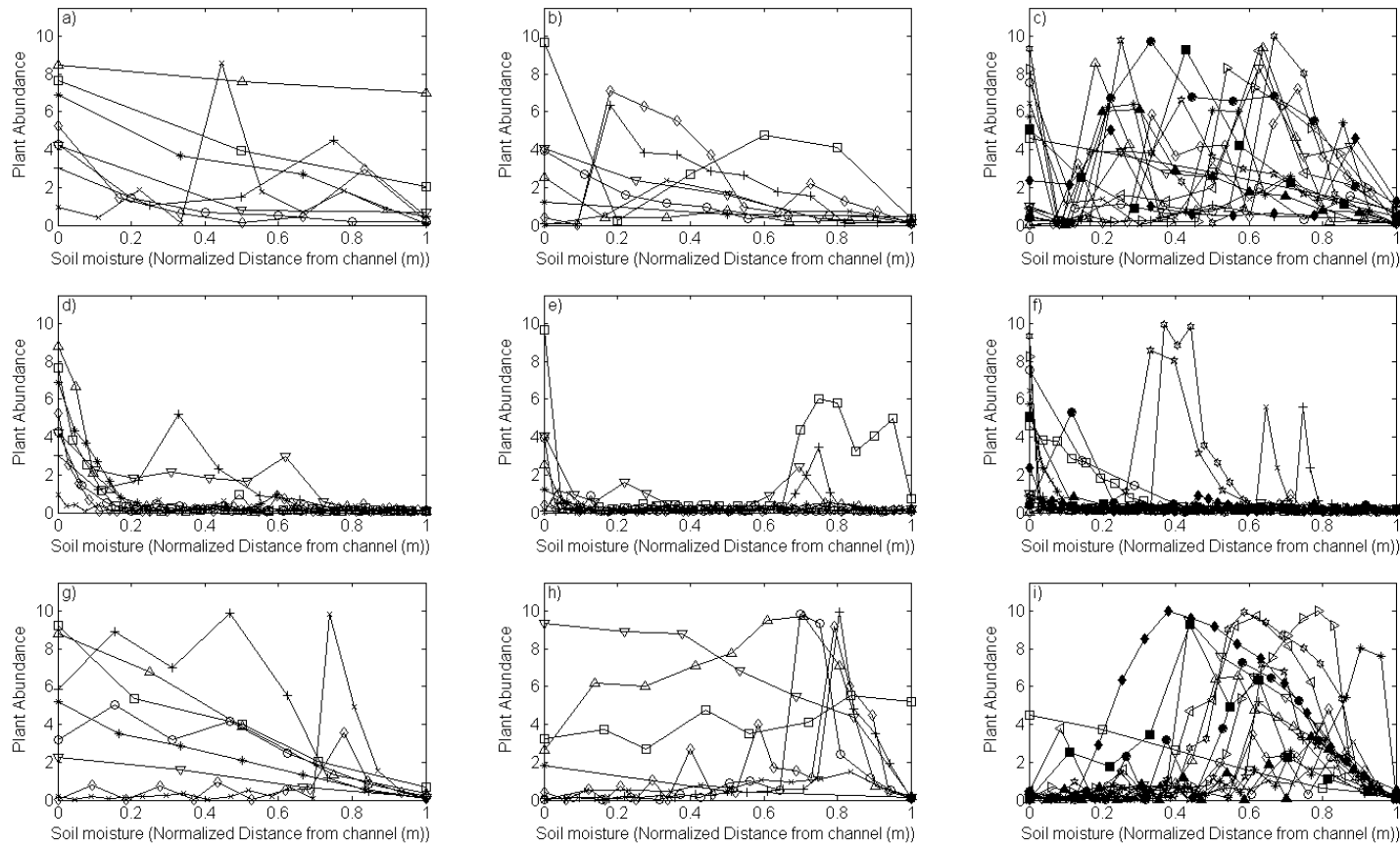
Figure B15. Overland flow-dominated landscape convergent-convex (left), convergent-planar (middle), and convergent-concave (right) hillslope plant tolerance curves where soil moisture is approximated by normalized distance from the channel (wet) to the ridgeline (dry) for a) - c) channel to ridgeline transects, d) - f) ascent transects, and g) - i) descent transects. The same symbol indicates data obtained from the same hillslope (ex. convergent-convex) for each of the three sampling methods (i.e. channel to ridgeline, ascent and descent).
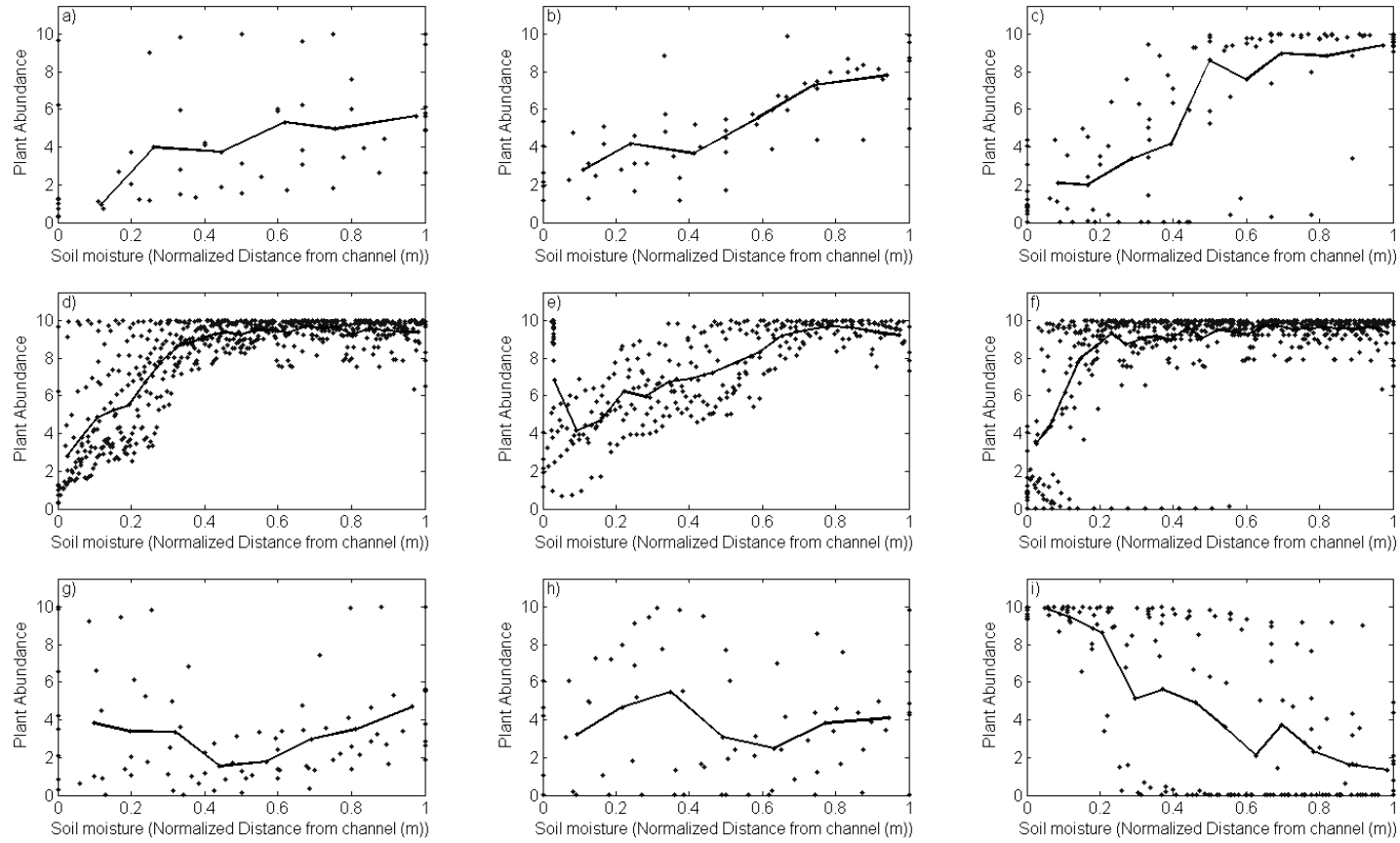
Figure B16. Landslide-dominated landscape divergent-convex (left), divergent-planar (middle), and divergent-concave (right) hillslope plant tolerance curves where soil moisture is approximated by normalized distance from the channel (wet) to the ridgeline (dry) for a) - c) channel to ridgeline transects, d) - f) ascent transects, and g) - i) descent transects. The same symbol indicates data obtained from the same hillslope (ex. divergent-convex) for each of the three sampling methods (i.e. channel to ridgeline, ascent and descent).
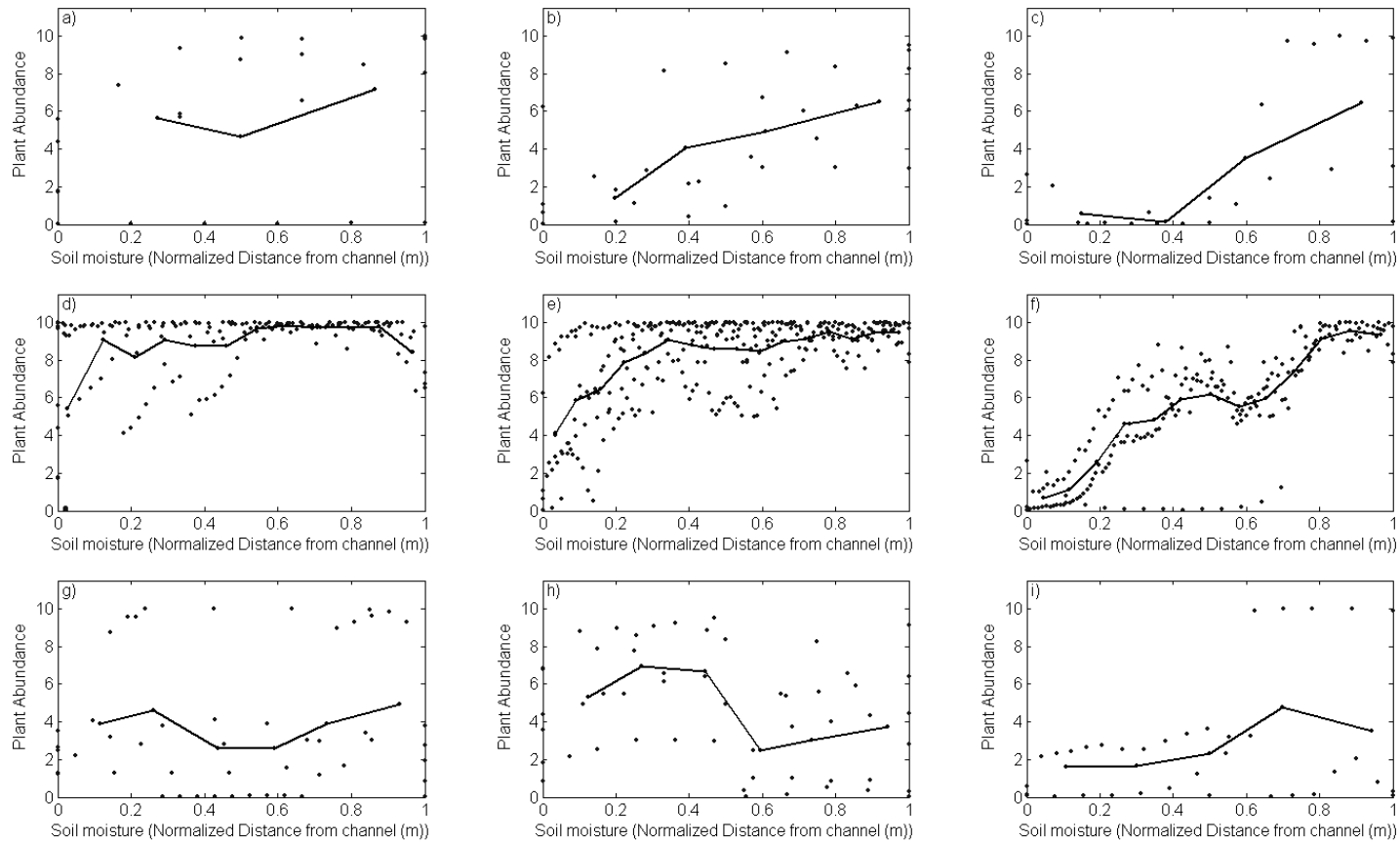
103

Figure B17. Landslide-dominated landscape parallel-convex (left), parallel-planar (middle), and parallel-concave (right) hillslope plant tolerance curves where soil moisture is approximated by normalized distance from the channel (wet) to the ridgeline (dry) for a) - c) channel to ridgeline transects, d) - f) ascent transects, and g) - i) descent transects. The same symbol indicates data obtained from the same hillslope (ex. parallel-convex) for each of the three sampling methods (i.e. channel to ridgeline, ascent and descent).
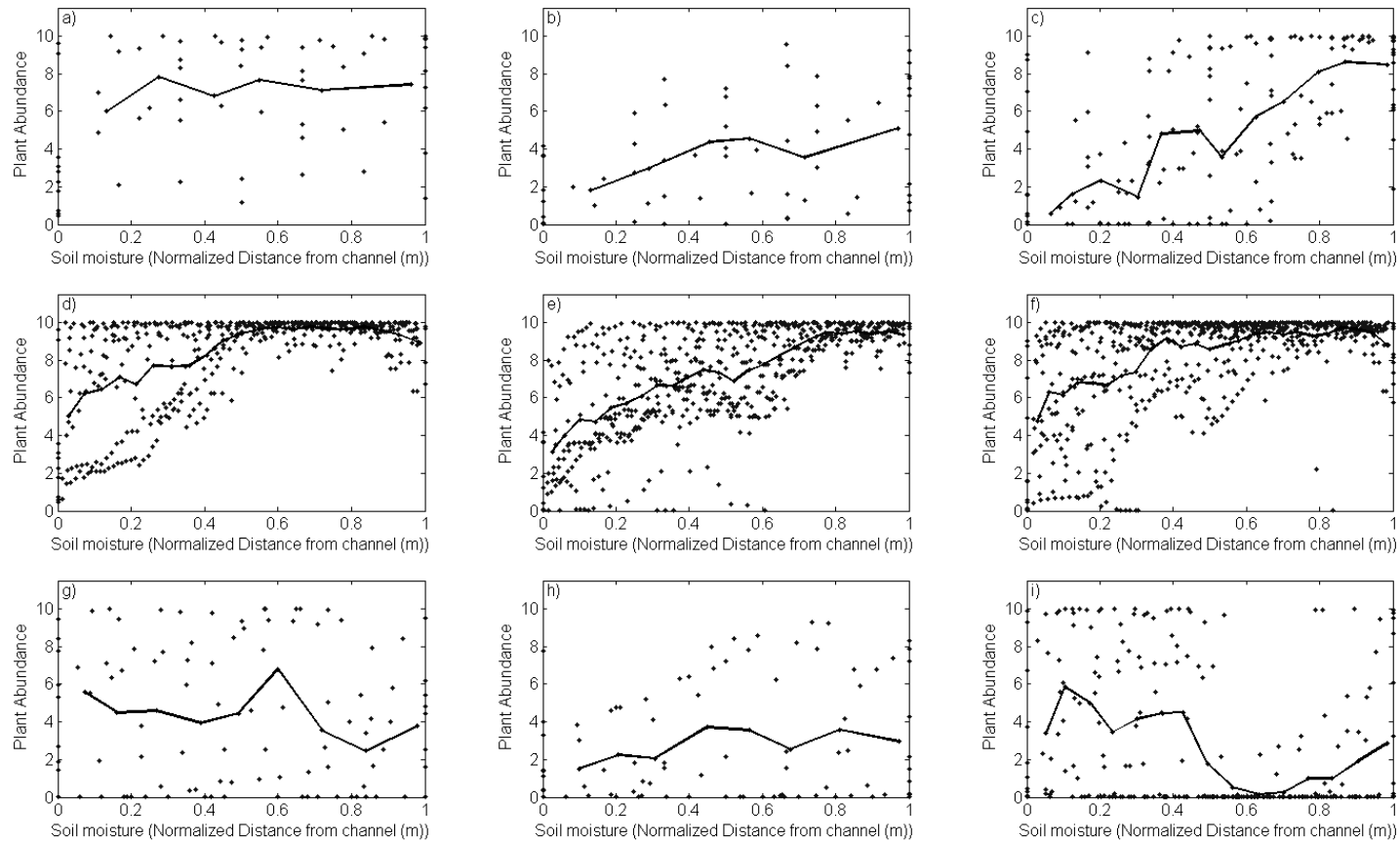
Figure B18. Landslide-dominated landscape convergent-convex (left), convergent-planar (middle), and convergent-concave (right) hillslope plant tolerance curves where soil moisture is approximated by normalized distance from the channel (wet) to the ridgeline (dry) for a) - c) channel to ridgeline transects, d) - f) ascent transects, and g) - i) descent transects. The same symbol indicates data obtained from the same hillslope (ex. convergent-convex) for each of the three sampling methods (i.e. channel to ridgeline, ascent and descent).
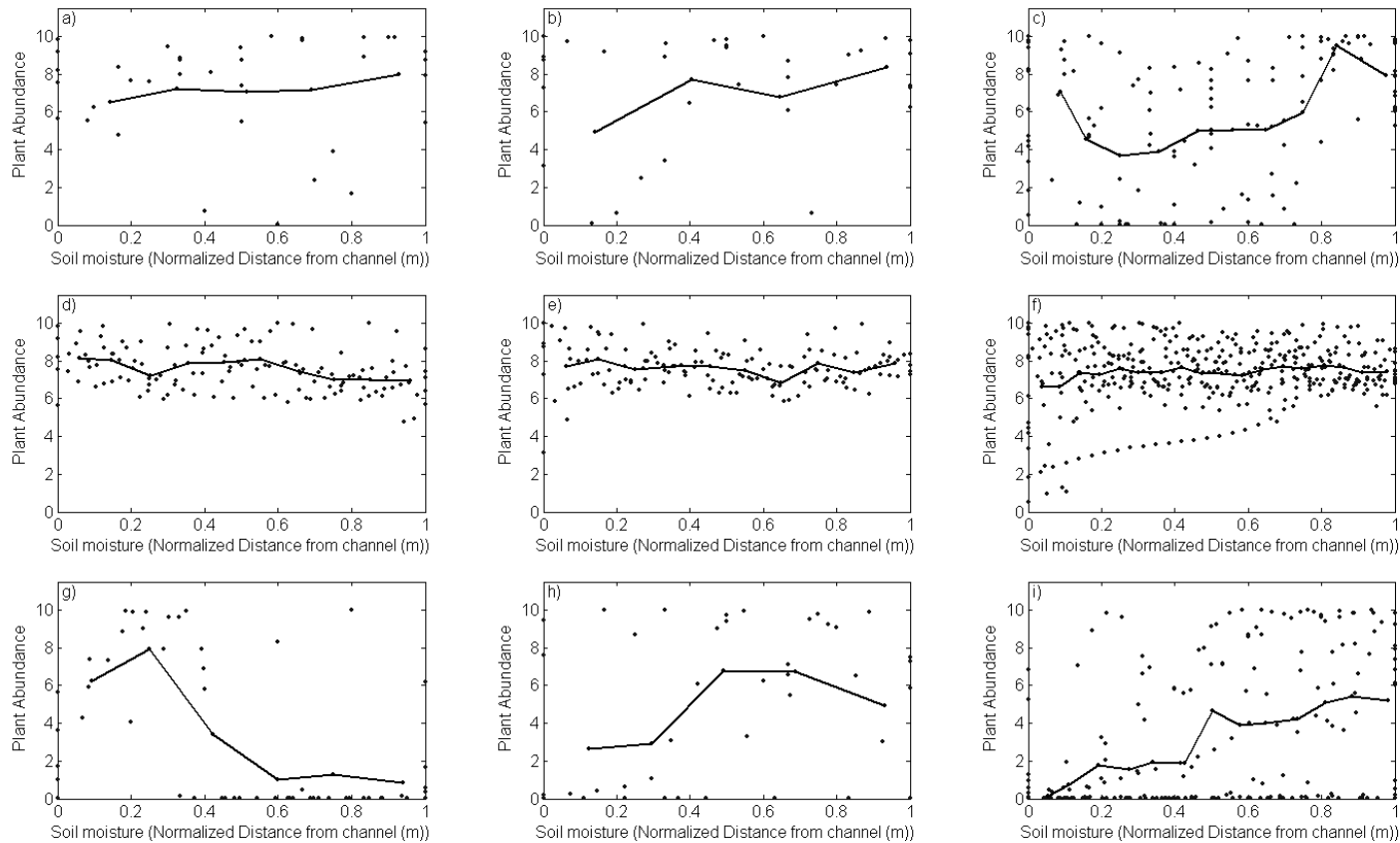
105

Figure B19. Creep-dominated landscape divergent-convex (left), divergent-planar (middle), and divergent-concave (right) hillslope plant tolerance curves generated when data for all transects in the hillslope category is binned by normalized distance according to the square root of sample size and soil moisture is approximated by normalized distance from the channel (wet) to the ridgeline (dry) for a) - c) channel to ridgeline transects, d) - f) ascent transects, and g) - i) descent transects. The solid line indicates binned data. Points represent unbinned data.

Figure B20. Creep-dominated landscape parallel-convex (left), parallel-planar (middle), and parallel-concave (right) hillslope plant tolerance curves generated when data for all transects in the hillslope category is binned by normalized distance according to the square root of sample size and soil moisture is approximated by normalized distance from the channel (wet) to the ridgeline (dry) for a) - c) channel to ridgeline transects, d) - f) ascent transects, and g) - i) descent transects. The solid line indicates binned data. Points represent unbinned data.
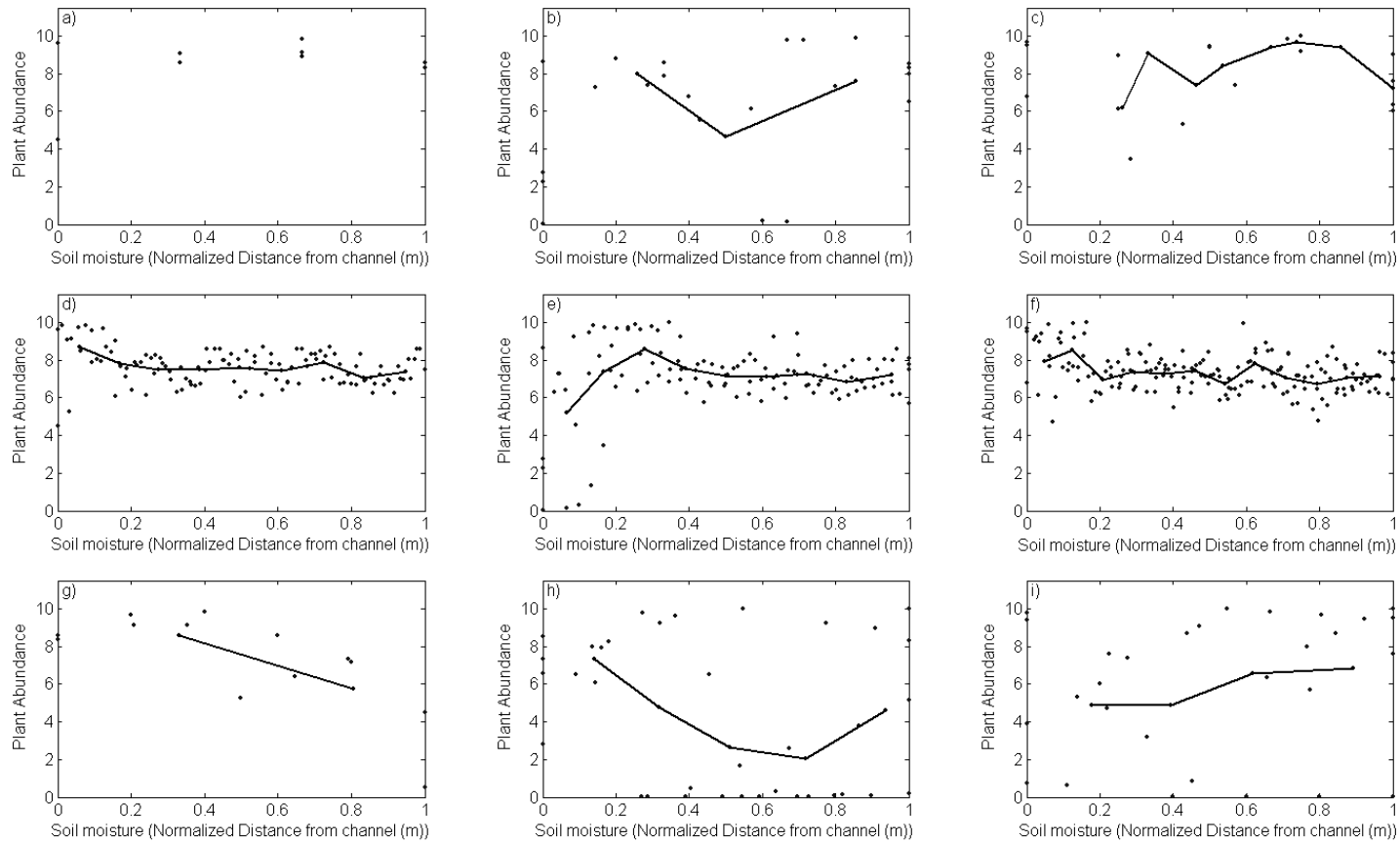
Figure B21. Creep-dominated landscape convergent-convex (left), convergent -planar (middle), and convergent -concave (right) hillslope plant tolerance curves generated when data for all transects in the hillslope category is binned by normalized distance according to the square root of sample size and soil moisture is approximated by normalized distance from the channel (wet) to the ridgeline (dry) for a) - c) channel to ridgeline transects, d) - f) ascent transects, and g) - i) descent transects. The solid line indicates binned data. Points represent unbinned data.
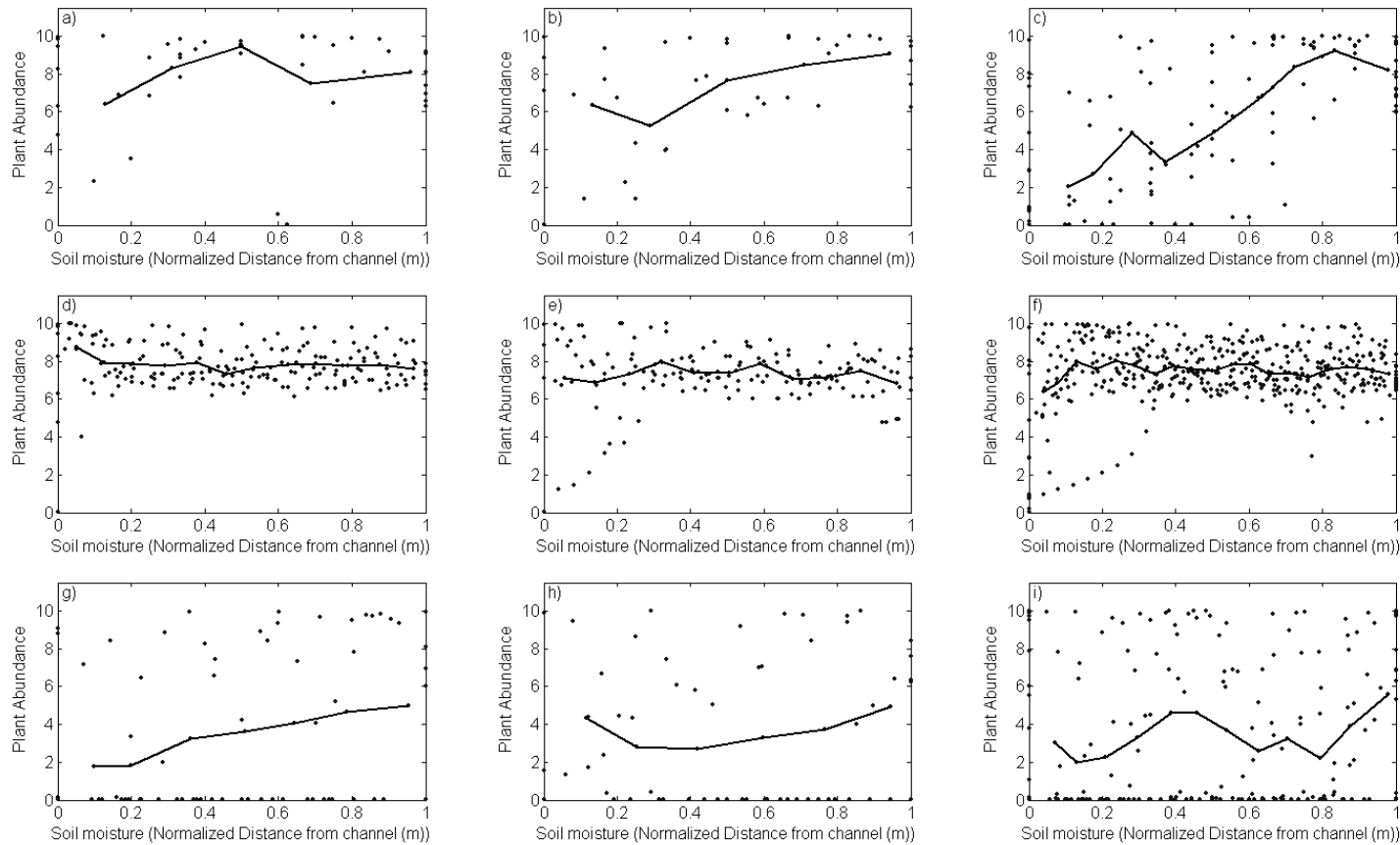
Figure B22. Overland flow-dominated landscape divergent-convex (left), divergent-planar (middle), and divergent-concave (right) hillslope plant tolerance curves generated when data for all transects in the hillslope category is binned by normalized distance according to the square root of sample size and soil moisture is approximated by normalized distance from the channel (wet) to the ridgeline (dry) for a) - c) channel to ridgeline transects, d) - f) ascent transects, and g) - i) descent transects. The solid line indicates binned data. Points represent unbinned data.
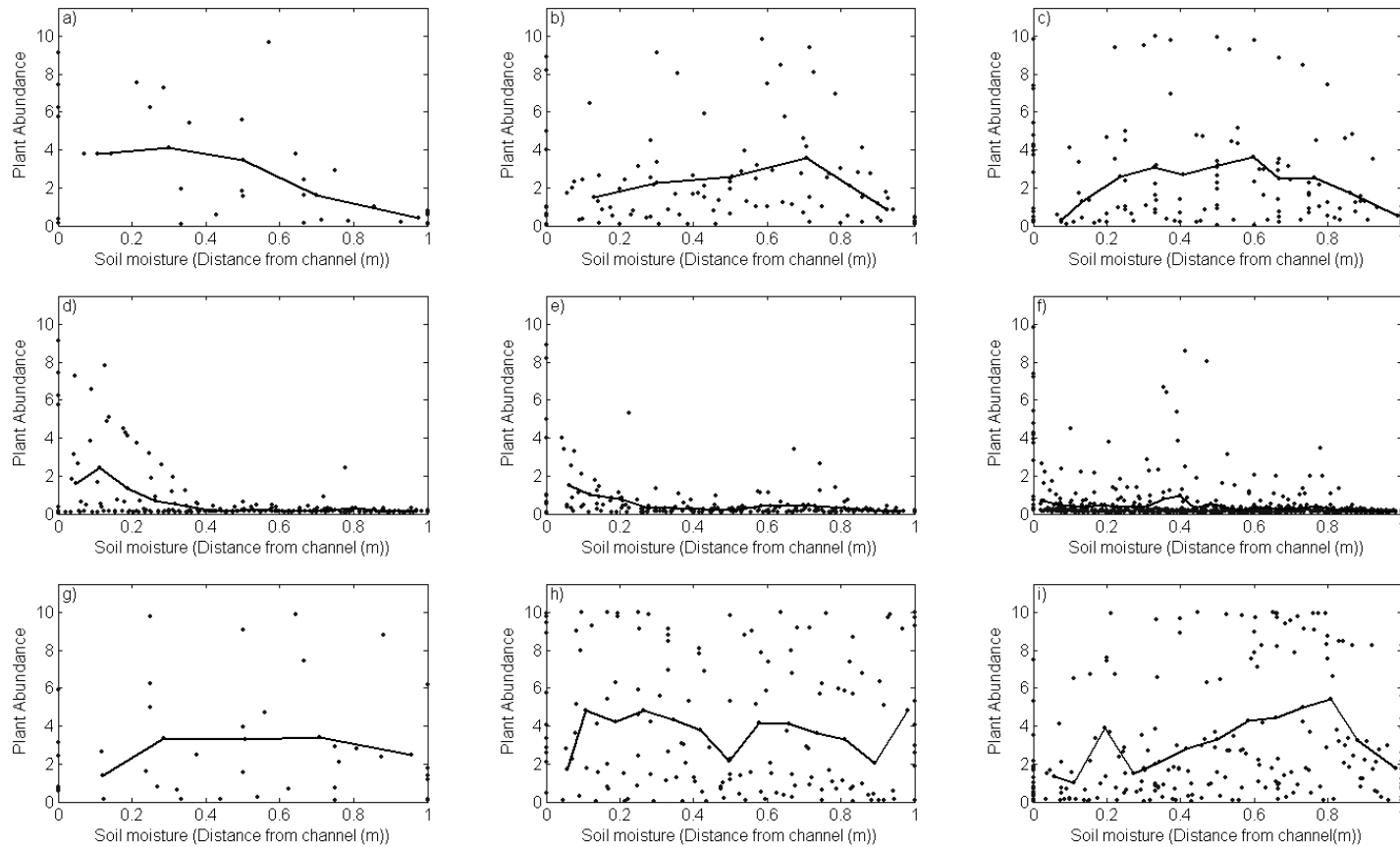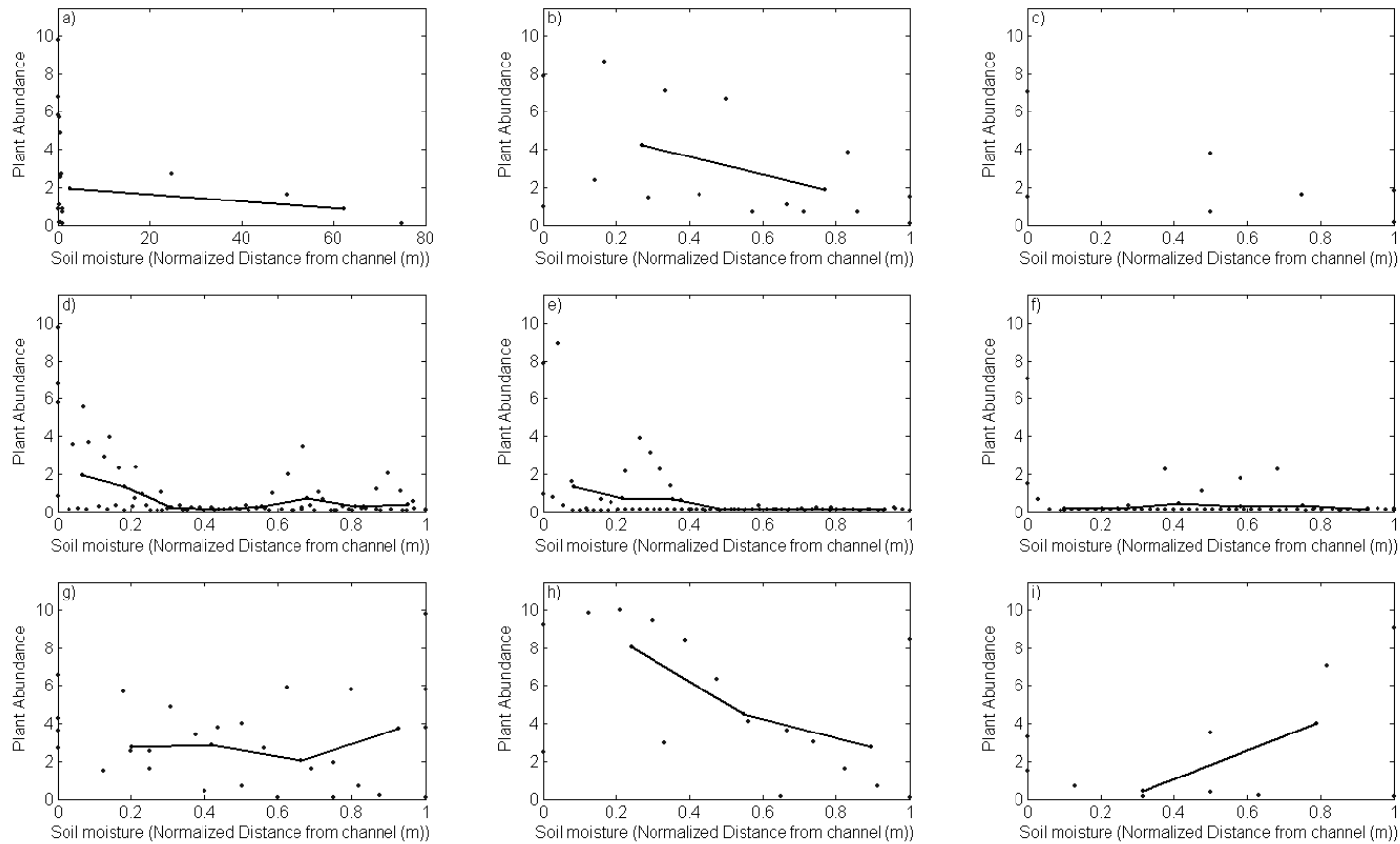
109

Figure B23. Overland flow-dominated landscape parallel-convex (left), parallel-planar (middle), and parallel-concave (right) hillslope plant tolerance curves generated when data for all transects in the hillslope category is binned by normalized distance according to the square root of sample size and soil moisture is approximated by normalized distance from the channel (wet) to the ridgeline (dry) for a) - c) channel to ridgeline transects, d) - f) ascent transects, and g) - i) descent transects. The solid line indicates binned data. Points represent unbinned data.
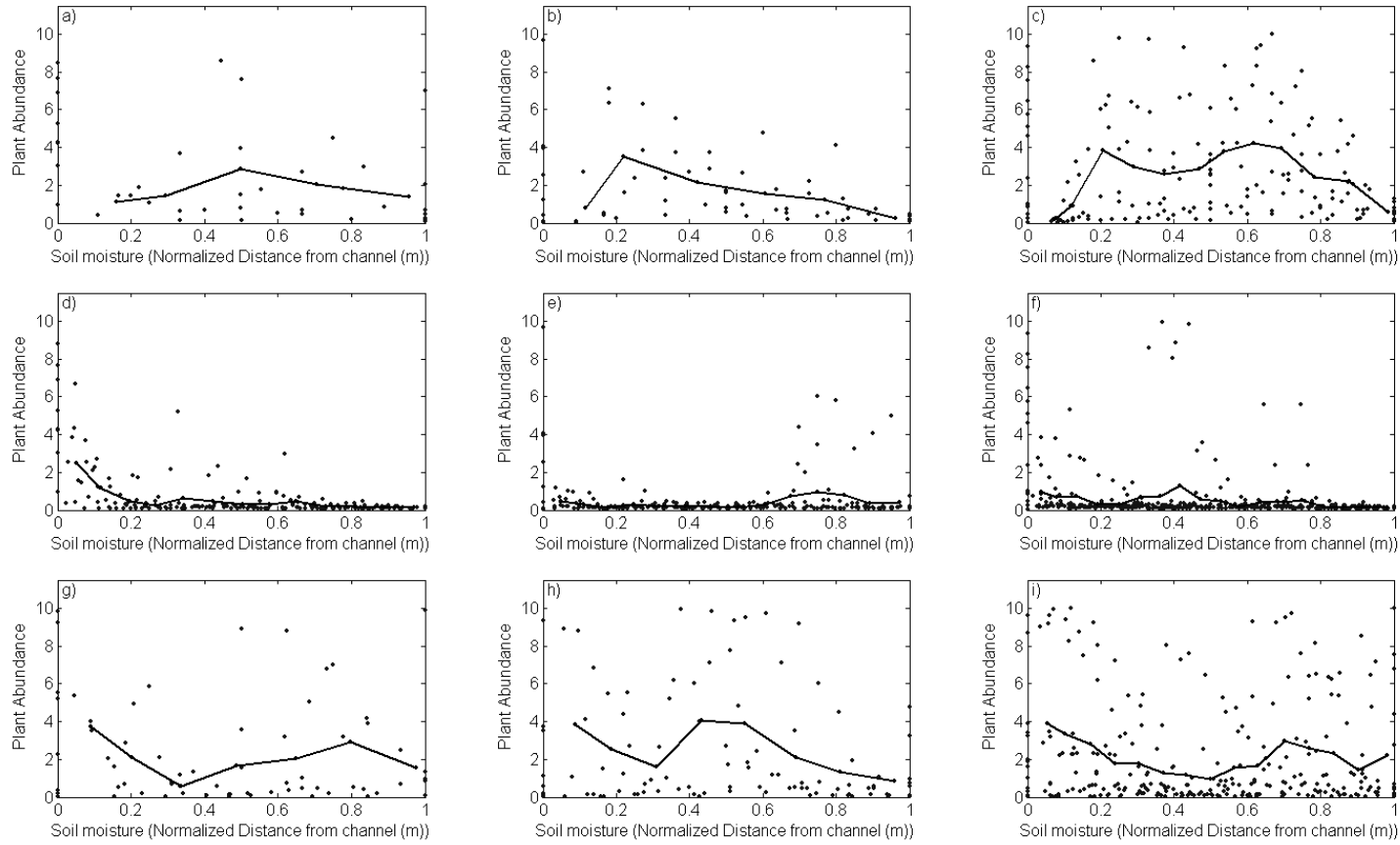
Figure B24. Overland flow-dominated landscape convergent-convex (left), convergent -planar (middle), and convergent - concave (right) hillslope plant tolerance curves generated when data for all transects in the hillslope category is binned by normalized distance according to the square root of sample size and soil moisture is approximated by normalized distance from the channel (wet) to the ridgeline (dry) for a) - c) channel to ridgeline transects, d) - f) ascent transects, and g) - i) descent transects. The solid line indicates binned data. Points represent unbinned data.
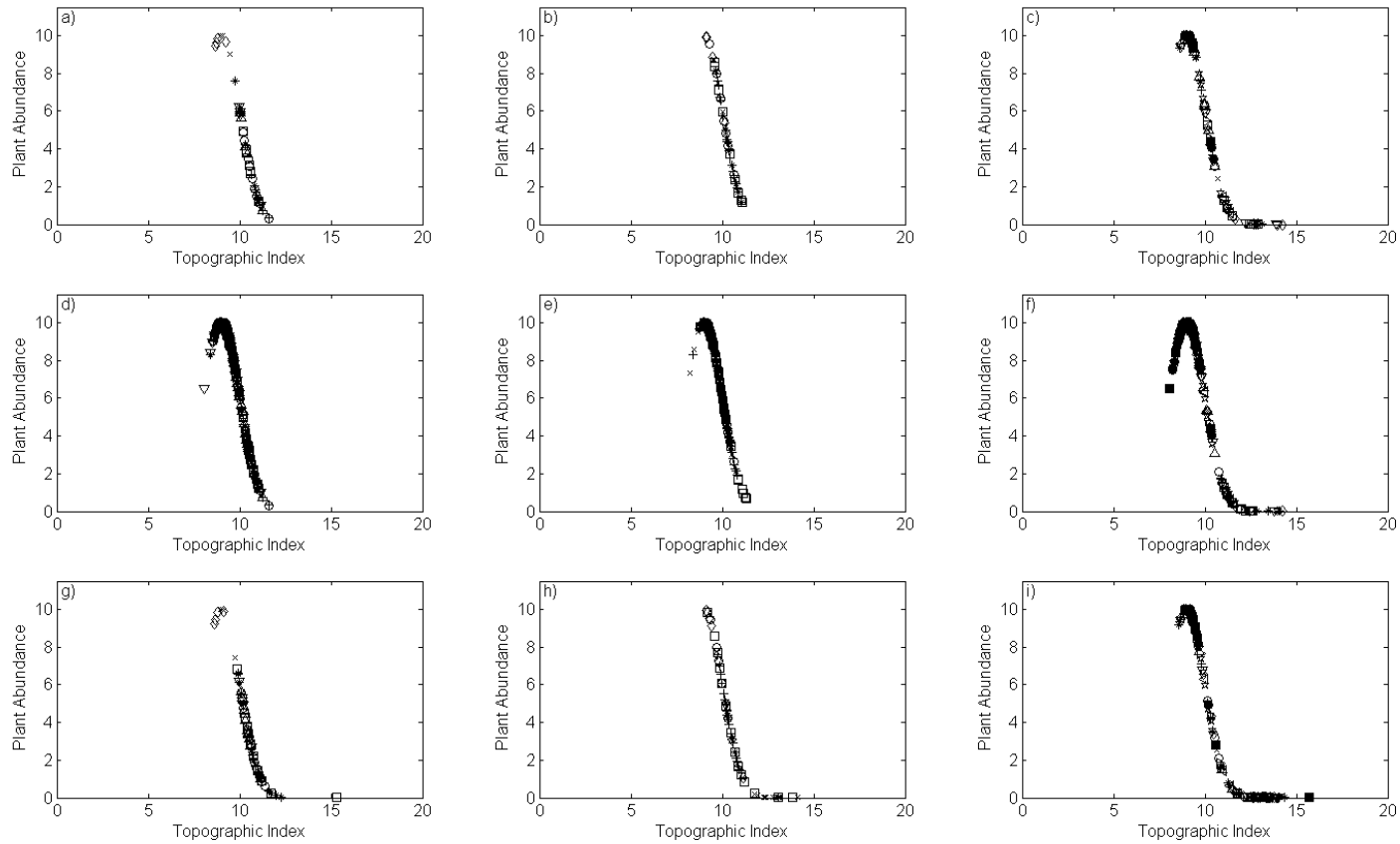
Figure B25. Landslide-dominated landscape divergent-convex (left), divergent-planar (middle), and divergent-concave (right) hillslope plant tolerance curves generated when data for all transects in the hillslope category is binned by normalized distance according to the square root of sample size and soil moisture is approximated by normalized distance from the channel (wet) to the ridgeline (dry) for a) - c) channel to ridgeline transects, d) - f) ascent transects, and g) - i) descent transects. The solid line indicates binned data. Points represent unbinned data.
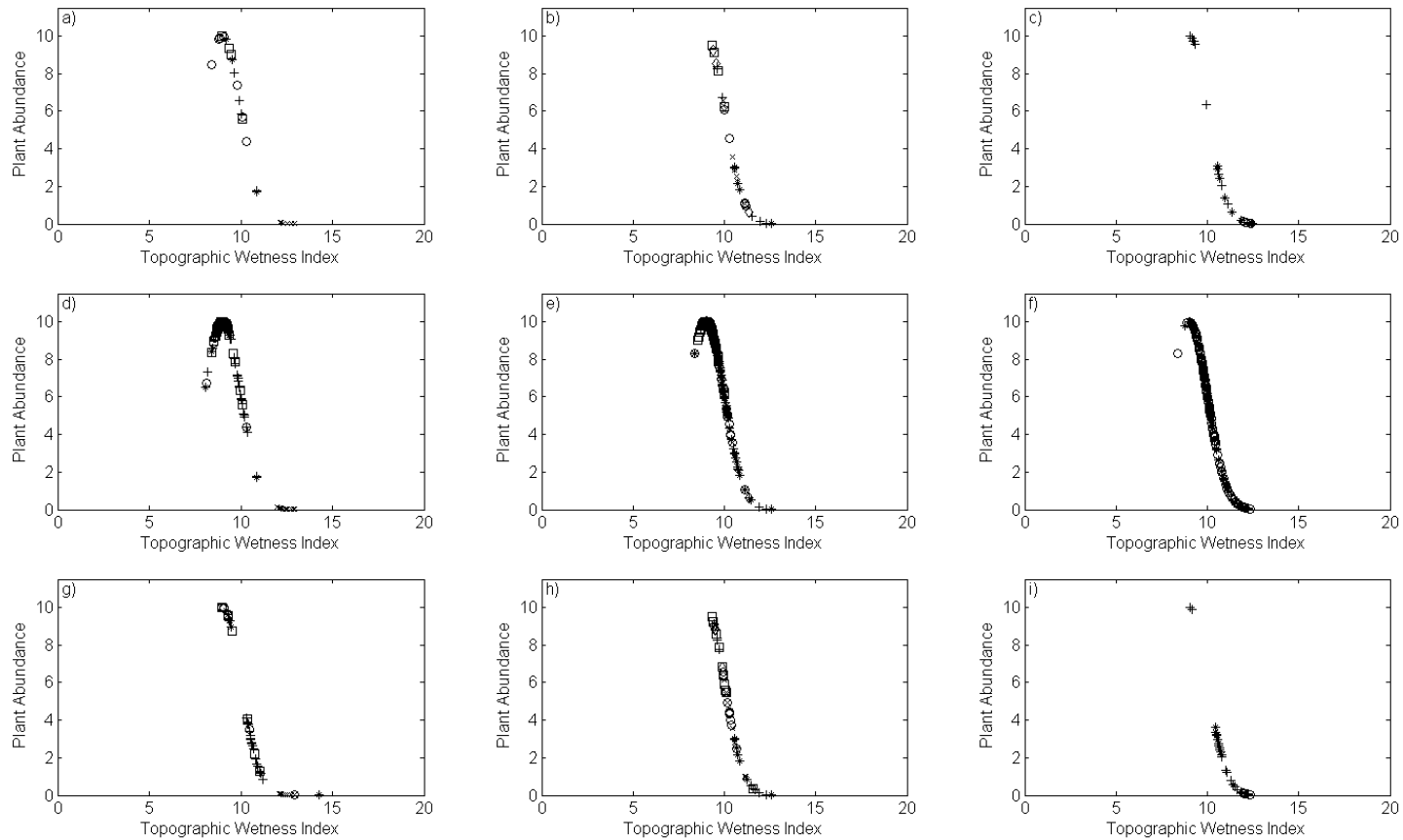
Figure B26. Landslide-dominated landscape parallel-convex (left), parallel-planar (middle), and parallel-concave (right) hillslope plant tolerance curves generated when data for all transects in the hillslope category is binned by normalized distance according to the square root of sample size and soil moisture is approximated by normalized distance from the channel (wet) to the ridgeline (dry) for a) - c) channel to ridgeline transects, d) - f) ascent transects, and g) - i) descent transects. The solid line indicates binned data. Points represent unbinned data.
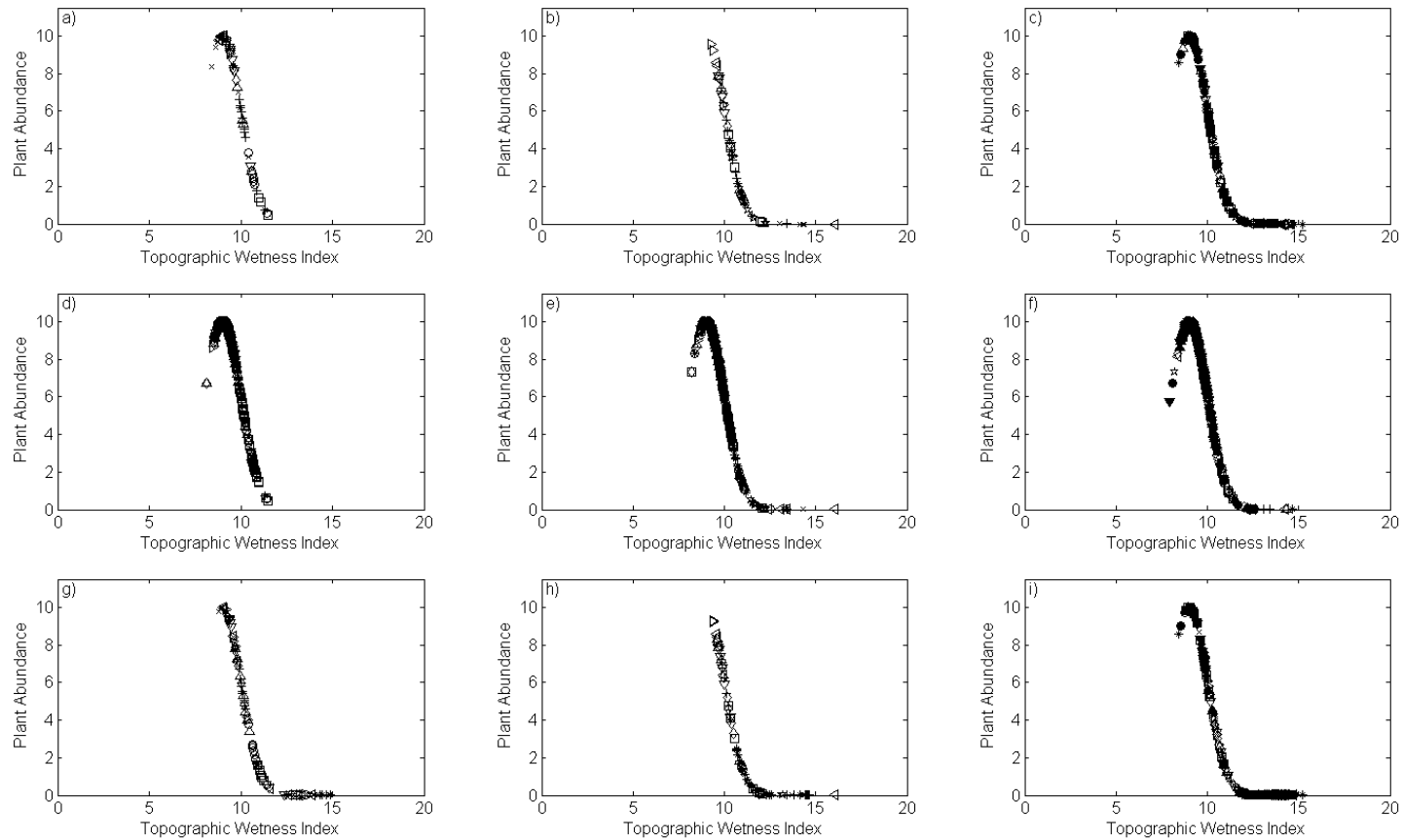
Figure B27. Landslide-dominated landscape convergent-convex (left), convergent-planar (middle), and convergent-concave (right) hillslope plant tolerance curves generated when data for all transects in the hillslope category is binned by normalized distance according to the square root of sample size and soil moisture is approximated by normalized distance from the channel (wet) to the ridgeline (dry) for a) - c) channel to ridgeline transects, d) - f) ascent transects, and g) - i) descent transects. The solid line indicates binned data. Points represent unbinned data.

114

Figure B28. Creep-dominated landscape divergent-convex (left), divergent-planar (middle), and divergent-concave (right) hillslope plant tolerance curves generated when abundance is plotted as a function of the topographic index for a) - c) channel to ridgeline transects, d) - f) ascent transects, and g) - i) descent transects. The same symbol indicates data obtained from the same hillslope (ex. divergent-convex) for each of the three sampling methods (i.e. channel to ridgeline, ascent and descent).
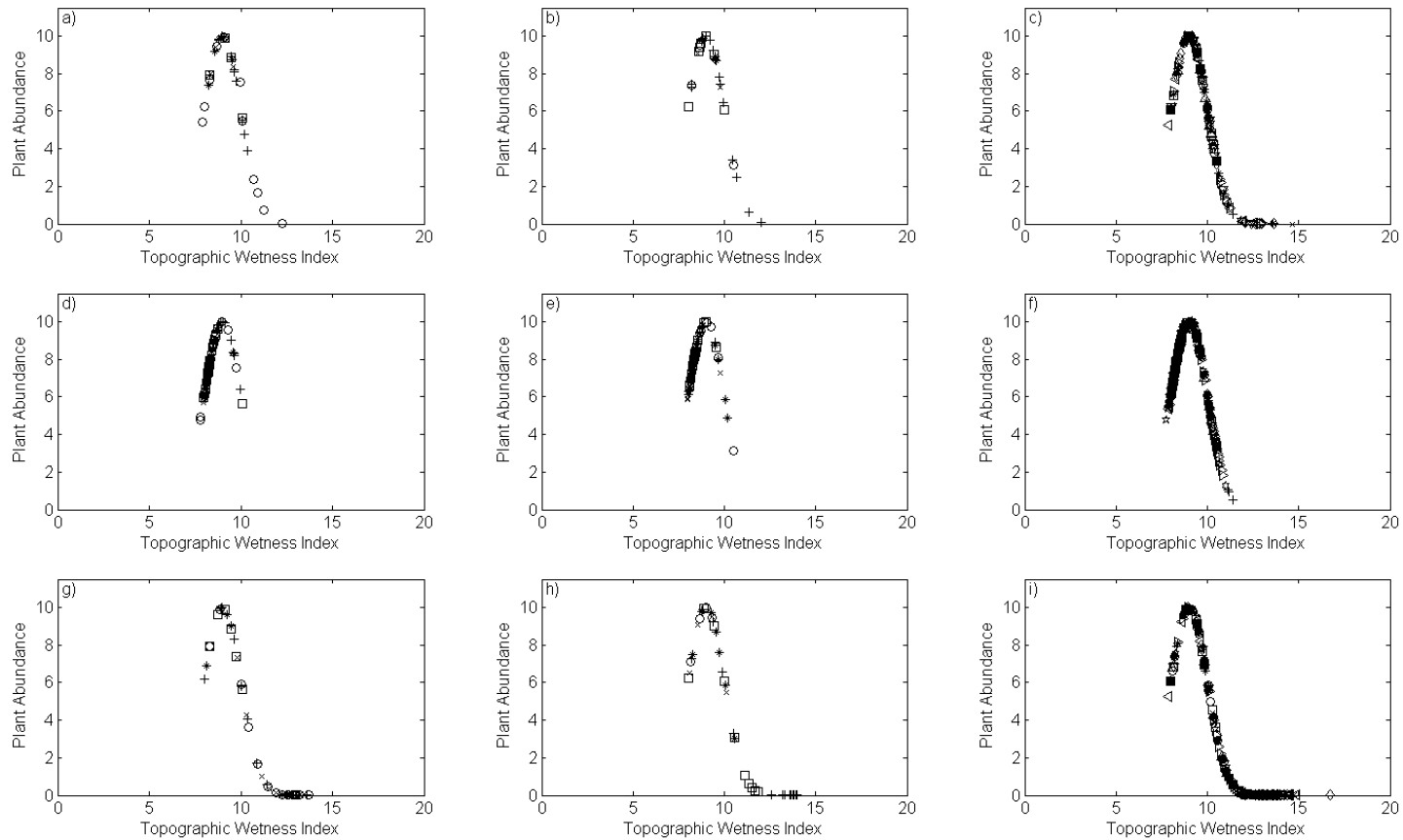
Figure B29. Creep-dominated landscape parallel-convex (left), parallel-planar (middle), and parallel-concave (right) hillslope plant tolerance curves generated when abundance is plotted as a function of the topographic index for a) - c) channel to ridgeline transects, d) - f) ascent transects, and g) - i) descent transects. The same symbol indicates data obtained from the same hillslope (ex. parallel-convex) for each of the three sampling methods (i.e. channel to ridgeline, ascent and descent).
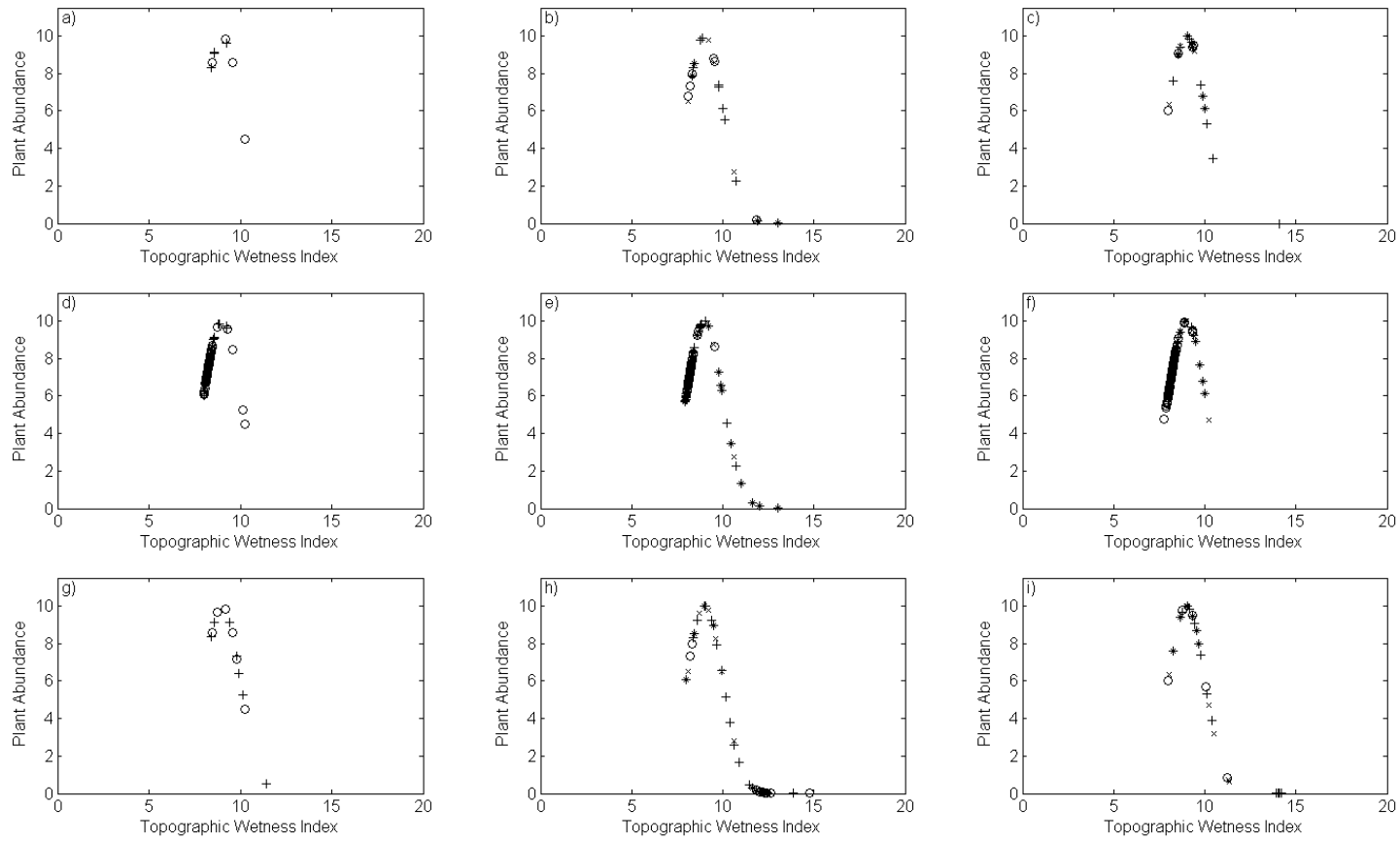
116

Figure B30. Creep-dominated landscape convergent-convex (left), convergent-planar (middle), and convergent-concave (right) hillslope plant tolerance curves generated when abundance is plotted as a function of the topographic index for a) - c) channel to ridgeline transects, d) - f) ascent transects, and g) - i) descent transects. The same symbol indicates data obtained from the same hillslope (ex. convergent-convex) for each of the three sampling methods (i.e. channel to ridgeline, ascent and descent).
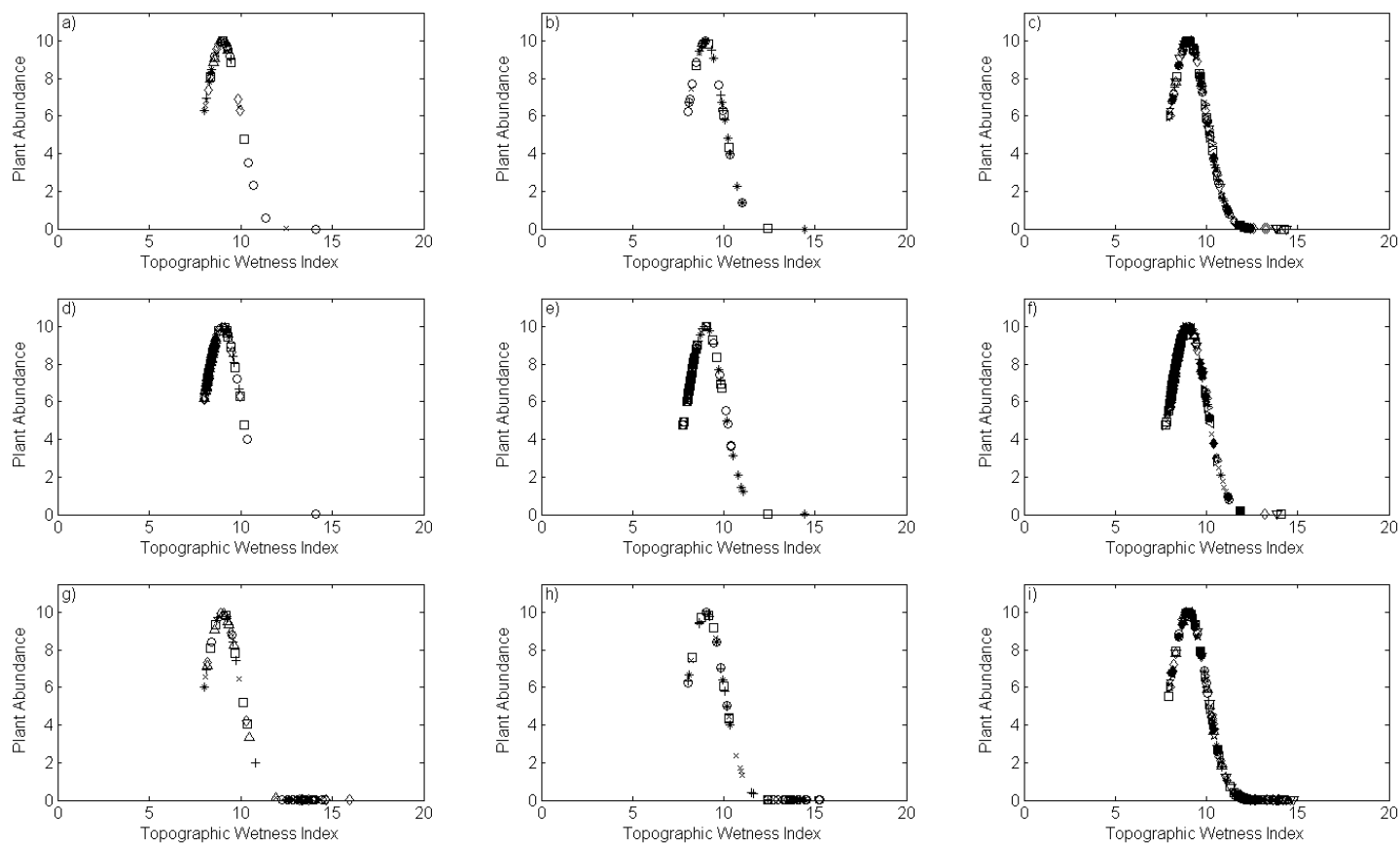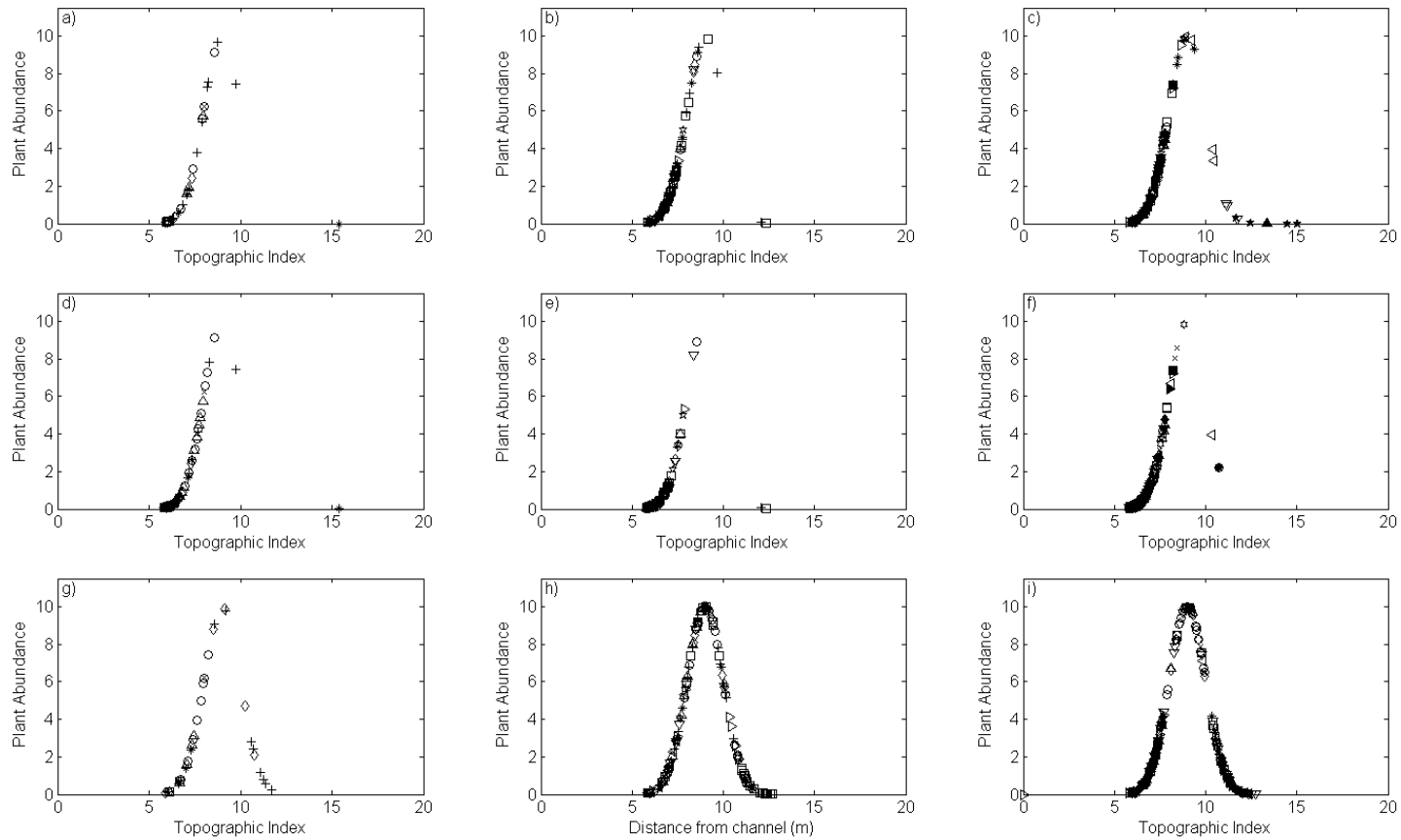
117

Figure B31. Overland flow-dominated landscape divergent-convex (left), divergent-planar (middle), and divergent-concave (right) hillslope plant tolerance curves generated when abundance is plotted as a function of the topographic index for a) - c) channel to ridgeline transects, d) - f) ascent transects, and g) - i) descent transects. The same symbol indicates data obtained from the same hillslope (ex. divergent-convex) for each of the three sampling methods (i.e. channel to ridgeline, ascent and descent).
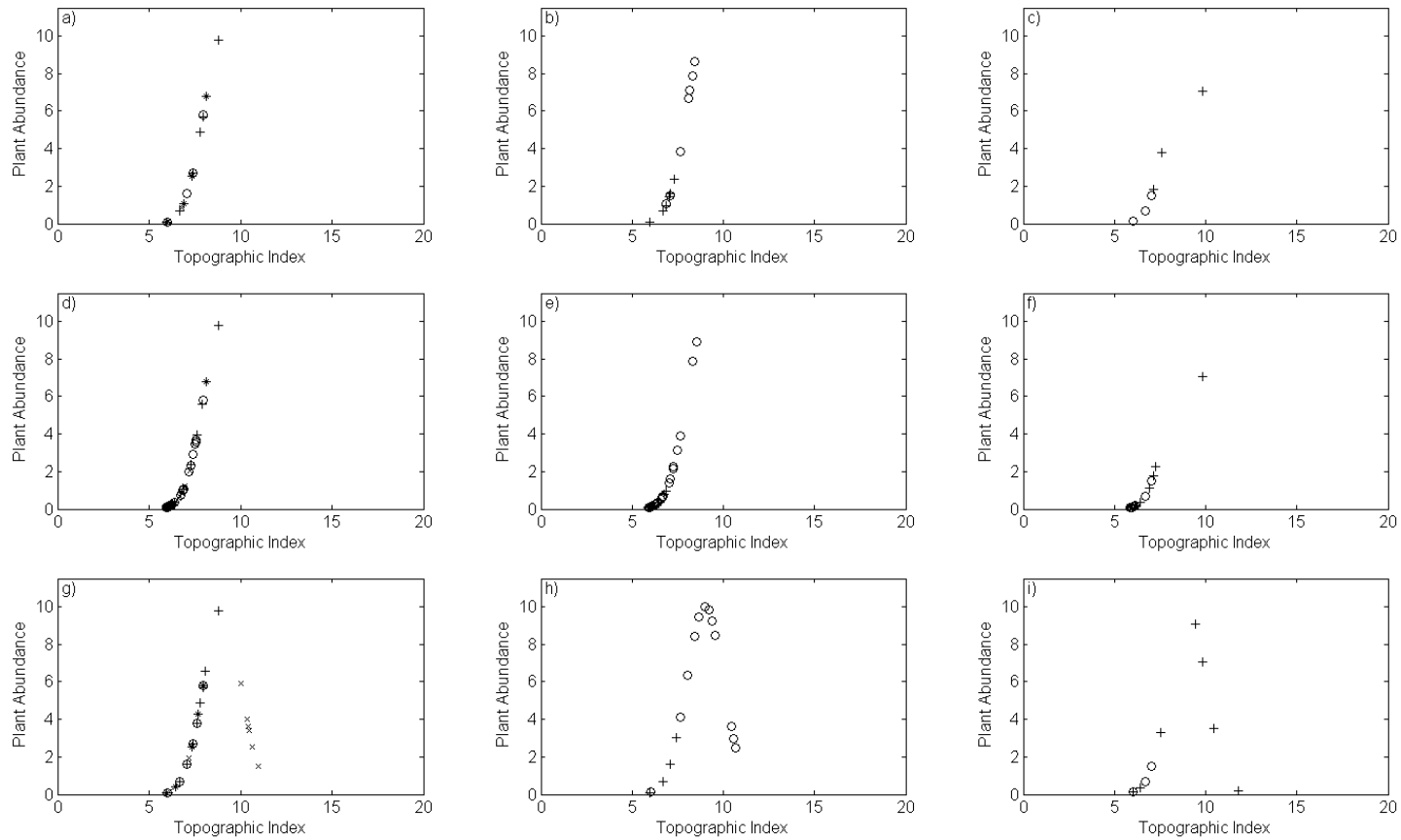
118

Figure B32. Overland flow-dominated landscape parallel-convex (left), parallel-planar (middle), and parallel-concave (right) hillslope plant tolerance curves generated when abundance is plotted as a function of the topographic index for a) - c) channel to ridgeline transects, d) - f) ascent transects, and g) - i) descent transects. The same symbol indicates data obtained from the same hillslope (ex. parallel-convex) for each of the three sampling methods (i.e. channel to ridgeline, ascent and descent).
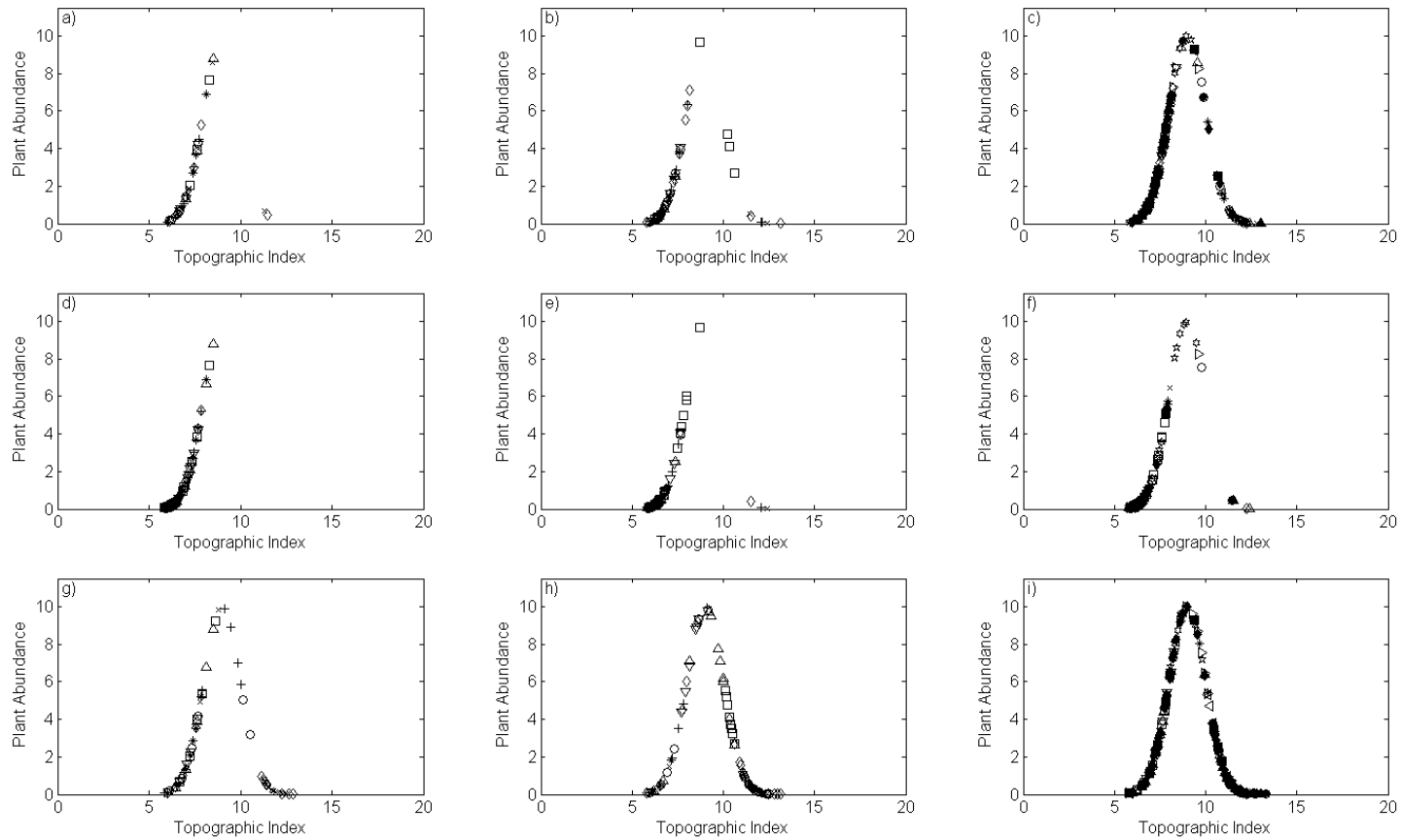
Figure B33. Overland flow-dominated landscape convergent-convex (left), convergent-planar (middle), and convergent-concave (right) hillslope plant tolerance curves generated when abundance is plotted as a function of the topographic index for a) - c) channel to ridgeline transects, d) - f) ascent transects, and g) - i) descent transects. The same symbol indicates data obtained from the same hillslope (ex. convergent-convex) for each of the three sampling methods (i.e. channel to ridgeline, ascent and descent).

120

Figure B34. Landslide-dominated landscape divergent-convex (left), divergent-planar (middle), and divergent-concave (right) hillslope plant tolerance curves generated when abundance is plotted as a function of the topographic index for a) - c) channel to ridgeline transects, d) - f) ascent transects, and g) - i) descent transects. The same symbol indicates data obtained from the same hillslope (ex. divergent-convex) for each of the three sampling methods (i.e. channel to ridgeline, ascent and descent).

121

Figure B35. Landslide-dominated landscape parallel-convex (left), parallel-planar (middle), and parallel-concave (right) hillslope plant tolerance curves generated when abundance is plotted as a function of the topographic index for a) - c) channel to ridgeline transects, d) - f) ascent transects, and g) - i) descent transects. The same symbol indicates data obtained from the same hillslope (ex. parallel-convex) for each of the three sampling methods (i.e. channel to ridgeline, ascent and descent).

Figure B36. Landslide-dominated landscape convergent-convex (left), convergent-planar (middle), and convergent-concave (right) hillslope plant tolerance curves generated when abundance is plotted as a function of the topographic index for a) - c) channel to ridgeline transects, d) - f) ascent transects, and g) - i) descent transects. The same symbol indicates data obtained from the same hillslope (ex. convergent-convex) for each of the three sampling methods (i.e. channel to ridgeline, ascent and descent).

123